Structural Basis for Dishevelled-2 Association to the Plasma Membrane

Andrew Thomas Lucas

Thesis submitted to the faculty of the Virginia Polytechnic Institute and State University in partial fulfillment of the requirements for the degree of

Master of Science
In
Biological Sciences

Dr. Carla Finkielstein
Dr. Daniel Capelluto
Dr. David Bevan

April 16th, 2010
Blacksburg, Virginia

Keywords: Dishevelled-2, DEP, phosphatidic acid, pH-dependent

Structural Basis for Dishevelled-2 Association to the Plasma Membrane

Andrew T. Lucas

ABSTRACT

The Wingless (Wnt) signaling pathway is one of the critical developmental pathways for control of cell differentiation, proliferation, and cell growth. The DEP domain, located on the C-terminus of Dishevelled (Dvl), plays a role in cytoplasm-membrane association, which branches the canonical and non-canonical Wnt signaling pathway within the cell. It has been suggested that the DEP domain requires the recruitment of ionic lipids, such as phosphatidic acid, to regulate its localization to the plasma membrane and association to the frizzle receptor. However, the physical mechanism for DEP association to the plasma membrane is still unknown.

We show that mDvl2-DEP interacts with phosphatidic acid at a distinct patch on the surface formed by a positively charged surface area by NMR spectroscopy. The binding of this interaction was also found at physiologically relevant concentration using fluorescence spectroscopy. We also determined that the interaction is pH-dependent and regulated through a 'histidine switch' mechanism at His464 and His465 where there is increased association of mDvl2-DEP to the plasma membrane at higher pH values (7.5). This association is based on tertiary structure conformational changes with rearrangement of the loop regions by a change in local pH, not its interaction with phosphatidic acid.

Overall, our work will contribute to elucidate how cells regulate their developmental pathways through localized molecular interactions.

Table of Contents

Abstract
Table of Contents……iii
Abbreviations……iv
List of Figures and Tables……v

Chapter 1: Background and Significance……1
A. Wingless (Wnt) Signaling Pathway……..1
B. Dishevelled-2 (Dvl-2)……....1
C. The DEP Domain……...3
C.1 Domain Architecture
C.2 Lipid Interaction
D. Relevance of Wnt pathways in disease……..6

Chapter 2: Specific Aims……....8

Chapter 3: Results……..10

Chapter 4: Discussion and Conclusions……23

Chapter 5: Materials and Methods……28

Chapter 6: Collaborations……..…31
A. **A novel heme-regulatory motif mediates heme-dependent degradation of the circadian factor Period 2.** Jianhua Yang, Kevin D. Kim, Andrew Lucas, Karen E. Drahos, Carlo S. Santos, Sean P. Mury, Daniel G. S. Capelluto, and Carla V. Finkielstein. *Molecular and Cellular Biology*. Aug. 2008: 4697-4711…….……..31
B. **Heme Binding to the Translationally Controlled Tumor Protein Induces Oligomerization.** Andrew Lucas, Jianhua Yang, Daniel G.S. Capelluto, and Carla Finkielstein. *Publication in process* ……....56

Appendices
A. Literature Cited……...…65

Abbraviations

APC	Adenomatous polyposis coli
CD	Circular dichroism
CK1α,γ	Casein kinase 1
Daam1	Disheveled-associated activator of morphogenesis 1
DEP	Dishevelled, Egl-10, and pleckstrin homology domain
Dvl	Dishevelled
Egl-10	Egg Laying defective 10
FPLC	Fast performance liquid chromatography
Fz	Frizzled transmembrane receptor
GSH	glutathione sepharose
GSK3β	Glycogen synthase kinase
GST	glutathione S-transferase
HSQC	Heteronuclear single quantum coherence
JNK	c-Jun N-terminal kinase
Kd	ligand dissociation constant
LBA	liposome binding assay
LDL	Low density lipoprotein
LRP	LDL-related protein
Nhe2	Na^+/H^+ Exhangers 2
NMR	Nuclear magnetic resonance spectroscopy
PA	phosphatidic acid
PC	phosphatidylcholine
PE	phosphatidylethanolamine
PG	phosphatidylglycerol
PCP	planar cell polarity
PH	pleckstrin homology
PRD	proline-rich domain
ROCK	Rho-associated, coiled-coil containing protein kinase
S3H	Proline-rich Src 3 homology
SDS-PAGE	sodium dodecyl sulfate polyacrylamide gel electrophoresis
SPR	surface plasmon resonance
TCF	Transcription Factor
Wnt	wingless type
Wnt-Fz	Wnt-Fz ligand-receptor pair

List of Figures and Tables

Chapter 1: Background and Significance

Figure 1.1: The Wingless (Wnt) Signaling Pathways……..2
Figure 1.2: Domains of Dishevelled-2…….2
Figure 1.3: Alignment of Dvl-DEP in noted Dishevelled proteins……..4
Figure 1.4: Structure and features of mouse Dishevelled-1…….4
Figure 1.5: Chemical structures of ionic lipids known to interact with the DEP Domain…….5
Figure 1.6: Proposed dependence of pH to Wnt signaling pathway branching……...6

Chapter 3: Results

Figure 3.1: Phosphatidic Acid binds to the DEP domain of mouse Dishevelled-2……...11
Figure 3.2: Homology Model of mDvl2-DEP……...12
Figure 3.3: Chemical Shift Analysis Demonstrates Two Sites of Interaction……...13
Figure 3.4: Coulombic Surface Charge Analysis of mDvl2-DEP ……....14
Figure 3.5: Phosphatidic acid does not perturb structural elements of mDvl2-DEP at pH 7.5…….16
Figure 3.6: Mutations to mDvl2-DEP alters binding capability to phosphatidic acid…...17
Figure 3.7: mDvl2-DEP interacts with phosphatidic acid in the micromolar range……..17
Figure 3.8: Changes in pH results in chemical shift perturbations of interacting residues……..19
Figure 3.9: Changes in pH alters tertiary structure of mDvl2-DEP……..20
Figure 3.10: Phosphatidic acid does not alter mDvl2-DEP structure at lower pH values…….…..21
Figure 3.11: mDvl2-DEP binding to phosphatidic acid is decreased at lower pH……22

Chapter 6: Collaborations

A. Yang *et al*

Figure 1: Heme modulates hPer2 stability in vitro and in vivo…….…35
Figure 2: Heme binds hPer2 in two distinct regions…….…36
Figure 3: A novel heme-regulatory motif is present in hPer2……...……37
Figure 4: Heme binds to the PAS domain and the HRM motif…….38
Figure 5: Degradation of hPer2 depends exclusively on the redox state of the heme bound to HRM…….…39
Figure 6: CD analysis of the heme-binding regions in hPer2……..……..40
Figure 7: The HRM modulates hPer2 stability in CHO cells……42
Figure 8: Binding of heme prevents hPer2/hCry1 heterodimerization……..……43
Figure 9: HRM-heme binding odulates the expression of Rev-erbα……...…..44

B. Lucas *et al*

Figure 1: Analysis of TCTP/heme and TCTP/calcium interaction using gel filtration chromatography and non-denaturing gel electrophoresis……...…48

Figure 2: Analysis of TCTP/heme and TCTP/calcium interaction shows structural conformation change and change to denaturation effects……..49
Figure 3: Absorption spectra of TCTP/heme and the effects of calcium……..50
Figure 4: Determination of novel interactions between TCTP with heme and calcium interaction demonstrates calcium dissociates the heme induced dimmer……..51
Figure 5: NMR titration proves TCTP dimer formation and dissociation…….……52
Figure 6: Pulldown of TCTP when mixed with heme shows dimer formation while calcium shows dissociation……...53

Chapter 1: Background and Significance

Wingless Signaling Pathways

The wingless (Wnt) signaling pathway is critical for controlling cell differentiation, proliferation, cell growth and, at least in Drosophila, is responsible for the segmented polarity of individual cells in relation to the body during embryogenesis. In mammals, it aids during limb formation (*1*). The Wnt signaling cascade is triggered by binding of wnt molecules to each of the nine Frizzled (Fz) transmembrane receptors. In large, this complex activates Disheveled (Dvl) proteins through phosphorylation (*2*), which signals the formation of a multi-protein complex that spans the fragment of the Fz receptor.

As result of Wnt-induced activation, there is alternate pathway determination (Fig 1.1). The canonical pathway is also known as the ß-catenin dependent pathway. Here, the multi-protein complex containing Axin, APC (Adenomatous polyposis coli), and GBP (GSK3 Binding Protein) inhibits GSK3 (glycogen synthase kinase 3) (*3*). While GSK3 usually phosphorylates ß-catenin marking it for degradation; now with GSK3 inhibited, an increase of ß-catenin begins to accumulate within the cell due to the lack of markers for degradation. Eventually, ß-catenin translocates to the nucleus, binding TCF, a transcription factor, modulating specific gene expression (*3*).

The second set of pathways that can be induced by wnt are the non-canonical pathways, otherwise known as the ß-catenin independent pathway. While there are three non-canonical pathways, only one is mediated by Dvl at all times: the planar cell polarity (PCP) pathway (*2*). This pathway is initiated when the protein Daam1 activates the GTPases Rho and Rac by inducing a Dvl-Rho or Dvl-Rac complex. These proteins in complex activate kinases ROCK and JNK that begin signaling cascades that lead to actin stability and cellular movement (*2*).

Dishevelled-2

There are a few structural characteristics of importance contained within Dvl. There is a highly conserved characteristic region of positively charged (basic) residues, several putative phosphorylation sites, and a proline-rich Src 3 homology binding domain (*4*). Dvl2 also has three well-conserved domains within its structure: the N-terminal DIX, central PDZ, and C-terminal DEP domain (Fig 1.2).

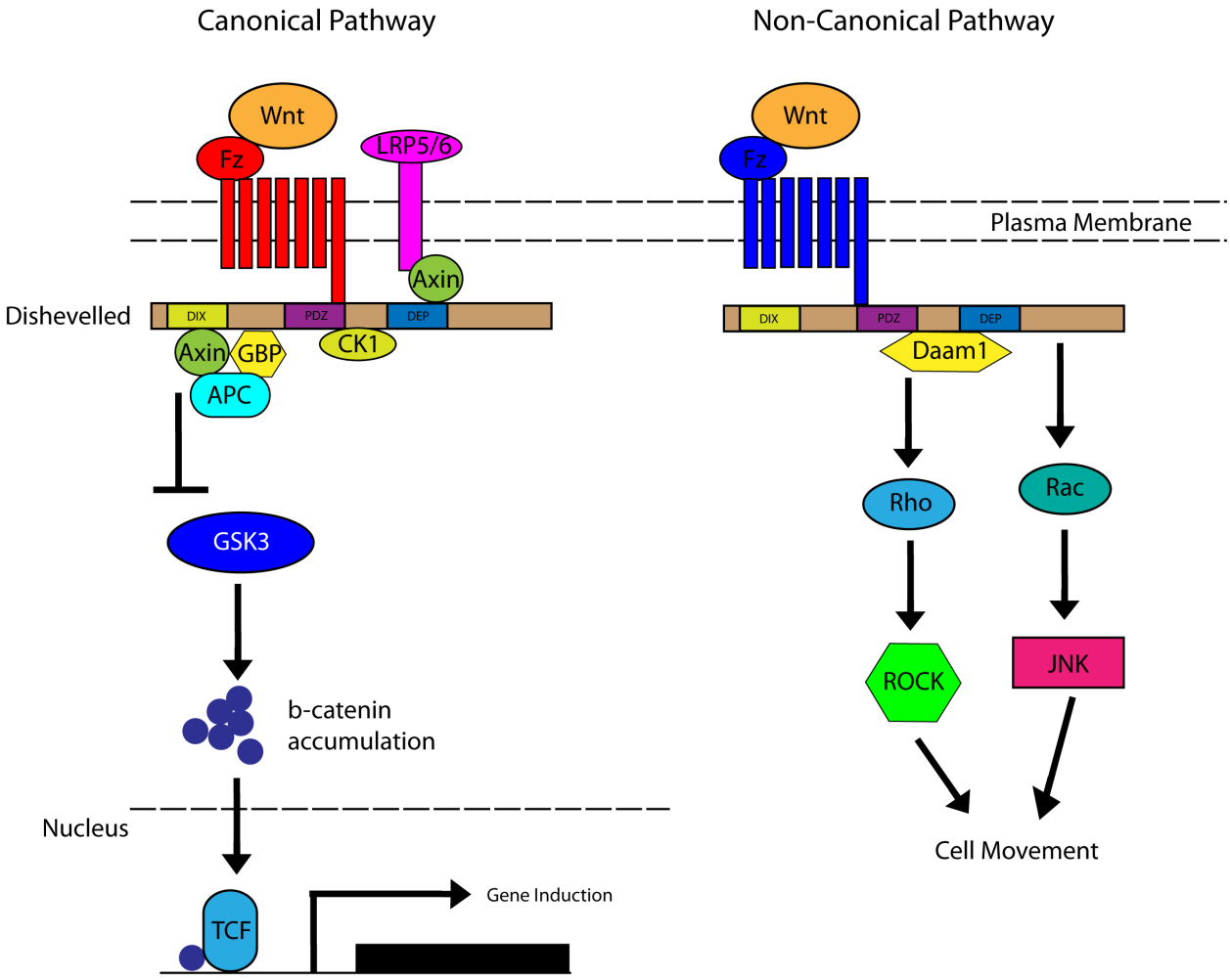

Figure 1.1: *The Wingless (Wnt) Signaling Pathways. Depending on which wnt molecule binds the Fz receptor, the signal can affect gene transcription, cell movement, or actin polymerization. In the canonical pathway, wnt binding causes a disruption of the ß-catenin destruction complex, where GSK3 would normally phosphorylate ß-catenin, marking it for proteolysis. This inhibition allows for an increase in cytoplasmic ß-catenin level, which translocates to the nucleus to modulate gene expression. In the non-canonical pathway, wnt binding signals the GTPases Rho and Rac, which through activation of other key molecules, mediates cytoskeleton changes.*

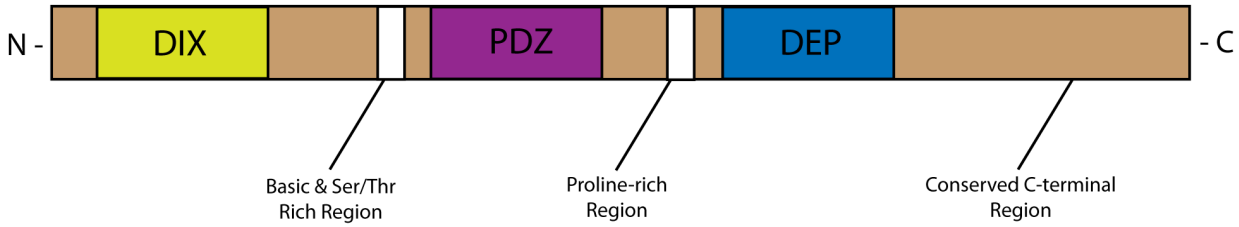

Figure 1.2: *Cartoon representation of the mDvl2 protein, showing known protein domain locations and characteristics of importance.: the N-terminal DIX, the central PDZ, and the C-terminal DEP domains.*

The DIX domain is named as such due to the conservation of sequence within Dishevelled and Axin. This domain is primarily used as a scaffold for the Wnt/ß-catenin pathway by associating with proteins needed for ß-catenin phosphorylation . Interaction among DIX domains was proven among Dvl1-DIX Dvl3 and rat Axin (*5*) , demonstrating that the DIX domain favors both homo- and hetero-oligomer formation. Deletion of the DIX domain however results in decreased distribution of mDvl2 in cytoplasmic vesicles, inferring a role in cytoplasmic vesicular association (*6*). The DIX domain does this by interacting with phosphatidylcholine (PC) through a conserved VKEEIS motif located near its axin-binding motif (*6*). In addition, ΔDIX-Dvl2 is unable to stabilize β-catenin (*6*). The stabilization of β-catenin is also lost when the vesicle associating sequence (VKEEIS) is mutated. These two results point towards a cytoplasmic vesicular pool of Dvl, which stabilizes β-catenin, thus branching it towards the canonical pathway (*6*).

The PDZ domain is named after three proteins in which it has been found: Post Synaptic Density- 95, discs-large, and Zonula occludens-1. It is best known for its interaction in binding to the Fz receptor and triggering signal transduction (*3*) and binding of other partners on the C-terminal region of trans-membrane proteins (*7*). It exhibits mostly of a pleated beta-sheet structure where a cleft is formed, acting as the site of binding (*3*). This domain has been shown to serve in a regulatory fashion (by controlling stability, localization, or structure) in opposition to a transduction module (*3*). Remarkably, when the PDZ domain is mutated, it has drastic effects on the β-catenin signaling, but not on the PCP pathway (*3*). For instance, the absence of a proper PDZ domain will inhibit the morphogenic movements of the gastrulation within *Xenopus laevis* embryos. It will also disrupt the canonical Wnt signaling pathway by preventing activation in certain marginal tissues (*5*).

The DEP Domain

Domain Architecture

The DEP domain, is named after the three proteins it was discovered in: Dishevelled, Egl-10, and pleckstrin (*8*). Its structure is mainly of a globular domain, roughly resembling a pyramid, with a three-helix bundle at its core (*8*) and is highly conserved through the mammalian phylogeny (Fig 1.3). There are two characteristics in this domain to note as well: the presence of an electrostatic dipole and a string of basic residues directly adjacent to this dipole. Whereas

this dipole is well suited for protein-protein interactions (*8*), the string of basic residues is hypothesized to interact with acidic phospholipids for membrane association (Fig1.4) (*8*). However, the evidence is variable in the requirements of the DEP domain for Dvl signaling (*4*). Whereas it is known that the DEP domain has a role in cytoplasm-membrane association (*9*), the mechanism(s) have not yet been determined. The DEP domain also plays a role in upstream communications between Fz and Dvl, but not on downstream signals (*10*).

```
hDvl2-DEP       GCEGRGLSVHTDMASVTKAMAAPESGLEVRDRMWLKITIPNAFLGSDVVDWLYHHVEGFP
mDvl2-DEP       -CEGRGLSVHMDMASVTKAMAAPESGLEVRDRMWLKITIPNAFLGSDVVDWLYHHVEGFP
mDvl1-DEP       QLEEAPLTVKSDMSAIVRVMQLPDSGLEIRDRMWLKITIANAVIGADVVDWLYTHVEGFK
                  *   *:*: **::::.:.*  *:****:**********.**.:*:******* *****

hDvl2-DEP       ERREARKYASGLLKAGLIRHTVNKITFSEQCYYVFGDLSG
mDvl2-DEP       ERREARKYASGLLKAGLIRHTVNKITFSEQCYYVFGDLSG
mDvl1-DEP       ERREARKYASSMLKHGFLRHTVNKITFSEQCYYVFGDLCS
                **********.:** *::********************..
```

Figure 1.3: Alignment of Dvl-DEP in noted Dishevelled proteins. Alignments were generated using CLUSTALW using sequences NM_07888.3 (mDvl2), NM_010091.3 (mDvl1), and NM_004422.2 (hDvl2) from Dvl-DEP domains found (*10*). Residues in blue represent identical residues, while green represents similar residue types, and the asterisks denote the consensus sequence.

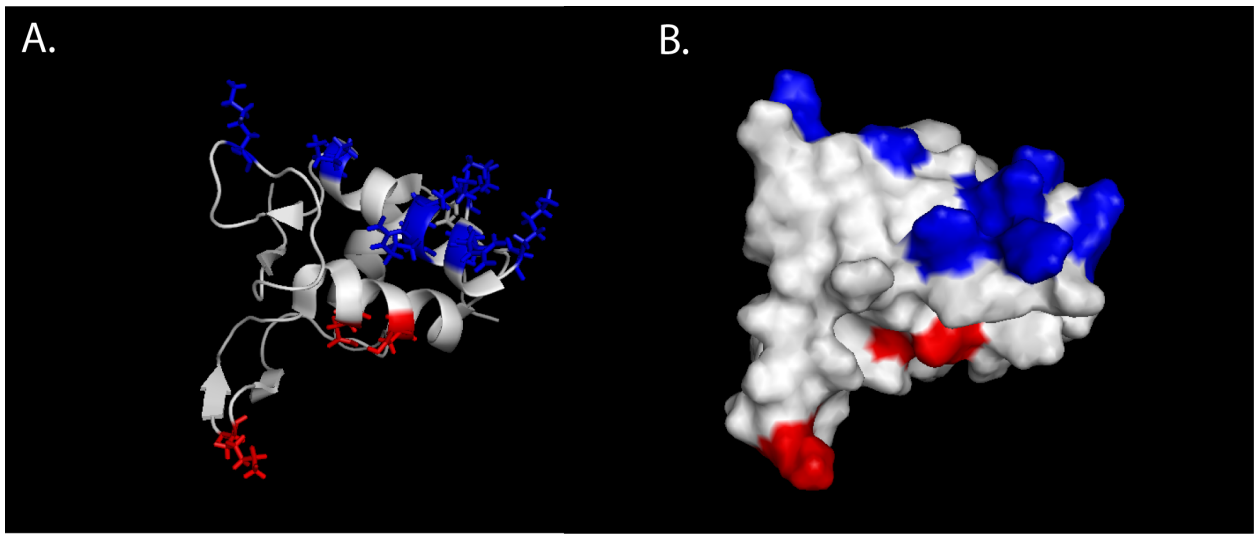

Figure 1.4: *Structure and highlighted features of mouse DEP Dishevelled 1. An electrostatic potential is created due to positively/negatively charged residues (in red) and the string of basic residues (in blue), which give a possible site for protein-protein interaction. In blue are basic residues associated with possible membrane interaction. Each is represented in (A) a ribbon and (B) surface model. Adapted from (10).*

Lipid Interaction

Dvl localizes to the plasma membrane in response to Fz activation; interestingly, multiple modes of interaction have been observed with the receptor. Current model proposes specificity of the pathway chosen is based on interaction with recruited lipids (*12*).

Recently, mouse Dvl1 was found to interact with charged lipids (Fig 1.5) in the plasma membrane (*13*). Specifically, the mDvl1-DEP domain interacts with negatively charged lipids and this interaction is essential for PCP signaling, but not Wnt/ß-catenin signaling (*14*). Binding has been proposed to occur in a pH-dependant manner, where a change from pH 7.4 to 7.1 decreased membrane localization of Dvl in cultured cells, despite the presence of Fz (*12*). Accordingly, mutations of basic residues within mDvl1-DEP domain to glutamate successfully abolished the interaction of DEP and negatively charged vesicles (*12, 13*). However, when treated with sphingosine, a cationic lipid that coats the plasma membrane, the localization of the mutated mDvl1 is rescued (*14*). These results denote the Dvl-DEP domain interacts with negatively charged phospholipids and this interaction is critical for Fz-dependent localization of Dvl (Fig 1.6).

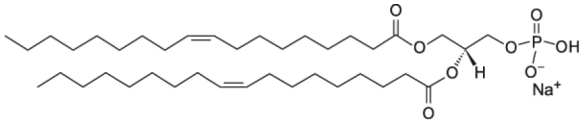

1,2-dioleoyl-sn-glycero-3-phosphate (DOPA)

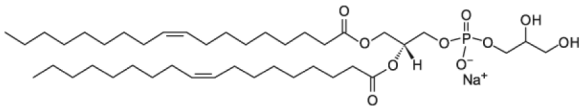

1,2-dioleoyl-sn-glycero-3-phospho-(1'-rac-glycerol) (DOPG)

Figure 1.5: *Chemical structures of the ionic lipds known to interact with the DEP domain*

However, it is still unknown as to how Dvl2-DEP physically interacts with ionic phospholipids in the plasma membrane. While this interaction also seems to occur in a pH dependent manner, we do not know the manner in which pH may change Dvl-DEP that alters the ability of ionic lipids to interact. Thus, we aim to characterize the specific residues required for interaction with ionic lipids. We also will determine the effects of pH on the capability of Dvl2-DEP binding to the plasma membrane.

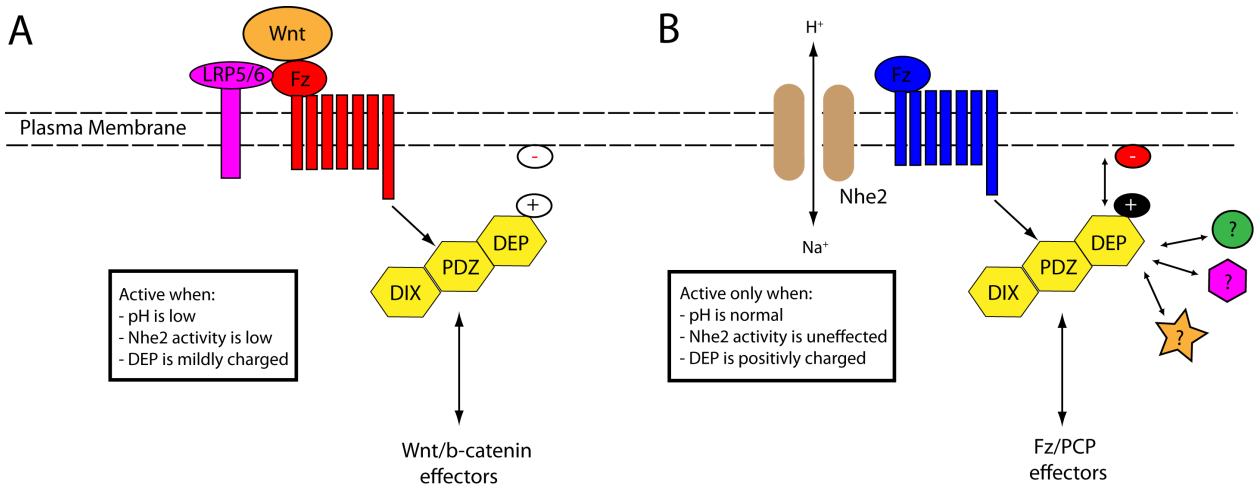

Figure 1.6: *Proposed dependence of pH to Wnt signaling pathway branching. A) In vivo the presence of Dvl near the Fz receptor can be a transient reaction, sufficient to activate the canonical signaling pathway, even at low intercellular pH values (14). B) However, a stable reaction between the DEP domain and the membrane surface is required for successful signaling of the non-canonical PCP pathway. At increased intercellular pH values, the relative charge on both the basic residues of the DEP domain and plasma membrane will hold a stronger charge, allowing for a more stable interaction.*

Relevance of Wnt Pathways in Disease

As the Wnt signaling pathway operates as a key mediator in cell to cell signaling events during embryogenesis and development, it is clear that problems will arise when the pathway breaks down or is altered. Faults in wnt signaling have been implicated in numerous sporadic types of cancer: including colon, lung, kidney, breast, and bone (*16-20*).

One of the most well-known colon cancer syndromes involves familial adenomatous polyposis (FAP). This syndrome is characterized through the numerous polyps grown from the colorectal epithelial cells (*21*). This cancer is particularly dangerous as it is highly invasive and has a high probability of metastasis (*21*). This, along with many other colorectal cancers, is found to be caused by the inactivation of both APC alleles, resulting in overall loss of APC functionality (*22*). The APC protein, classically thought of as a tumor suppressor protein, binds to β-catenin, de-stabilizing the protein and leading it towards the proteasome pathway (*23*). However, with APC unable to bind to β-catenin, high levels of 'stabilized' β-catenin accumulate within the cell. This pool of stabilized β-catenin is thought to elicit a transcriptional response that is thought to be important in the early stages of tumorigenesis. While FAP may be a particular form of colon cancer, colorectal cancer is still widespread, with 85% of these cancers having mutations in the APC (*24*).

Sustained loss of Wnt signaling functionality has been linked to Alzheimer's disease (AD) through changes in the cellular metabolism (*25*). Among proteins signaling within the wnt cascade, JNK and GSK3 are known to phosphorylate tau proteins responsible for stabilizing the microtubule network within neuronal cells (*26*). However, over expression of Dvl proteins might lead to inhibition of GSK3 from phosphorylating its targets, leading to changes in binding to the microtubule network (*25*). This change is also thought to aid in the development of amyloid β-peptide (Aβ) filaments, which begins an 'amyloid cascade' which ultimately results in the deposition of amyloid plaques in the brain. Dvl proteins can also activate c-Jun N-terminal kinases (JNK), a stress activated kinase, which controls expression of notable regulatory and tumor suppressor proteins p53 and c-Jun. Thus it is thought that Dvl works as a modular protein, aiding in the neuronal homeostasis through its control of JNK (*25*).

Chapter 2: Specific Aims

The goal of this project is to determine the structural basis for Dvl2-DEP association to the plasma membrane thru its interaction with ionic lipids. Specifically, we will evaluate structural features associated to phosphatidic acid binding to the DEP domain. We will also measure how changes in intracellular pH affect the interaction of mDvl2-DEP with ionic lipids. Our results will provide bases for understanding mDvl2-DEP binding to the plasma membrane and the branching mechanisms in the wnt signaling. Thus, we propose to investigate the following:

Specific Aim 1: To indentify the residues within mDvl2 DEP for binding to phosphatidic acid

Using NMR spectroscopy, we will be able to determine interacting residues for phosphatidic acid. Structural similarity among recombinant proteins will be determined by circular dichroism (CD). Conformational changes in secondary and tertiary structure will be measured using CD by titrating recombinant proteins samples with dihexanoyl-phosphatidic acid. We will also evaluate the interaction using fluorescence spectroscopy. Recombinant proteins will be tested using a liposome-binding assay (LBA) to measure and analyze the levels of mDvl2-DEP binding to phosphatidic acid (PA)-containing liposomes. We will also test whether altered mixtures of ionic lipids (such as PA with PG) will alter domain binding.

Specific Aim 2: To determine the relevance of pH in binding of phosphatidic acid to mDvl2-DEP

We hypothesize that mDvl2-DEP association to the plasma membrane is affected in a pH-dependent manner based on charged structural characteristics and localization events. By using NMR, Dvl2-DEP will be titrated at various pH values to observe the pH sensitivity of PA binding residues. We will employ circular dichroism to measure secondary structure content and tertiary structure conformations alterations in DEP caused by pH alterations.

Liposome binding assay will then be used to determine the effect of pH on binding of PA-containing liposomes by various mutant recombinant proteins of mDvl2-DEP. We will

also evaluate differences in binding affinity among mutants of mDvl2-DEP through fluorescence spectroscopy.

In summary, this research opens up new options of looking at how cells may regulate their developmental pathways thru localized molecular interaction.

Chapter 3: Results

A. <u>Specific Aim 1:</u> To indentify the residues within mDvl2 DEP for binding to phosphatidic acid

i. Rationale

Dvl localizes to the plasma membrane in response to Fz activation by wnt binding through its DEP domain (*1*). Recent studies have pointed towards wnt pathway specificity being chosen based on recruitment of specific lipids, specifically ionic lipids such as phosphatidic acid (PA) and phosphatidylglycerol (PG) (*3*) (*4*). By replacing a cluster of five basic residues on the surface of mDvl1-DEP to glutamate, the localization to the plasma membrane was successfully abolished. This binding could be rescued though by the addition of sphingosine (a cationic lipid) to the plasma membrane (*3*). This proves that mDvl1-DEP binds to negatively charged phospholipids. The interaction between Dvl-DEP with negatively charged lipids is essential for PCP activation, but not for Wnt/ß-catenin signaling (*3*). Results show that changing two basic residues acidic within mDvl1-DEP, leads to normal ß-catenin signaling, but a drastic perturbation in the PCP pathway.

Thus, we aim to identify the specific residues of mDvl2-DEP that interact with phosphatidic acid for further exploration into their role in plasma membrane association.

ii. Experimental Design

To determine the amino acid residues that interact with ionic lipids, we used NMR spectroscopy. Labeled mDvl2-DEP was titrated in set ratios (ranging from 0 to 32-fold) with phosphatidic acid and chemical shifts perturbations were monitored. As result, site-directed mutagenesis was performed on His464, His465, Lys477, and Lys 494. Mutant constructs were tested using circular dichroism to ensure the integrity of the overall secondary structure. We used liposome binding assays to observe the effects of each of these residues on PA interaction. We further characterized these interactions by fluorescence spectroscopy and determine binding affinities.

iii. Results

a. Phosphatidic acid binds Dvl2-DEP domain

Titration of N^{15} labeled Dvl2-DEP with PA by NMR spectroscopy was used to determine the interacting residues for binding.

With the levels of PA at a molar ratio of 32:1 (PA:Dvl2-DEP), we observed chemical shifts in different residues (Figure 3.1). Five residues had been previously identified by NMR titration with PA: His420, His465, Phe469, Lys477, and Lys494 (Capelluto, personal communication). Out of these residues in Dvl, all are conserved in higher mammalian phylogeny except for H464 (with changes between Lys and Thr) and H420 (absent in mDvl1, but present in human Dvl proteins). This makes His464 a special characteristic for mDvl2-DEP compared to its homolog mDvl1.

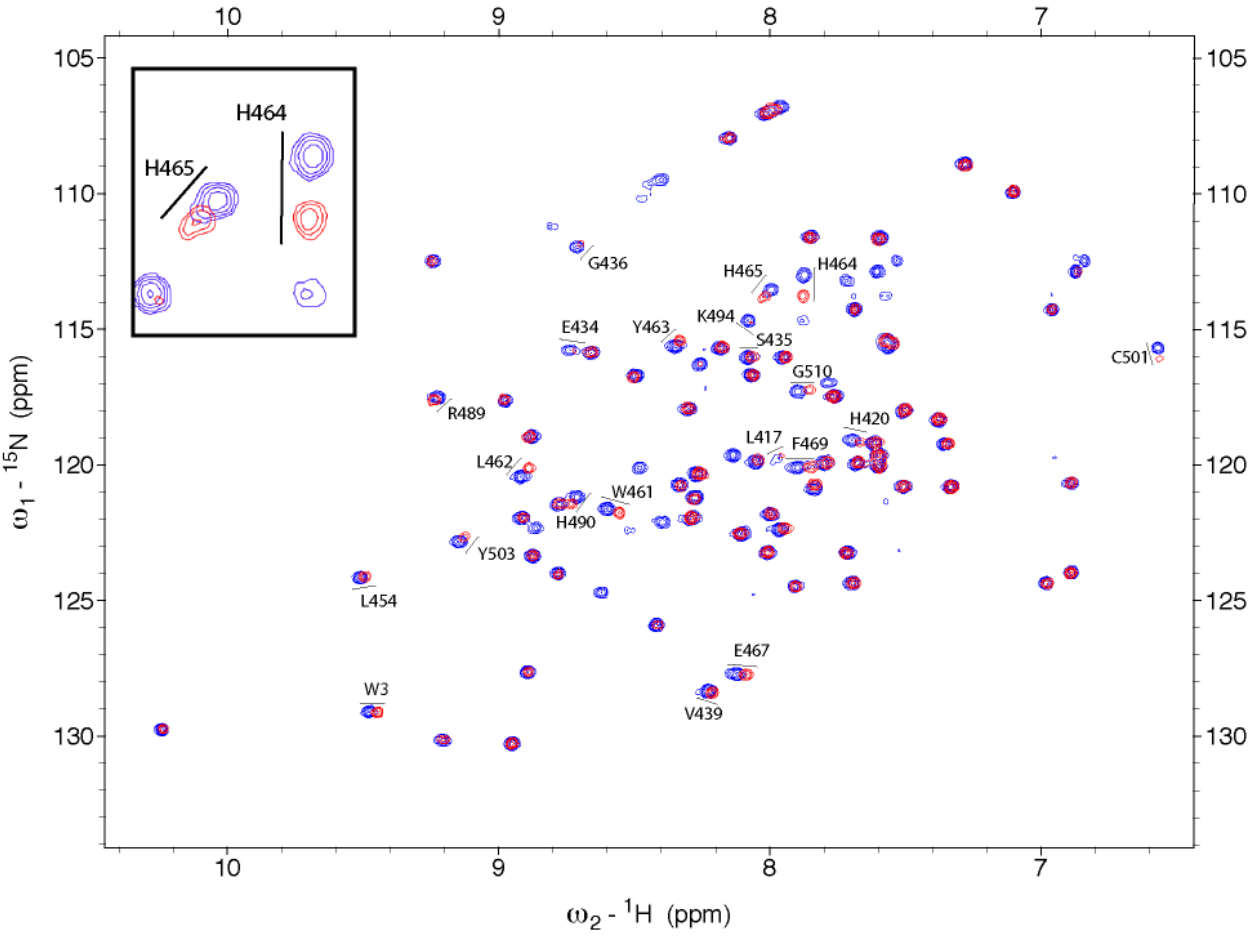

Figure 3.1: *Phosphatidic acid binds to the DEP domain of mouse Dishevelled-2. A 100 μM sample of N^{15}-labeled mDvl2-DEP was titrated with phosphatidic acid (PA) at a pH of 7.5 from 0:1 to 64:1 (PA : protein ratio). Shown are the 0:1 (blue) and the 32:1 titration (red) HSQC spectra points. Observed chemical shifts are marked and labeled.*

To determine the significance of the shifting for mDvl2-DEP by PA, we determined the deviation of the chemical shifts between 0:1 (PA : mDlv2-DEP) and 32:1 ratio samples (Figure 3.3A). We used the algorithm as described by Utrecht NMR Spectroscopy Research group of $\sigma = [(H^1 \text{ shift})^2 + (N^{15} \text{ shift} / 6.51)^2]^{1/2}$ to determine the resulting deviation in chemical shifts (*5*).

Any shift greater than one standard deviation from the data set was counted as significant. There was a large grouping of interactors centralized around residues 461 to 469, 501 to 504, and two histidine residues (H420 and H490). Out of these, residues 461 to 469 are over two deviations away.

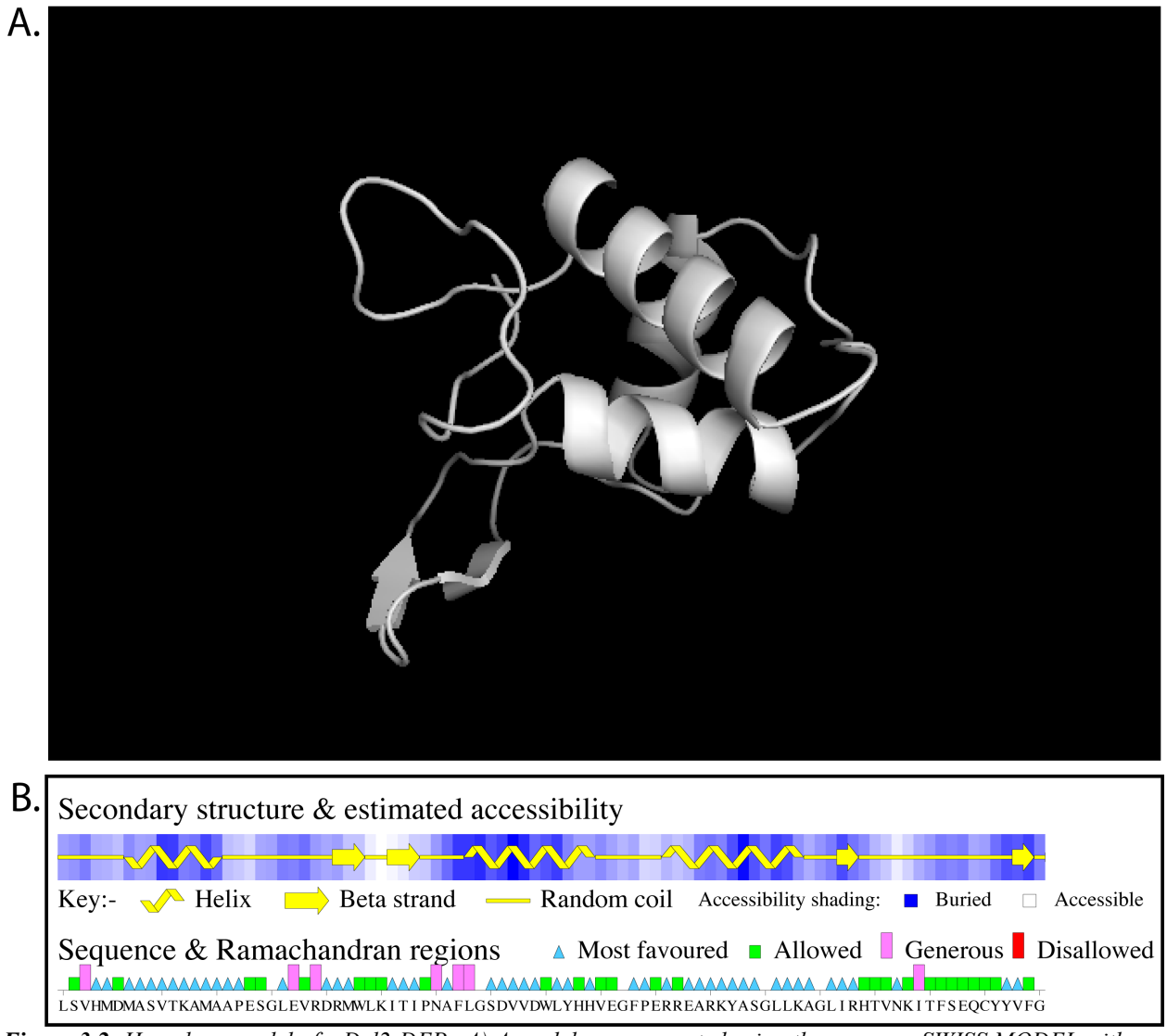

Figure 3.2: *Homology model of mDvl2-DEP. A) A model was generated using the program SWISS MODEL with the structure of mouse Dvl1-DEP as a template sequence (PDB code: 1FSH). B) The structure was confirmed using the analysis algorithm PROCHECK, generating the Ramachandran plot. The Ramachandran regions are presented in comparison with the sequence and secondary structures for the model generated. The model can be considered accurate, with over 90% of the residues falling into favorable or allowable regions.*

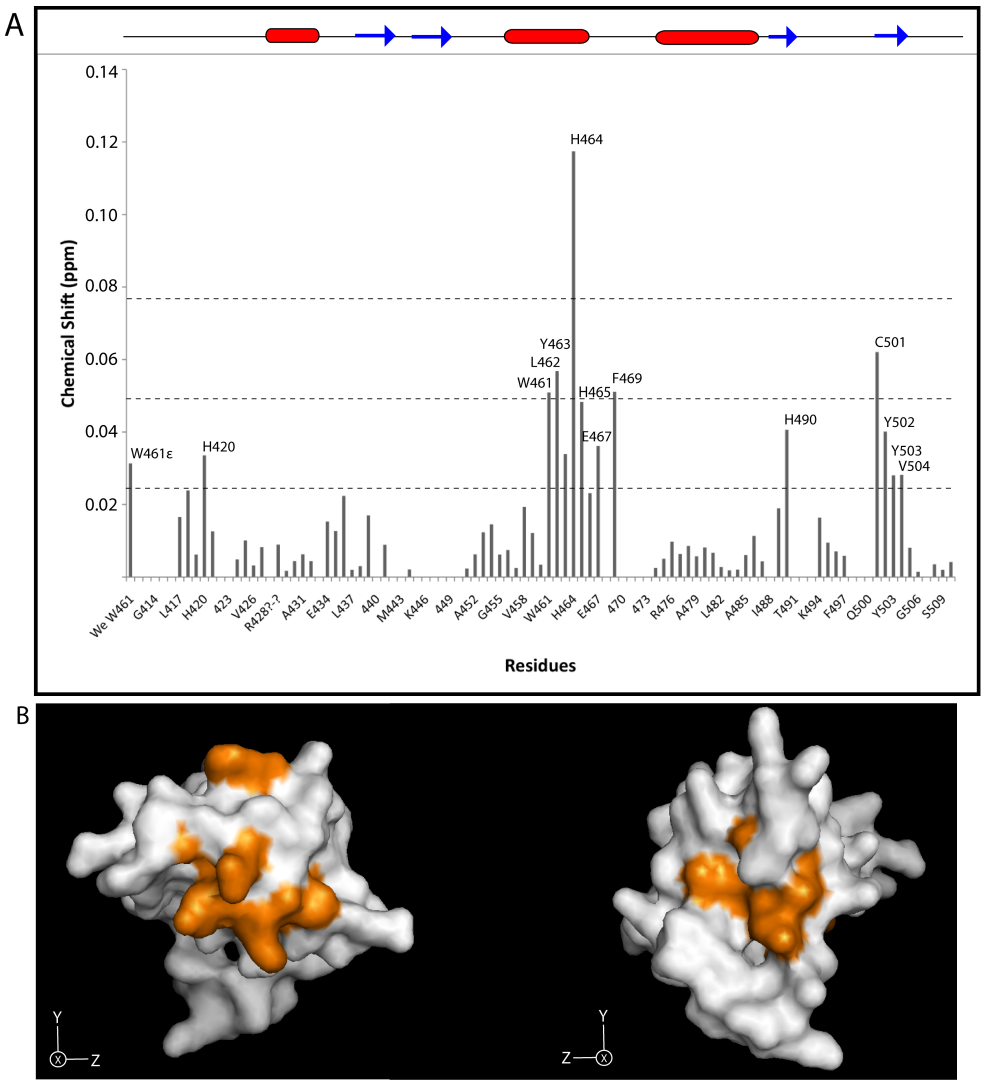

Figure 3.3: *Chemical shift analysis demonstrates two sites of interaction. A) Chemical shift analysis with standard deviations of the data set represented by dashed lines on the graph. Location of predicted secondary structure shown above denoted alpha helicies (red) and beta strands (blue). Two small groupings of interacting residues, which are over one standard deviation away from residues 461-469 and 501-504, along with two histidine residue are identified. B) Significant interacting residues (orange) are mapped on a surface model of mDvl2-DEP.*

To model the structure of mDvl2-DEP (Figure 3.2A), we used mouse Dvl1-DEP (PDB code: 1FSH) as a template. To perform the actual modeling, SWISS MODEL was used to both sequence alignment and homology model. The structure was further validated using PROCHECK (Figure 3.2B). The Ramachandran plot generated shows that over 90% of the residues are in favorable or allowable regions (data not shown).

When these residues are mapped on the surface of a structural model (orange) of mDvl2-DEP, two patches are seemingly shown (Figure 3.3B).

A Coulombic charge analysis of the surface area of mDvl2-DEP was performed using Chimera (Figure 3.4) (*6*). We observe both the large basic patch of residues across the top of the protein and the electrostatic dipole, similar to mDvl1-DEP. However, a large positively charged region is located on the right-hand x-axis whereas the left-hand x-axis is neutrally charged. This suggests that the patch of interacting residues on the left-hand x-axis is a false reading due partially to free ligand in solution (not constrained to a micelle or bi-layer) and the hydrophobic nature of the supposed interacting residues.

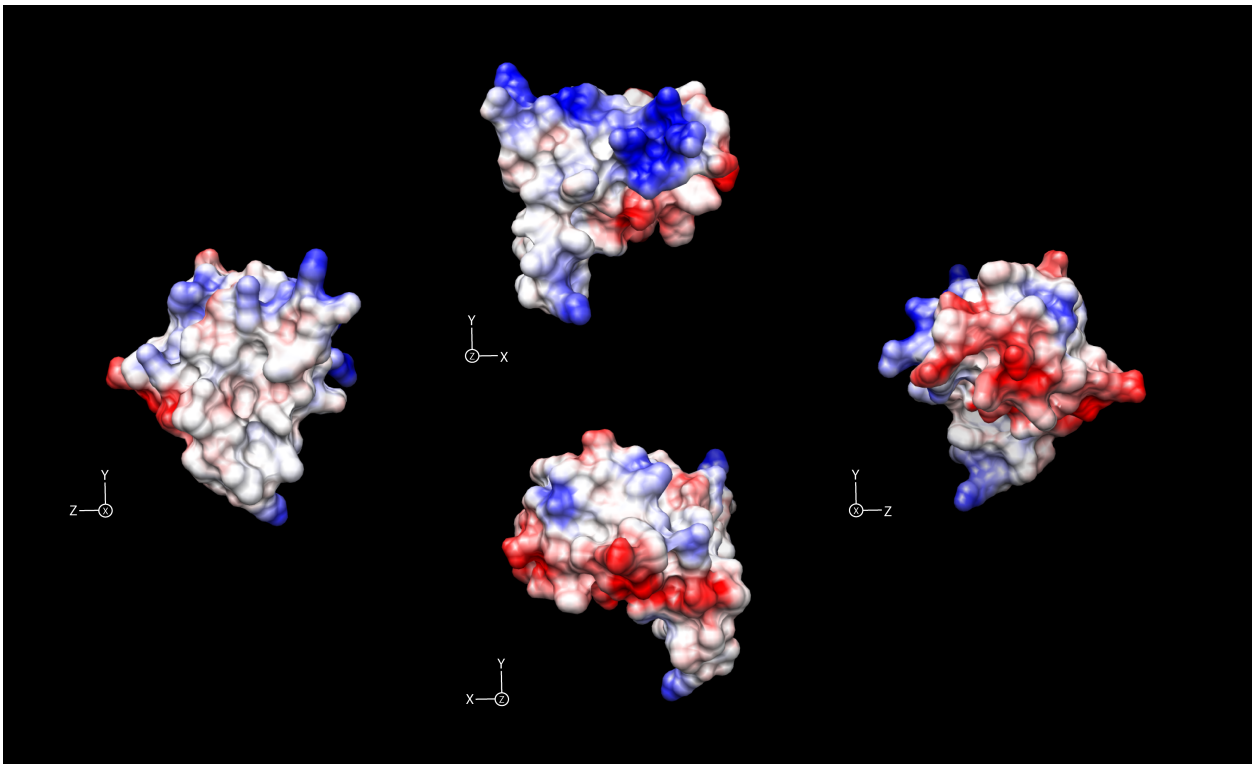

Figure 3.4: *Coulombic surface charge analysis of mDvl2-DEP. The presence of a large basic (negatively charged in blue) on the top surface and the electrostatic dipole presents us with similar features as the mDvl1-DEP. However, we also see a large positively charged area (red) located on the right-handed side of the protein, located around possible interacting residues found by NMR.*

b. Phosphatidic acid does not perturb mDvl2-DEP structure

Site directed mutagenesis was performed on His464 and His465 to Asn, (referred to as mDvl2-DEP 2N). To confirm first that these mutations did not affect the structure of mDvl2-DEP, circular dichroism spectroscopy was performed in both far-UV (190 nm-260 nm) and near-UV (250 nm-350 nm) ranges to observe secondary and tertiary structure elements, respectively (Figure 3.5A). The spectra gathered for both regions allow us to conclude that the secondary structures are not affected by the mutations. However, there is a change in the tertiary structure

conformation, with an increased exposure of phenylalanine and tryptophan residues. This is most likely to occur due to reorganization of the loop regions.

To determine the effects of phosphatidic acid on the structure of mDvl2-DEP, we titrated a 10 μM sample of mDvl2-DEP wild type (Figure 3.5B) and mDvl2-DEP 2N (Figure 3.5C) at pH 7.5 with PA in ratios ranging from 0 to 32-fold using circular dichroism. In both cases, far-UV spectra and near-UV spectra showed no changes in secondary and tertiary structure conformation.

c. Mutations to mDvl2-DEP alters binding capability to phosphatidic acid

To determine the effects of each mutation in mDvl2-DEP, we used a liposome binding assay to visualize the strength of interaction to PA-containing liposomes and recombinant mutant forms of mDvl2-DEP.

We observe a relatively strong interaction of mDvl2-DEP wild type to the PA-containing liposomes (1:1 PA:PC) with 68% bound to the liposome pellet. However, we observe a slight decreased binding with mDvl2-DEP 2N, of 3-5%. We do detect a dramatic difference in comparison with both mDvl2-DEP K477A and K494A, both dropping to below 10% total binding (Figure 3.6).

We are still able to notice a difference between mDvl2-DEP wild type and the 2N mutant, denoting that the two histidine residues do play a role in binding of phosphatidic acid. This can be attributed to the fact that the mutation to Asn is 'softer', meaning that the bulkiness of the residue is relatively conserved and the relative charge is gone (but still polar). This allows us to make a more accurate determination as the 'softer' mutation should keep the overall tertiary structure intact. However, we do see a much larger decrease in binding with the lysine to alanine mutations. This can possibly be explained though as the change of a lysine (long and charged) to an alanine (short and neutral) is dramatic and would most likely result in secondary issues that could alter binding.

d. Binding affinity of mDvl2-DEP is in the micromolar range for phosphatidic acid

To determine a relative affinity of mDvl2-DEP to phosphatidic acid, we used fluorescence spectroscopy to chart the exposure of tryptophan in response to a titration of dihexanoyl-phosphatidic acid (Figure 3.7). We titrated 1 μM of recombinant mDvl2-DEP with up to 32-fold excess of dihexanoyl-phosphatidic acid and plot the maximum response for each

titration point. An IC_{50}, defined as half of the maximum inhibitory concentration, value of 5.3 μM could be extrapolated from the logarithmic regression ($r^2 = 0.9816$).

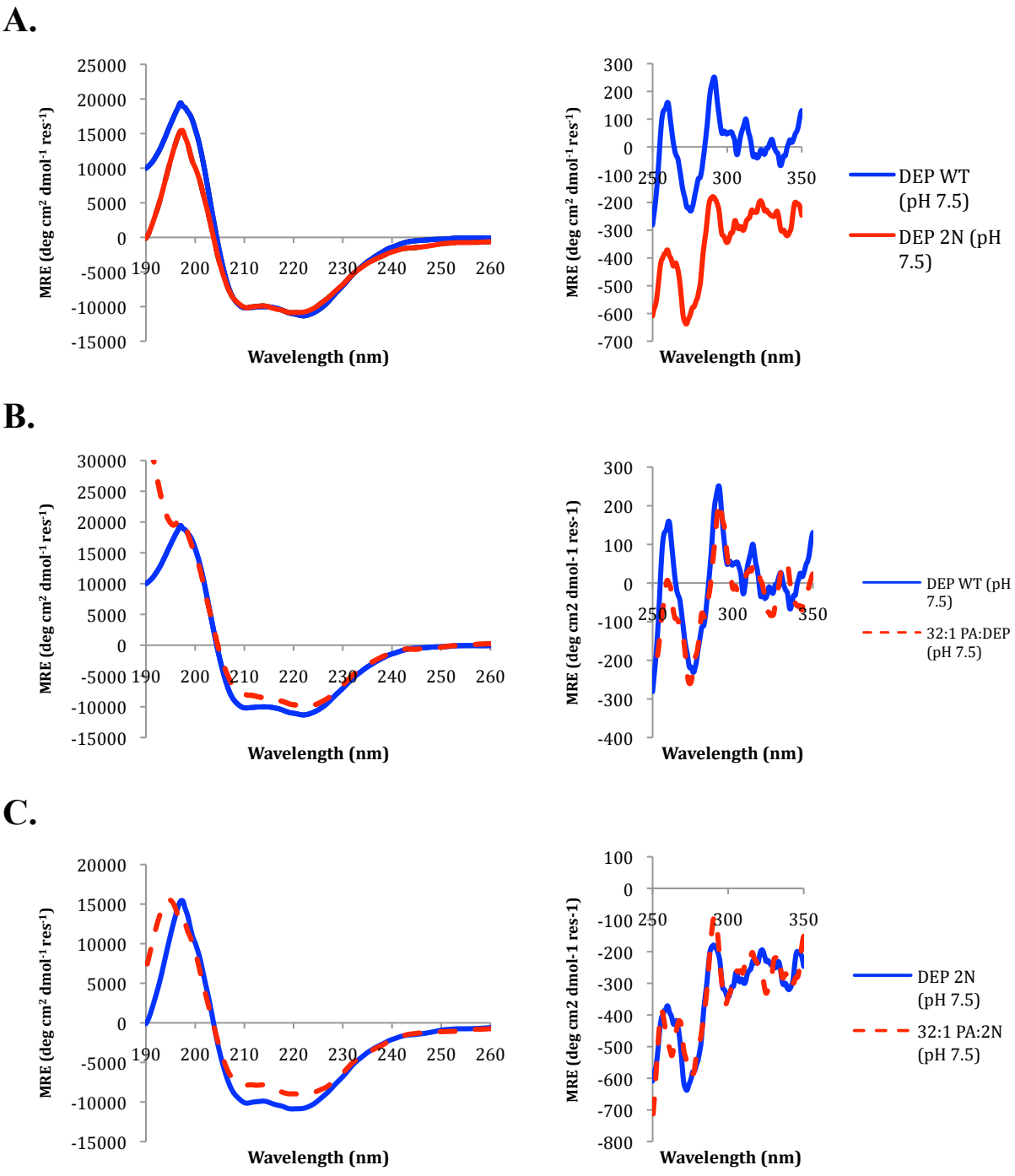

Figure 3.5: *Phosphatidic acid does not perturb structural elements of mDvl2-DEP at pH 7.5. A) Far-UV (190 nm-260 nm) and near-UV (250 nm-350 nm) CD spectroscopy scans of 10 μM mDvl2-DEP wild type (blue) and mDvl2-DEP 2N (red) demonstrates that their overall secondary and tertiary structures remain similar after mutation of His 464 and His 465 to Asn. B) Far-UV and near-UV spectra of samples of mDvl2-DEP and C) mDvl2-DEP 2N (10 μM, blue) were titrated with PA in ratios ranging from 0 to 32-fold (red).*

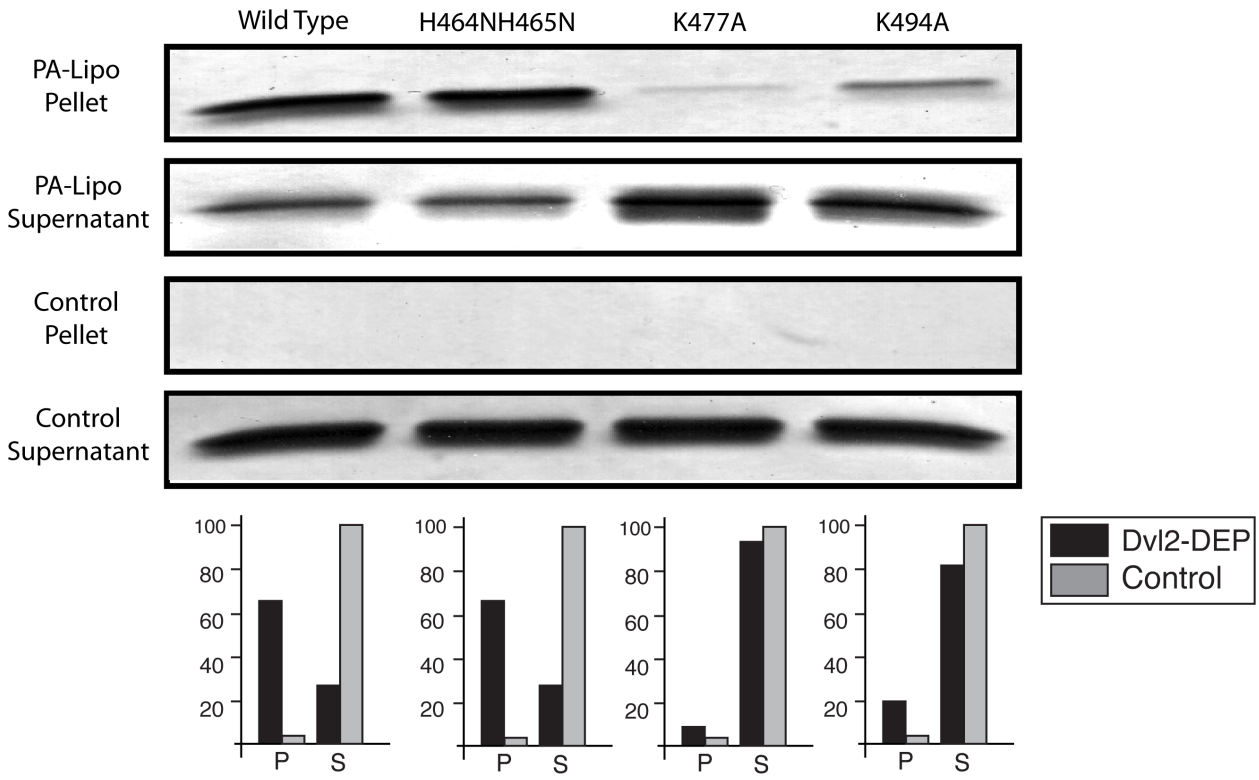

Figure 3.6: *Mutations to mDvl2-DEP alters binding capability to phosphatidic acid. Lanes labeled with 'P' and 'S' represent the amount of protein in the pellets and supernatant fractions after centrifugation. The y-axis represents the percentage of the protein sample. Samples were quantified using the program FluorChem (Alpha Innotech) through spot densometry compared to a 10 ug protein input.*

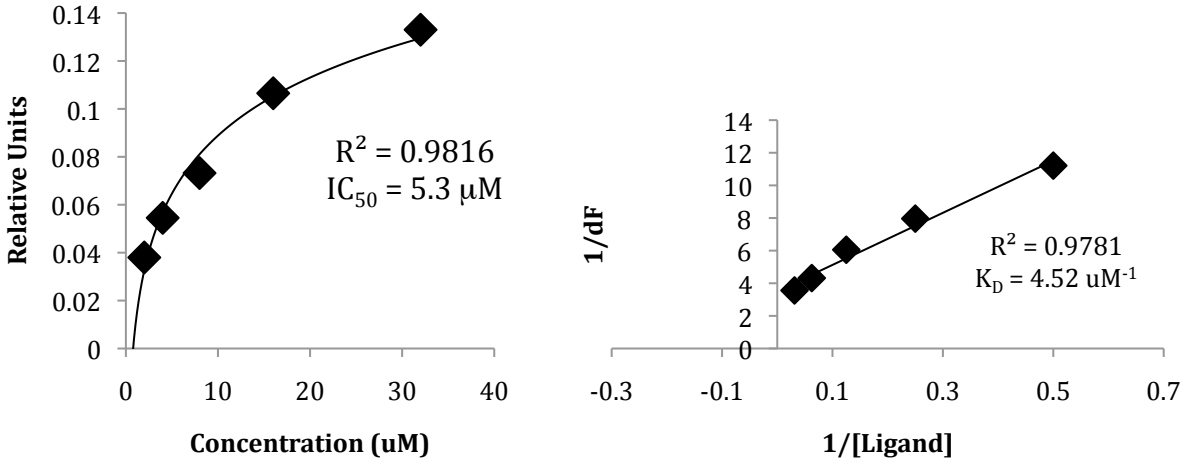

Figure 3.7: *mDvl2-DEP interacts with phosphatidic acid in the micromolar range. Using fluorescence spectroscopy, we titrated a 1 μM sample of mDvl2-DEP recombinant protein with dihexanoyl-phosphatidic acid (0 to 32-fold). IC50 and Kd values were extrapolated using logarithmic regression and Lineweaver-Burke kinetics respectively.*

B. Specific Aim 2: To determine the relevance of pH in phosphatidic acid binding to mDvl2-DEP

i. Rationale

Using S2 cells, a *Drosophila* intestinal cell line, a decrease in intracellular pH from 7.4 to 7.1 led to a decrease in Dvl recruitment to the membrane, despite the presence of the Frizzled receptor (*7*). It was hypothesized this effect was based on the possibility of decreased activity of Nhe2, a sodium/hydrogen pump, though it is not investigated. This pH sensitivity is similar to the FYVE domain and its interactions with PtdIns(3)P. The FYVE domain binds in a pH-dependent manner where lower pH values increase the binding affinity and localization to endosomes (*8*). This change in binding is caused by conformation and charge alterations in binding residues as a cause of pH; specifically it was found the change in protonation state of certain histidine residues located in close proximity to one another yielded the binding location. If mDvl2-DEP is affected in a pH-dependent manner through specific residues, then we would expect to see a change in binding to phosphatidic acid when these residues are mutated.

ii. Experimental Design

Initial experiments were performed using liposome binding assays, where we change the pH of the reaction solution to determine the effects on Dvl2-DEP binding. We will also test mutant constructs, such as H464H465N, to determine if these residues affect binding due to pH effects. To determine why a change in binding occurred, we titrated a labeled sample of Dvl2-DEP at various pH values of 5.5, 6.5, and 7.5 using by NMR. This allowed us to determine which residues are pH sensitive and, in relation, which interacting residues demonstrate chemical shift perturbations. We further quantified the change of binding affinity based on fluorescence spectroscopy to determine if the binding affinity falls out of physiological ranges.

iii. Results

a. Changes in pH Results in Chemical Shift Perturbations of Interacting Residues

To determine the effects of pH on mDvl2-DEP, we used NMR spectroscopy to evaluate an N^{15} labeled sample, titrated to different pH values. The titration was performed at pH value of 5.5, 6.5, and 7.5 respectively. These values were chosen to assess pH values close to physiological conditions as well as extremes to show a difference. Based our previous findings

in identifying interacting residues, we looked to see how these residues would behave in the decreased pH environment (Figure 3.8). Represented are the values for pH 5.5 (red) and pH 7.5 (blue). When comparing the residues, we did find that most, if not all, of the interacting residues do change position due to a change in pH. Some of the key residues, including the histidine residues, have been marked for ease. It is also important to note that these histidine molecules undergo some of the larger conformational changes within the spectra, denoting their seemly sensitivity to the environment in which they are surrounded.

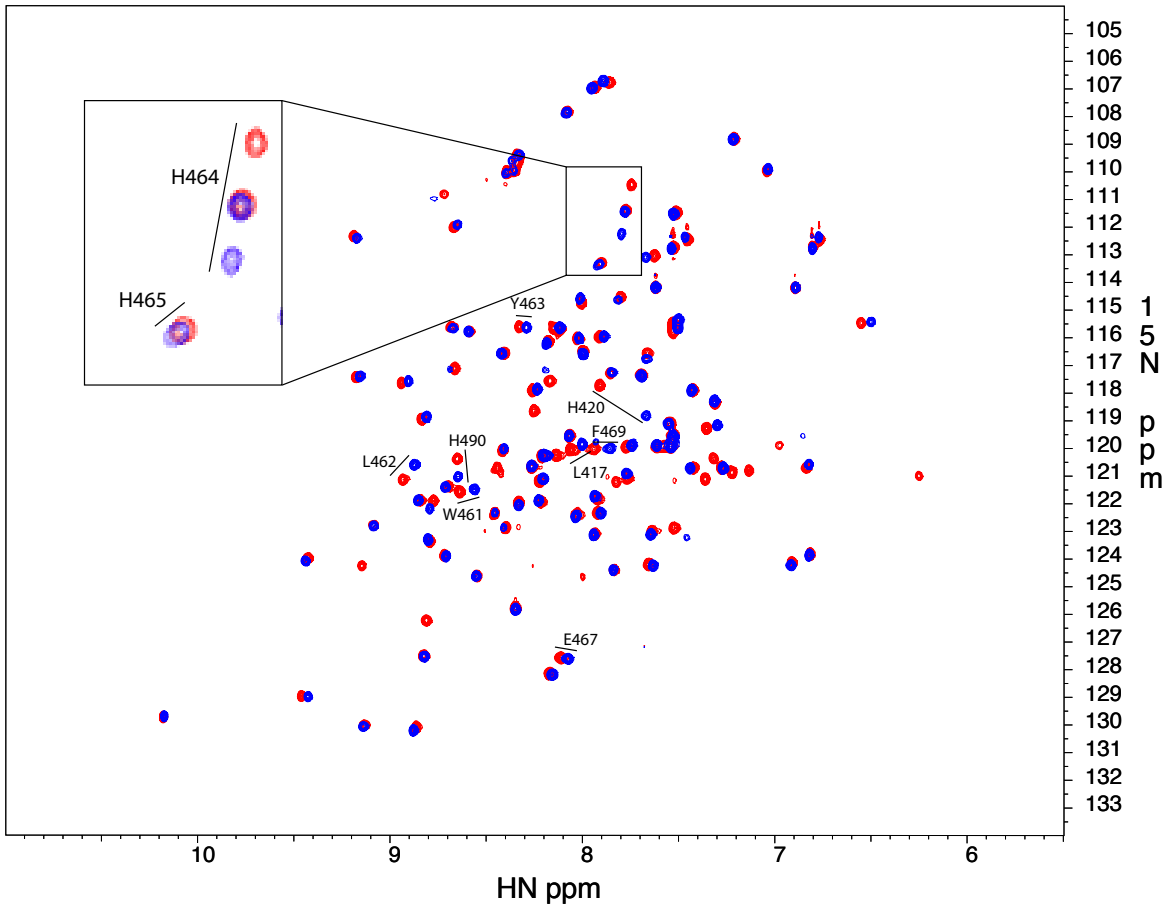

Figure 3.8*: Changes in pH causes chemical shift perturbations of conformation of PA-binding residues. A 300 μM sample of N^{15} labeled mDvl2-DEP at pH 5.5 (red) and pH 7.5 (blue). Marked are some of the more dramatic chemical shifts that occur within the found PA-interacting residues.*

b. Changes in pH alters tertiary structure of mDvl2-DEP

As we detect a large number of chemical shift perturbations due to a change in pH, we ran 10 μM sample of mDvl2-DEP wild type and mDvl2-DEP 2N at pH 7.5 and 6.25 to determine the changes in secondary and tertiary structure that occur (Figure 3.9). Far-UV spectra showed no change in overall secondary structure content in either mDvl2-DEP or mDvl2-DEP 2N.

However, in the near-UV spectra, we observe a slight change in tertiary structure with the wild type protein in the region showing changes to phenylalanine. But this change in binding is not observed in mDvl2-DEP 2N. This difference between mDvl2-DEP wild type and 2N lets us conclude that the two histidine residues (His 464 and His 465) do play a role in altering mDvl2-DEP structure in response to pH.

To determine if the structure of mDvl2-DEP is more susceptible to conformational change by PA at lower pH values, we titrated a 10 μM sample of mDvl2-DEP wild type (Figure 3.10A) and mDvl2-DEP 2N (Figure 3.10B) at pH 6.25 with phosphatidic acid (ranging from zero to 32-fold) to determine if structural perturbations occur. Again, phosphatidic acid does not affect the overall secondary structure content or the tertiary structure conformation at pH 6.25. This suggests that the only conformational change occurring is in response to pH and not the interaction with the ligand.

A.

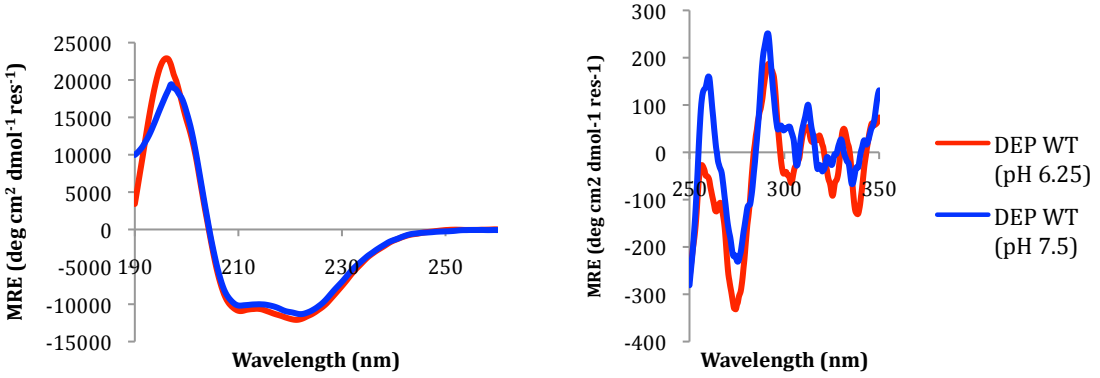

B.

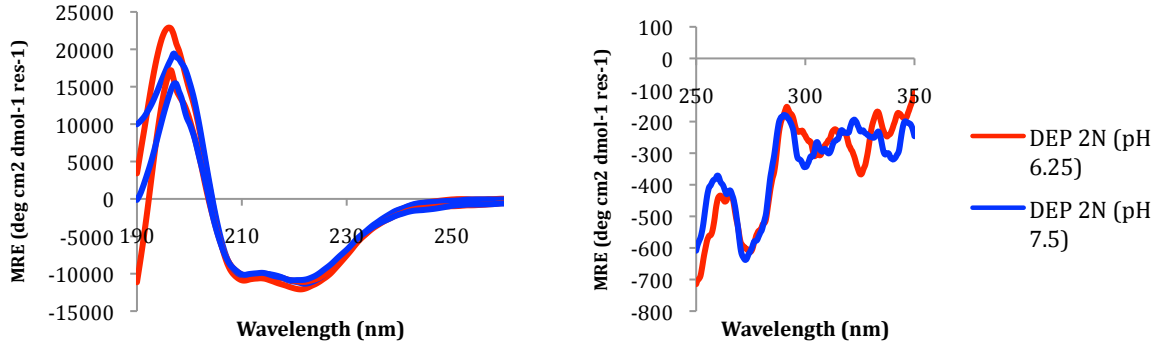

Figure 3.9: *Changes in pH alters tertiary structure of mDvl2-DEP. 10 μM Far-UV (190 nm-260 nm) and 50 μM near-UV (250 nm-350 nm) spectra CD spectroscopy scans of mDvl2-DEP wild type and mDvl2-DEP 2N at pH 7.5 (blue) and 6.25 (red).*

A.

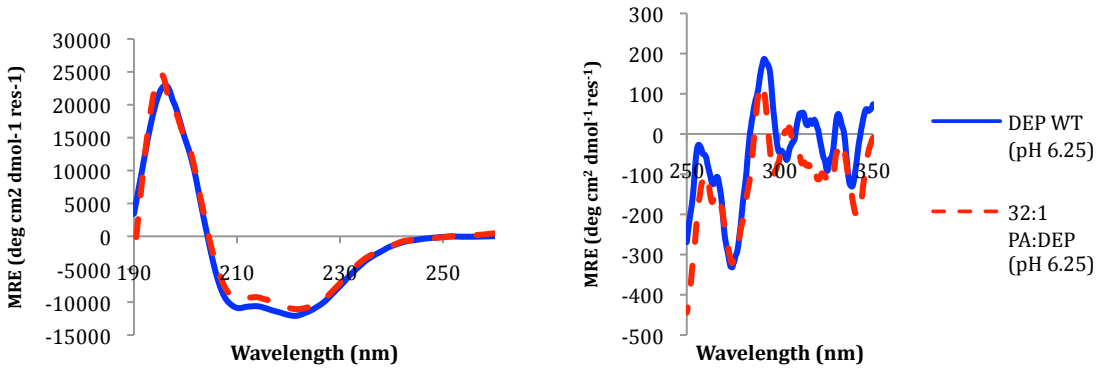

B.

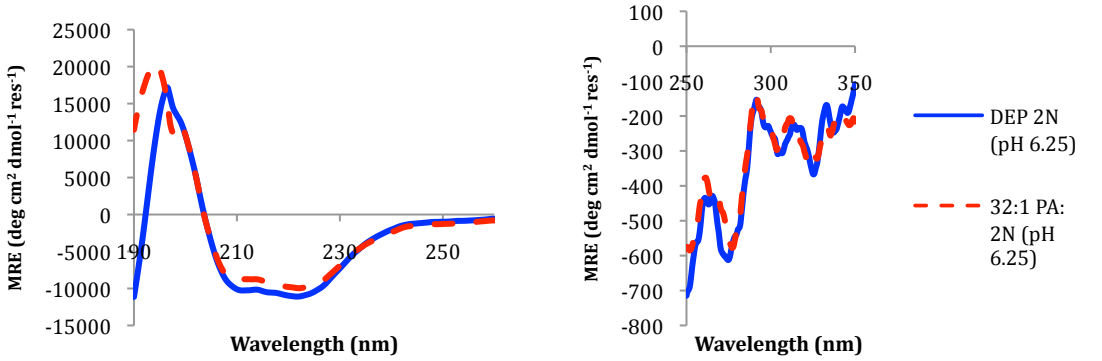

Figure 3.10: *Phosphatidic acid does not alter mDvl2-DEP structure at lower pH values. 10 μM samples of mDvl2-DEP wild type (A) and mDvl2-DEP 2N (B) were titrated with PA in ratios ranging from 0 (blue) to 32-fold (red). Far-UV and near-UV spectra were obtained from each.*

c. mDvl2-DEP binding to phosphatidic acid is decreased at low pHs

To observe how the change in tertiary structure conformation in response to pH affects binding of phosphatidic acid, we employed liposome binding assays. Using PA-containing liposomes, we performed a titration of different pH values ranging from 6.25 to 7.5 to observe changes in bound recombinant protein to PA-containing liposomes.

We still observe a relatively strong binding at the higher pH (pH 7.5), with about 68% of mDvl2-DEP wild type associating with the liposomes. As the pH decreases, we see a progressive drop to about 32% bound at a pH of 6.8. Any pH values lower than this kept a similar binding of around 35%. When we look at the binding of mDvl2-DEP 2N, we see its highest binding rate is about 65%, with all other points hovering around 60%.

This lets us conclude that pH plays a role in mDvl2-DEP binding to phosphatidic acid. It is also of note that the difference between the maximum and minimum binding is changed in a

relatively short pH range (7.5 maximum to 6.8 at minimum). We can also see the effect of both His464 and His 465, as their mutation reduces the binding to the minimal level. While this may seem to contradict the NMR results before, the alterations are most likely local conformational changes that are not sensitive to biophysical techniques such as circular dichroism.

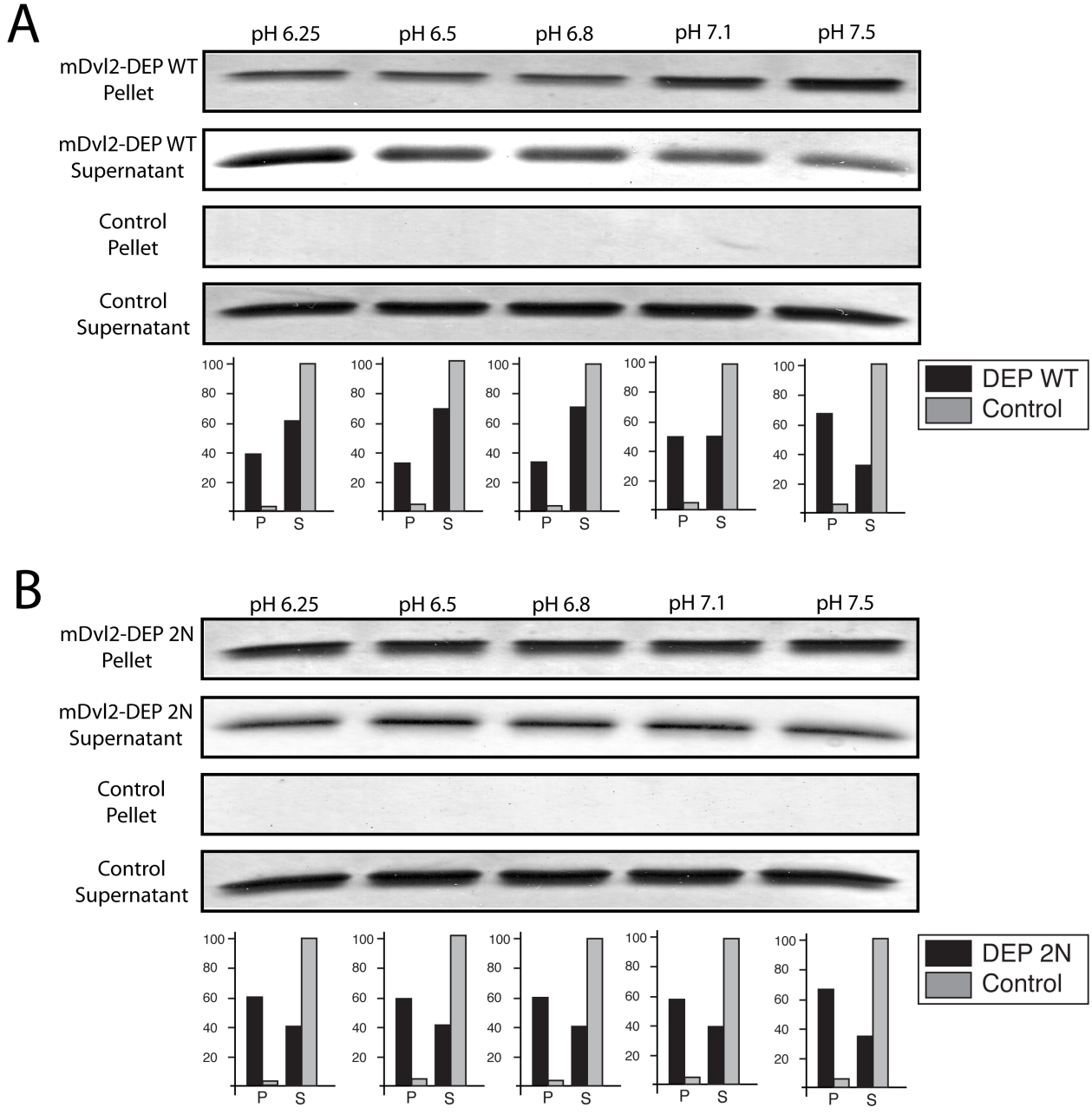

Figure 3.11: *mDvl2-DEP binding to phosphatidic acid is decreased at lower pH. We observe a strong binding at pH 7.5 of roughly 68% with the mDvl2-DEP wild type recombinant protein. This binding is decreased to a minimal level of roughly 35% bound at pH values of 6.8 and below. The binding of mDvl2-DEP 2N however hovers around 20% no matter what pH the liposomes are contained. This lets us conclude that the binding of mDvl2-DEP is pH-dependent and that it reaches its lowest levels of binding around a pH of 6.8.*

Chapter 4: Discussion and Conclusions

While many others had hypothesized that Dvl recruites specific lipids to differentiate pathway specificity (*1*), Simons et al. showed that mDvl1-DEP specifically interacted with ionic lipids such as phosphatidic acid (PA) and phosphatidylglycerol and that this interaction was necessary for PCP pathway signaling. The β-catenin pathway can still activate without mDvl1-DEP localization to the membrane. The interaction between PA and mDvl1-DEP is proposed to occur in a pH dependent manner. By changing the intracellular pH from 7.45 to 7.1, the authors detect changes in mDvl2-DEP localization within S2 (*Drosophila* intestinal) cells. They continue by mutating five basic (Lys and Arg) residues to glutamate along the proposed membrane binding surface; these mutations abolished the localization of mDvl1-DEP, as well as full-length mDvl1, from localizing to the plasma membrane. However, this localization could be rescued when the S2 cells were treated with sphingosine, a cationic lipid, which coated the plasma membrane. Thus, mDvl1-DEP interacts with negatively charged phospholipids (such as PA) and this interaction is critical for Fz- dependent localization of mDvl1.

Interaction of mDvl2-DEP and phosphatidic acid

Using NMR spectroscopy, we were able to detect an interaction between mDvl2-DEP and phosphatidic acid, supporting DEP mDvl2 act similarly to mDvl1. We were able to identify two distinct areas where PA interacted with mDvl2-DEP: 461 to 469 and 501 to 504. We also see significant chemical shift perturbations in His420 and His 490. However, each of these areas of interaction contain histidine residues. The residue that showed the greatest chemical shift perturbations was His494, moving over three deviations, marking it a significant interactor. Histidine has been implicated in numerous proteins as a binding residue, especially in membrane binding proteins. For instance, the alteration of three histidine residues in Aβ-peptide, a protein thought to be neurodegenerative and leading to Alzheimer's disease, changed the toxicity by altering its membrane binding capacity (*2*). Another example is the membrane binding of P-type cardiotoxin, found in snake venom, which contains key histidine residues at its membrane binding motif and impair the functionality of cell membranes (*3*). The histidine residues in PAP_{20}, an enzyme that catalyzes the dephosphorylation of phosphatidic acid, shows that upon binding to PC in the membrane, the enzyme is significantly inhibited in its functionality (*4*). Even in plants, the regulation of violaxanthin de-epoxidase (VDE), an enzyme that keeps the

thykaloid membranes from overexcitation by light, becomes fused with the thykaloid membrane through its histidine residues, which also serve as its regulator (*5*).

Using our model, the plotted interacting surface could be mapped to determine there are two patches formed where phosphatidic acid interacts. It is also important to note that His residues (His464His465 and H490) seem to form the center of each of these patches. When you observe the charge characteristics of each of these regions, there is a strong positive charge surrounding His464His465, even up to His420. This is similar to both the FYVE domain (*7*) and Protein-Tyrosine Phosphatase SHP-1 (*8*) interact with their phospholipid ligands. The other patch, containing His490, does not seem to have any charge on its surface. However, the interaction that we see could be occurring due more to hydrophobicity rather than charge (*9*). It is also possible that the region between residues 501 to 504 is a false interactor due to the free ligand in the NMR solution due to saturation (*10*).

Recombinant proteins were used to test possible effects of the varying interacting residues identified by chemical shift perturbations, determining residues using the resonance assignments generated by Dr. Capelluto. Using PA-containing liposomes, we tested the initial level of binding between three mutations: H464NH465N, K477A, and K494A. Binding to these liposomes with mDvl2-DEP K477A and K494A demonstrated a dramatically diminished binding; however, this could simply be because of nature of the mutation. The change from a large, charged residue to a small, neutral residue would vastly affect its ability of interacting with a charged phospholipid. The absence of which could also affect the surrounding charge surface of protein (*11, 12*) and weakening the electrostatic attraction (*13*), ultimately resulting in decreased binding.

Residues His464 and His465 were obvious candidates for mutation due to their large chemical shift perturbations and the possibility of forming a 'histidine switch' (to be discussed further later on). Instead of an alanine mutation, we opted for a softer mutation to asparagine, as this will retain the bulkiness of the histidine residue as, though uncharged, is polar (*14*). This construct (to be referred to as mDvl2-DEP 2N) showed a slightly decreased amount of binding compared to the wild type. Based on circular dichroism spectroscopy, we do not observe a change of secondary or tertiary structure caused by the addition of PA to either the wild type or 2N mutant, so the interaction with PA is not causing the change. However, while secondary structure is conserved in both proteins, we do see a change in tertiary structure with the 2N,

showing an increased exposure of Trp, Tyr, and Phe residues. This is most likely caused by a reordering of the loop regions, allowing for a slightly greater exposure of the fluorophore residues (*15, 16*).

Finally, we were able to extrapolate an IC_{50} value of 5.3 μM and a K_D of 4.52 μM^{-1} for phosphatidic acid interaction with mDvl2-DEP using fluorescence spectroscopy. This is low binding affinity site compared to other PA binding proteins, such as Protein Phosphatase-1 (PP1c) at 8 nM (*18*), or Protein-Tyrosine Phosphatase SHP-1 at 13.4 nM (*8*). It is also considerably lower than other PA binding proteins, such as the capping protein for Arabidopsis thaliana (atCP) with 17 μM (*19*). In the larger picture of membrane binding proteins, this is a low affinity compared to regions such as the N-PTB region of Dab2 to sulfatides at 600 nM (*20*), or the Phox (PX) domain of Phosphoinositide 3-Kinase-C2α to PtdIns(4,5)P_2 at 25 nM (*21*). However, this is a lower equilibrium constant than the FYVE domain binding to PtdIns(3)P at 71 μM (*7*). However, all of these values can be considered relevant depending on the area of interaction in the plasma membrane. While the affinity would be low for a single phospholipid interaction, patches of specific phospholipids could increase the favorability of interaction (*22*). The increased surface area of a specific set of phospholipids could increase the effectiveness of membrane association by amplifying its properties. It is also possible that phospholipids with similar characteristics could aid in association, but not the actual binding to the protein. For instance, PA could be surrounded by phosphatidylglycerol (PG), another negatively charged phospholipid, and aid in drawing mDvl2-DEP towards a section of plasma membrane.

Sensitivity of mDvl2-DEP to the effects of pH

By titrating a N^{15}-labeled sample of mDvl2-DEP at various pH values, we are able to observe that the protein will change its conformation in response to pH. While this is to be expected with a decreased pH due to changes in protonation state (*23*), this titration showed the sensitivity of the lysine (*24*) and histidine (*25, 26*) residues within mDvl2-DEP to changes in pH (Fig 3.8). Thus, we conclude that changes in pH increases the exposure of Phe and Tyr thru near-UV circular dichroism while retaining secondary structure elements (*13*). Fluorescence spectroscopy also confirms increased exposure of Trp at decreased pH through an increase in quenching due to the low pH (*27*). These tertiary structure alterations are most likely due to reorganization of loop regions in response to the increased protonation of the solvent (*28*).

The regulation of membrane binding proteins is an important fundamental mechanism within the cell. The 'histidine switch' hypothesis is a biochemical hypothesis first argued by Kampmann et al in viral membrane fusion proteins (*29*), where histidine residues act as pH sensitive switches for association/release from membranes. These switches can then lead to altered structural conformations or transitions, leading to a more stable "postfusion" conformation (*29*). For these switches to function properly, they must only be protonated when the pH becomes low enough, while being resilient enough not to be protonated again (*30*). It is this protonation that determines if the electrostatic association is strengthened or weakened to the negatively charged surface of the plasma membrane (*13*).

While it is known that mDvl2-DEP will localize to the plasma membrane at the normal membraneous pH of 7.45 (*31*), how does the pH decrease to levels enough to alter mDvl2-DEP association to phosphatidic acid? One explanation is that the interaction takes place in a locally altered pH environment by mediating membrane pumps (*7*). It has been hypothesized that the Fz-receptor may physically interact with Nhe2, a Na^+/H^+ pump, to change the local pH surrounding the receptor intracellularly. It is also possible that the pKa of histidine can shift in the presence of its ligand, closer to more physiological values (*7*), explaining why we see a decrease in binding before the pKa.

We are able to illustrate that the binding of mDvl2-DEP is pH-dependent through our liposome binding assay results. The decrease in mDvl2-DEP association to PA-containing liposomes at lowered pH values is apparent, with a drop from roughly 68% binding stabilizing to 35% around pH 6.8. However, mDvl2-DEP 2N seems to have lost pH sensitivity, remaining at a near constant level of association (~65%) at all pH values tested. While we know there are tertiary structure changes, the reaction is going to be affected by a change in the relative charge surface of mDvl2-DEP. This change in charge surface will not remain in a localized region of interaction though, but instead affect the surface of the protein as a whole; similar to plastocyanin interacting with the cell membrane, where changes in tertiary structure are shown to affect the entire protein surface and alter other biophysical characteristics (*e.g.* thermal stability) (*32*).

Histidine has a pKa between 6.0 and 6.5 (*33*), where the histidines will experience a change in charge approaching and surpassing this point. However, the estimated pI of mDvl2-DEP is roughly 7.08, denoting that the protein itself will experience changes in its charge surface

before coming close to the pKa of histidine. Thus, the pKa of two residues could be overcome by the overall pI of the protein in determining behavior. The environment in which the histidine residues are surrounded will affect the pKa, possibly altering them from their expected values (6.0-6.5) to more extremes (6.9-7.6) (*34*). However, others have shown that at a pH of 7.4, histidine residues are responsive enough even close to 1 pH unit away from its pKa (*7*).

Conclusions

In conclusion, our research has shown that mDvl2-DEP also interacts with phosphatidic acid. This interaction takes place in two distinct patches formed by a positively charged surface area. We have also demonstrated that this interaction occurs at a physiologically relevant concentration of 4.5 μM. The interaction of mDvl2-DEP and phosphatidic acid does not cause significant changes in structural conformation. However, a change in pH will alter the tertiary structure conformation by relaxing the loop regions of mDvl2-DEP. We have also shown that histidine residues (His 464 and His 465) contribute as a regulator of plasma membrane association by acting in a pH-dependent manner known as a 'histidine switch.'

Chapter 5: Materials and Methods

Protein Purification

Proteins was expressed in Luria Broth (or minimal media containing $N^{15}H_4Cl$ for N^{15}-labeled protein) using *E. coli* Rosetta containing a GST-fusion vector previously inserted with the cDNA of mDvl2-DEP. Bacterial cells were grown at 37°C to an optical density of ~0.8 before adding 1 mM IPTG. Cultures were then be induced at 25°C for 4 hours before cells are harvested by centrifugation. Protein are then purified using glutathione-sepharose affinity chromatography following manufacturer's instructions. Untagged proteins were obtained by cleaving off the GST-tag with PreScission Protease (12 units / 450 μg protein for 2 h at room temperature). Proteins were resolved using a 16/60 Superdex 75 column in an AKTApurifier Fast Performance Liquid Chromatography (FPLC) system. For untagged mDvl2-DEP purifications, the S75 column was equilibrated with 20 mM Sodium Citrate pH 6.8, 100 mM NaCl, and 1 mM DTT. Peak fractions will be pooled and concentrated prior to use. For untagged NMR samples, protein solutions were further exchanged into 20mM d-Citrate pH 6.5, 100 mM NaCl, and 1 mM d-DDT. For non-NMR samples, the buffer was composed similarly, but without deuterated-items.

Homology Modeling of mDvl2-DEP

The sequence for mouse Dvl2-DEP was aligned with that of mouse Dvl1-DEP (NM_010091.3) using SWISS MODEL. As sequence identity was relatively high (>70%), no adjustment was made to the alignment. Homology modeling was carried out using SWISS MODEL using the template for mDvl1-DEP (PDB IDcode 1FSH). The model was confirmed using PROCHECK.

NMR Phosphatidic Acid Titration

Samples were diluted to 100 μM to make a final buffer composition also containing 10% D_2O and 0.1% sodium azide. DHPA preparation includes pH correction of ligand solution within the range of the NMR sample (pH 7.5). The sample was mixed with corresponding molar ratios of DHPA:mDvl2-DEP at 0:1, 4:1, 8:1, 16:1, 32:1 and 64:1 concentrations. Sample pH was confirmed and adjusted if needed using an NMR pH probe before each run. Samples were analyzed on a 600 MHz Bruker Avance III at the Virginia Tech Chemistry Department NMR

Facility at 1 atm and 298°K. HSQC data will be processed and refined using NMRDraw (NIH) and spectra corrections were performed using Sparky (UCSF).

Alternatively, a sample of 300 μM for pH titration was equilibrated to a pH of 5.5, and then adjusted using NaOH to pH values of 6.5 and 7.5 before being processed.

Dvl2-DEP Mutant Synthesis

Primers were designed based on the Stratagene QuickChange Site-Directed Mutagenesis protocol, changing the residue into an alanine or asparagine. Sequence was confirmed in both DNA strands.

Liposome Binding Assay

Dioleyl (DO) lipids were dissolved in solutions of chloroform: methanol: water (65:53:8) and 400 μg aliquoted in mass ratios of 1:1 DOPA:DOPC or 1:1 DOPC:DOPE, dried under a nitrogen stream and desiccated overnight to remove residual water. Lipids were then hydrolyzed for forty minutes at room temperature in 200 μL of LBA buffer solution (20 mM Tris pH 7.5, 100 mM NaCl, 180 mM sucrose), mixing the contents of the tube every ten minutes to ensure all lipids are in solution. The tubes were then flash frozen in liquid nitrogen and thawed in a 60°C water bath three times to aid in liposome formation. Uni-lamellar vesicles were formed using water bath sonication for eight minutes at thirty-second intervals. An additional 600 μL of LBA buffer solution was added, where the liposomes will then be extruded at room temperature through a 1 μm membrane twenty one times before being centrifuged at 14,5000 rcf for 10 minutes at 4C to pellet formed uni-lamenar liposomes. Supernatants were resuspended in 30 μL of LBA binding buffer solution (50 mM Sodium Citrate pH 7.5, 100 mM NaCl). Proteins were first centrifuged at 14,500 rcf for 10 minutes at 4°C before adding a total of 10 μg to the resuspended liposomes. Samples were placed on an inverter at room temperature for twenty minutes and then centrifuged at max speed for 15 minutes at 4°C to pellet liposome-protein complexes. Supernatant and pellets were resuspended in laemmli buffer and boiled for 2 minutes.

For pH titration, we followed essentially the same procedure albeit a solution of LBA binding buffer at various pH values was used to resuspend the liposome pellet. For pH values tested include 7.5, 7.1, 6.8, 6.5, and 6.25 in 20 mM Sodium Citrate and 100 mM NaCl buffer.

Circular Dichroism

Far and near-UV CD spectra were obtained on a Jasco-815 spectropolarimeter using a 1 mm slit-width quartz cuvette. Untagged Dvl2-DEP protein (10 μM) were titrated with increasing concentrations of DHPA (ranging from 0:1 to 32:1 PA:DEP) in 5 mM citrate pH 7.5, 100 mM KF. Spectra will also be obtained in similar buffers with pH values of 6.25. Five accumulations were gathered for each sample from 190 to 260 nm with 0.5 nm increments, a scan rate of 50 nm min^{-1}, a response time of 4s, and a sensitivity of 50 millidegrees at 25°C. Blanks were subtracted from the spectra. Data was converted into mean residue ellipticity (degrees cm^2 $dmol^{-1}$), processed using DICHROWEB and deconvoluted using CDSTTR.

Fluorescence Spectroscopy - Tryptophan Quenching

Fluorcence was performed on the Jasco J-815 with monochrometer attachment using a quartz cuvette at 25°C. Samples contained 1 uM of mDvl2-DEP in a final volume of 2 mL. Increasing amounts of ligand (DHPA) will be added in rations ranging from 0:1 to 32:1 (DHPA to protein). Samples were equilibrated for five minutes after mixing. Emission spectra were obtained using an excitation wavelength of 295nm and then measuring emission from 310 to 410nm. Three accumulations were gathered for each point at a DIT of 4 s, sensitivity of 1000 volts, and 5nm bandwidth. Spectra were corrected by subtracting buffer blanks.

Chapter 6: Collaborations

A. A Novel heme-regulatory motif mediates heme-dependent degradation of the circadian factor Period 2. Jianhua Yang, Kevin D. Kim, Andrew Lucas, Karen E. Drahos, Carlo S. Santos, Sean P. Mury, Daniel G. S. Capelluto, and Carla V. Finkielstein. *Molecular and Cellular Biology*. Aug. 2008: 4697-4711. Reprinted with permission, American Society for Microbiology License Number 2186140420519.

Contributions I have made to this project are stated in the Acknowledgements section of the publication (see attached):

"…A.L. and D.G.S.C. performed and analyzed CD experiments,…"

A Novel Heme-Regulatory Motif Mediates Heme-Dependent Degradation of the Circadian Factor Period 2

Jianhua Yang,[1] Kevin D. Kim,[1] Andrew Lucas,[1] Karen E. Drahos,[1] Carlo S. Santos,[1] Sean P. Mury,[1] Daniel G. S. Capelluto,[2] and Carla V. Finkielstein[1]*

Department of Biological Sciences[1] and Department of Chemistry,[2] Virginia Polytechnic Institute and State University, Blacksburg, Virginia 24061

Although efforts have been made to identify circadian-controlled genes regulating cell cycle progression and cell death, little is known about the metabolic signals modulating circadian regulation of gene expression. We identify heme, an iron-containing prosthetic group, as a regulatory ligand controlling *h*uman *Per*iod-2 (hPer2) stability. Furthermore, we define a novel heme-regulatory motif within the C terminus of hPer2 (SC841PA) as necessary for heme binding and protein destabilization. Spectroscopy reveals that whereas the PAS domain binds to both the ferric and ferrous forms of heme, SC841PA binds exclusively to ferric heme, thus acting as a redox sensor. Consequently, binding prevents hPer2 from interacting with its stabilizing counterpart cryptochrome.

In vivo, hPer2 downregulation is suppressed by inhibitors of heme synthesis or proteasome activity, while SA841PA is sufficient to stabilize hPer2 in transfected cells. Moreover, heme binding to the SC841PA motif directly impacts circadian gene expression, resulting in altered period length. Overall, the data support a model where heme-mediated oxidation triggers hPer2 degradation, thus controlling heterodimerization and ultimately gene transcription.

INTRODUCTION

Cellular homeostasis depends on a delicate balance between metabolic activity and gene expression. Heme is a prosthetic group essential for transport and storage of oxygen that is involved in the generation of cellular energy by respiration and synthesis and degradation of lipids and in oxidative damage. Heme-based sensor proteins detect and respond to variations in oxygen, carbon monoxide, and nitric oxide levels and cellular redox state by acting on transcription, translation, protein translocation, and protein assembly (8, 25).

Heme binding to transcription factors is found in both prokaryotes and lower eukaryotes; however, only three cases have been identified in higher eukaryotes: the basic leucine zipper transcription factor Bach1, the circadian transcription factor NPAS2, and the nuclear orphan receptor Rev-erb_ (6, 23, 30, 43). Although structurally unrelated, both NPAS2 and Bach1 regulate the transcription of genes impacting heme synthesis and degradation (15, 36). Heme binds to NPAS2 through a region of homology called PAS (*P*er-*A*RNT-*S*im) to form a gas-regulated sensor (6). Although DNA binding of NPAS2 depends on its heterodimerization with another basic-helixloop-helix-PAS protein termed Bmal1, heme is not required for the dimer to bind DNA (6). Heme-bound NPAS2 acts as a gas-sensing protein by binding carbon monoxide, causing inhibition of the DNA-binding capacity of NPAS2/Bmal1 (6). Interestingly, heme binding to Rev-erb is mediated by a histidine residue located in the carboxy tail of the ligand-binding domain, but unlike NPAS2, Rev-erb activity is not responsive to diatomic gases and is unlikely to sense redox conditions (30, 43).

Along with PAS, a second domain has been identified as a heme-binding site. The *h*eme-*r*egulatory *m*otif (HRM) comprises a stretch of residues where only a Cys-Pro core is absolutely conserved and a preferred hydrophobic residue is located in the fourth position (X-CP-_). This motif has been identified in functionally diverse proteins and is thought to govern the activity of a neighboring transmitter domain in response to heme binding (45). For example, heme binds to the

transcriptional repressor of the *h*eme *o*xygenase-1 (HO-1) gene, Bach1, through multiple HRMs (37). Binding inhibits Bach1/MafK association with the HO-1 promoter, inducing subcellular relocalization of Bach1 and degradation (37, 44). In addition to Bach1, various heme-mediated protein functions require HRMs: the yeast transcriptional activator Hap1 that transcribes genes encoding various cytochromes, catalase, and Rox1, which represses anaerobic genes under high heme concentration (see reference 12 and references within); the hemeregulated inhibitor kinase that controls the activity of the translation initiator factor eIF-2_ in stressed erythroid cells (4, 11); the erythroid 5-aminolevulinic acid synthase precursors whose transport to the mitochondria is mediated by heme binding to HRMs (20); the heme lyase found in both *Saccharomyces cerevisiae* and *Neurospora crassa* (35); the mammalian nuclear factor erythroid 2 that plays a critical role in erythroid differentiation (22); the HO-2 that metabolizes heme (21); the *i*ron *r*egulatory *p*rotein 2 (IRP2), a regulator of iron metabolism in mammals (13), and the *i*ron *r*esponse *r*egulator (Irr) in bacteria whose turnover depends on the cellular iron availability (28, 42).

A second PAS-containing circadian molecule, Per2, has also been implicated in heme binding and mediates *per1* and *per2* transcription in vivo by a mechanism involving NPAS2 (15). Disruption of either the *per1* or *per2* gene in mice leads to circadian deregulation of heme biosynthesis by altering the expression levels of the rate-limiting enzymes Alas1 and Alas2 (15, 46). Unlike NPAS2, Per2 does not contain a basic-helixloop- helix domain, and it is hypothesized that heme control of Per2-mediated gene transcription takes place indirectly by modulating the expression of Bmal1. Consequently, while we know much about how heme and Per2 signaling molecules operate in cell metabolism and circadian rhythms, we lack a clear understanding of how these two circuitries are integrated and operate to directly modulate gene expression.

Here we report the discovery of a previously uncharacterized heme-regulatory motif in Per2 with a functional link to protein stability. We show that (i) heme binds to two distinct regions of *h*uman *Per*iod-2 (hPer2) and the oxidation state of the heme iron determines binding specificity and degradation; (ii) hPer2 stability is compromised when heme binds to the outermost C-terminal domain of the protein, preventing hPer2 from binding its heterodimeric counterpart *h*uman *cry*ptochrome 1 (hCry1); (iii) downregulation of hPer2 is suppressed in the presence of inhibitors of heme synthesis or proteasome activity; and (iv) a point mutation in the C-terminal HRM is sufficient to stabilize hPer2 in vivo. Together, our data indicate that an uncharacterized HRM functions as a binding site and triggers heme-induced degradation of hPer2, likely regulating cellular signaling by modulating the formation of hPer2/hCry1 complex.

MATERIALS AND METHODS

Plasmid constructs and site-directed mutagenesis. Various hPer2 and hCry1 cDNA fragments were cloned into the SalI and NotI sites of pGEX-4T-3. Fragments of hPer2 comprising residues 1 to 172, 173 to 355, 356 to 574, 173 to 574, 822 to 872, and 822 to 1255 are referred to as hPer2(I), hPer2(II), hPer2(III), hPer2(II-III), hPer2(V4), and hPer2(V4-VII), respectively. The Cys residue of each putative HRM (Cys841 and Cys962) and Ser662 in hPer2 was mutated to Ala by site-directed mutagenesis using QuikChange (Stratagene). The hPer2, hPer2(SA841PA), hPer2(II-III), and hPer2(V4-VII) cDNAs were cloned into pCS2_*myc*-tag vector modified for ligation-independent cloning (Novagen).

Protein pull-down and hemin-agarose-binding assays. Glutathione *S*-transferase (GST) fusion proteins were expressed in *Escherichia coli* strain Rosetta (Novagen) and purified by glutathione-Sepharose chromatography following the manufacturer's instructions (GE HealthSciences). Untagged proteins were generated by digestion of fusion proteins with thrombin followed by concentration and buffer exchange (10 mM Tris-HCl [pH 8.0]). For pulldown assays, a total of 5 μg of GST-hCry1-bound beads or an equivalent amount of glutathione beads was washed in binding buffer A (20 mM Tris-HCl [pH 7.4], 100 mM NaCl, 5 mM EDTA, and 0.1% Triton X-100) and incubated with 2 μl of in vitro-transcribed

and -translated 35S-labeled hPer2 or the indicated fragments at 4°C for 1 h. After the beads were washed with low- and high-salt binding buffer A (with 100 mM and 1 M NaCl, respectively), bound proteins were eluted by boiling in Laemmli sample buffer and analyzed by sodium dodecyl sulfate-polyacrylamide gel electrophoresis (SDS-PAGE) and autoradiography. In other experiments, hemin [Fe(III)-heme, 10 μM] was added to either hPer2 or the preformed GST-hCry1/hPer2 complex and incubated at 4°C for 1 h. In the first scenario, hPer2/hemin was loaded onto GST-hCry1 beads, and binding proceeded at 4°C for an additional hour. Samples were analyzed by autoradiography.

For hemin-agarose binding, 20 μl of hemin-agarose beads (Sigma) was washed, resuspended in binding buffer B (10 mM sodium phosphate buffer [pH 7.5], 500 mM NaCl, 5 mM EDTA, 1% Triton X-100) and incubated with 5 μg of the indicated recombinant proteins at 4°C for 1 h. Beads were washed with lowand high-salt binding buffer B (with 250 mM and 1 M NaCl, respectively), and proteins were analyzed by SDS-PAGE.

Spectroscopic analysis of heme-protein binding. Ferric heme binding was determined by absorption spectra of 1 μM hemin in the absence or presence of 1 μM of indicated proteins in 10 mM Tris-HCl, pH 8.0. The protein/hemin molar ratio ranged from 0.25 to 8. Results were plotted as absorbance at the peak versus the molar ratio of protein to hemin. To determine ferrous heme-binding properties, 30 mM sodium dithionite was added to reduce hemin to ferrous heme. Absorption spectra were recorded between 300 and 700 nm on a Beckman DU-640 UV-visible spectrophotometer.

CD spectroscopy. Far-UV circular dichroism (CD) spectra were measured on a Jasco J-720 spectropolarimeter using a 1-mm-slit-width cuvette. The hPer2(V4-VII) protein (8.3 μM) was titrated against increasing concentrations of hemin (molar protein/hemin ratios of 1:1, 1:2, and 1:4) in 10 mM phosphate buffer (pH 7.6) and 150 mM NaCl. Five accumulated scans for each sample were recorded from 190 to 240 nm with an increment of 0.5 nm, a scan rate of 50 nm min_1, a response time of 4 s, and a sensitivity of 50 millidegrees at room temperature. All CD spectra were corrected by subtraction of the background from the spectrum obtained with either buffer alone or buffer containing hemin. Raw data were converted to mean residue ellipticity, _, in degrees cm2 dmol_1. A similar procedure was followed for hPer2(II-III) and hPer2(V4-VII-SA841PA). Data were analyzed for protein secondary structure using DICHROWEB (38) and deconvoluted using CDSSTR (34).

In vitro degradation assays. For protein degradation experiments, *C*hinese *h*amster *o*vary (CHO) cell extracts were prepared in lysis buffer (Promega) containing 25 mM Tris-HCl (pH 7.8), 2 mM EDTA, 2 mM dithiothreitol (DTT), 10% glycerol, and 1% Triton X-100. Alternatively, commercially available HeLa cell extracts (fraction S100 from Biomol) were also used in these experiments.

For in vitro degradation assays, 35S-labeled fragments of Cry1, Mdm2, hPer2, hPer2(S662A), and hPer2 proteins were incubated with cell extracts at 37°C supplemented with ubiquitin (0.1 mg/ml) and an energy-regenerating system. Hemin was added to the mixture to a final concentration of 10, 25, 50, or 100 μM. Reactions were stopped by the addition of Laemmli sample buffer, resolved by SDS-PAGE, and visualized by autoradiography. Densitometric quantitation was carried out using a FluoChem digital imaging system (Alpha Innotech).

Cell culture and analysis of endogenous Per2 protein. CHO cells were maintained in F-12K medium (Invitrogen) supplemented with 10% fetal bovine serum and gentamicin (50 μg/ml). To detect endogenous levels of Per2, cells were cultured in serum-free medium containing 5 mM succinylacetone for 24 h prior to hemin addition (10 μM). Cells were harvested at the indicated times after treatment, and pellets were resuspended in lysis buffer (50 mM Tris-HCl [pH 7.5], 10 mM MgCl2, 200 mM NaCl, 1% NP-40, 5% glycerol). For detection of hCry1 levels, the procedure was essentially the same as the one described above except that cells were first transfected with pCS2_*myc*-hCry1 using Lipofectamine (Invitrogen) and the protein was allowed to express for 12 h before the addition of succinylacetone. Endogenous Per2 and *myc*-hCry1 levels were detected by immunoblotting using specific antibodies (Santa Cruz).

Serum shock procedures and sample collection. Low-density CHO cells were plated 4 days before the experiment, transfected with 0.5 _g of pCS2_*myc*-hPer2 or -hPer2(SA841PA) using Lipofectamine and cultured for 12 h before synchronization (1). Briefly, at time zero, the medium was exchanged with 50% F-12K medium supplemented with 50% horse serum and gentamicin (50 μg/ml). After 2 h of incubation, cells were washed twice with phosphate-buffered saline (PBS), and the medium was replaced with serum-free F-12K medium containing 5 mM succinylacetone. Hemin (10 μM) was added 24 h after serum shock, and the cells were maintained for 6 h before the medium was replaced with serum-free F-12K medium containing 5 mM succinylacetone. At the indicated times, cells were washed with PBS, frozen, and kept at -80°C until the extraction of whole-cell RNA. Reverse transcription-PCRs were performed using specific primers for *Rev-erb*_ and *GAPDH* (glyceraldehyde-3-phosphate dehydrogenase gene) (see supplemental material for details).

Cell transfection and immunofluorescence assays. CHO cells were cultured on coverslips for 24 h. Cells were then transfected with 0.5 μg of pCS2_*myc*-hPer2 or -hPer2(SA841PA) using Lipofectamine (Invitrogen) and cultured for an additional 12 h. The effects of heme on *myc*-hPer2 and -hPer2(SA841PA) levels were determined using transfected cells treated with either 10 μM hemin or solvent for 2 h. After incubation, cells were maintained in serum-free medium for an additional 6 h and fixed in 3.7% formaldehyde–PBS–0.5% Triton X-100 at room temperature. Fixed cells were washed with PBS containing 0.5% Triton X-100 and then 0.1% Triton X-100 and blocked with goat serum at room temperature for 30 min. Subcellular localization of myc fusion proteins was detected using an Cy3-conjugated anti-*myc* antibody (Sigma). Nuclei were detected by incubating fixed cells with 4,6-diamidino-2-phenylindole (DAPI) (Molecular Probes). Fluorescence was visualized using a DeltaVision Core microscope equipped with a CoolSnap HQ2 camera (Applied Precision) at 457 nm, 528 nm, and 617 nm. Signal intensities were measured using the profile plot analysis.

RESULTS

Heme regulates hPer2 stability. Like other cellular pathways, the circadian clock relies on mechanisms of synthesis and degradation of some of its components to sustain oscillations. Heme stimulates the expression of transcription factors that regulate circadian rhythms by modulating the activity of the Bmal1/NPAS2 complex, which transcriptionally controls the expression of the mammalian *period* genes and of the *alas1* gene (6, 15). Because there is little evidence regarding the mode by which heme acts on eukaryotic circadian transcription factors, we aimed to elucidate the molecular basis by which heme binding influences hPer2 function. First, we monitored the degradation of radiolabeled hPer2 in a cell-free system in response to hemin [Fe(III)-heme] treatment. ^{35}S-labeled hPer2 was incubated with a cell extract as the source for ubiquitination enzymes and proteasome in the presence of various concentrations of hemin. Results show hPer2, but not a nonspecific control protein (Mdm2 [see Fig. S1 in the supplemental material]), is degraded shortly after the addition of hemin in a dose-dependent manner (Fig. 1A). Incubation with 1, 10, and 100 _M of ligand resulted in a rapid reduction (_20, 60, and 90%, respectively) of hPer2 levels (Fig. 1A and data not shown). Importantly, this effect was inhibited when cell extracts were preincubated with the proteasome inhibitor MG-132, suggesting that heme-dependent degradation of hPer2 is mediated by the ubiquitin-proteasome pathway (Fig. 1A). Next, we investigated whether heme binding to the hPer2 PAS domain mediates hPer2 turnover. Interestingly, ^{35}S-labeled hPer2(II-III) (residues 173 to 574, comprises the PAS domain) remained stable in a cell-free assay even at high hemin concentrations (Fig. 1B), suggesting that regions other than PAS contain heme-regulated instability elements mediating hPer2 degradation.

*C*asein *k*inase I *e*psilon (CKIε), a central component of the mammalian circadian clock, is the prime kinase involved in hPer2 downregulation by direct targeting of Ser$_{662}$ for phosphorylation (3, 7). To rule out any contribution of CKIε to heme-mediated degradation of hPer2, we analyzed ^{35}S-labeled hPer2(S$_{662}$A) in a cell-free system for its stability in the presence of hemin (Fig. 1C). hPer2 levels remained stable in the absence of hemin in cell extracts, ruling out the

contribution of other phosphorylation events in hPer2 stability. Results indicate that hPer2($S_{662}A$) levels remain sensitive to hemin addition, supporting the existence of a novel mechanism for hPer2 degradation that is independent of CKIε phosphorylation but dependent on the presence of heme.

Because hPer2 can be efficiently degraded in vitro, we were prompted to look for evidence of heme-mediated degradation in vivo. First, endogenous Per2 levels were monitored in CHO cells after hemin addition. Time course experiments showed reduced levels of Per2 protein but not its mRNA upon incubation with hemin (Fig. 1D). This result excludes the possibility of heme-mediated transcriptional effects on the *per2* gene and points toward heme-mediated control of protein stability, since untreated cells showed steady levels of Per2 (Fig. 1D). To further explore the dependence of heme on Per2 stability, CHO cells were pretreated with succinylacetone, an inhibitor of sigma-aminolevulinic acid dehydratase, to prevent de novo synthesis of endogenous heme (Fig. 1E). Consistent with our in vitro data, downregulation of Per2 in CHO cells was inhibited by succinylacetone but induced by further addition of exogenous hemin, indicating that heme synthesis is essential for Per2 degradation.

Heme binds within the C-terminal domain of hPer2. To identify the region on hPer2 involved in heme targeting, purified GST-hPer2 fragments [GST-hPer2(I), GST-hPer2(II), GST-hPer2(III), GST-hPer2(II-III), and GST-hPer2(V4-VII) (Fig. 2A)] were analyzed for heme-binding activity using hemin- agarose affinity chromatography (Fig. 2B). Direct interactions between hemin and PAS domain-containing fragments GST-hPer2(II), GST-hPer2(III), and GST-hPer2(II-III) were detected, confirming both the role of the PAS domain in heme binding and the reliability of the method to define heme interacting domains (Fig. 2B). Based on this result, it seems two regions within the PAS might be involved in heme binding. This can be addressed based on the functional homology among the PAS domains of the circadian NPAS2 and Per2 proteins. The PAS domain in NPAS2 typically encompasses 150 amino acids and contains two highly degenerate 50-residue subdomains termed A and B repeats, each of which binds one molecule of heme (for a review, see reference 10). Our results show that hemin is able to bind the truncated forms of PAS domain comprising either subdomain (Fig. 2 and see Fig. 4) (see Fig. S2 in the supplemental material) with equimolar stoichiometry suggesting that, like NPAS2, two independent regions within the hPer2-PAS domain are capable of hemin binding. Interestingly, while the N-terminal fragment of hPer2 comprising residues 1 to 172 [GST-hPer2(I)] did not exhibit any association with hemin-agarose beads (Fig. 2B, right panel), a distinct segment of the protein located within the C-terminal region, GST-hPer2(V4-VII), exhibited strong association with hemin, suggesting that a heme-binding motif is located within this region.

A novel heme-regulatory motif mediates hPer2-heme interaction. Heme-protein interaction is alternatively mediated by evolutionary conserved heme-regulatory motifs where Cys-Pro residues are invariant and where there is a tendency for a hydrophobic amino acid to be in the fourth position. Inspection of the hPer2 sequence determined the presence of two putative HRMs (Fig. 3A). Interestingly, both HRMs were located within hPer2(V4-VII), a fragment that exhibits hemebinding capacity (Fig. 2). Comparative analysis of global multiple Per2 sequence alignments exhibits conserved residues clustered in the HRMs and surrounded by sequence elements of high (for $SC_{841}PA$) and low (for $AC_{962}PA$) conservation (Fig. 3A). Phylogenetic analyses indicate that both putative HRMs are highly conserved modules in Per2 proteins among metazoan lineages, especially in mammals, suggesting that the sequences under investigation have a comparatively young most recent common ancestor (Fig. 3A).

Unlike other heme-binding sites, HRMs establish bonding between the cysteine sulfur and the iron atom of heme (45). Accordingly, we tested whether any of the putative HRMs identified in hPer2(V4-VII) were able to directly bind heme. Untagged hPer2(V4-VII) and its $SA_{841}PA$ and $AA_{962}PA$ mutant forms were analyzed after hemin addition by absorption spectroscopy (Fig. 3B). The hPer2(V4-VII) protein fragment shifted the peak of the strongest heme absorption band (388 nm), the Soret band, toward a shorter wavelength by _19 nm (369 nm [Fig. 3B]), consistent with heme binding to HRMs

(45). The $SA_{841}PA$ mutant form of hPer2(V4-VII), but not the $AA_{962}PA$ mutant form, abolished the protein's ability to shift the hemin absorption spectrum to shorter wavelengths and confirmed the essential role of Cys_{841} in heme binding (Fig. 3B). A second slight shift in the Soret peak (421 nm) was detected in the wild-type fragment (Fig. 3B). Whereas an additional residual shoulder was observed at a shorter wavelength for the $SA_{841}PA$ protein, we believe this shoulder results from excess amounts of free hemin in the sample. Our studies indicate that neither Cys_{841} nor Cys_{962} is responsible for the peak observed at 421 nm, suggesting the existence of a secondary component involved in heme binding that we later mapped between residues 1,121 and 1,255 of hPer2 (data not shown). Overall, our results pinpoint $SC_{841}PA$ as a novel heme-binding motif located at the C terminus of hPer2. As a direct test of the role of the $SC_{841}PA$ motif in heme binding, we examined whether a shorter fragment of hPer2 [GSThPer2(V4), residues 822 to 872] and its HRM mutant form [GST-hPer2(V4-$SA_{841}PA$)] were able to bind hemin by affinity chromatography (Fig. 3C). As expected, GST-hPer2(V4) displayed a strong interaction for hemin, and the mutation on Cys_{841} completely abrogated binding. Collectively, these data indicate that heme binds to hPer2 directly through Cys_{841}.

Binding of heme to both HRM and PAS follows a precise stoichiometry. Further evidence of direct binding of heme to hPer2(V4) and the PAS domain-containing fragment hPer2(III) was obtained by absorption spectra and titration experiments. Among hPer2 PAS-containing fragments, hPer2(III) was chosen because of its signal intensity. Hemin binding to hPer2(V4) shifted the Soret band from 388 to 370 nm, an event that was prevented by the mutation of Cys_{841} to Ala, confirming Cys_{841} as the axial heme ligand (Fig. 4A, left panel). Since hPer2(V4) does not have any appreciable absorption between 300 and 700 nm, the observed spectral changes on free hemin are due to alterations in the electronic structure and coordination state of the heme iron caused by its interaction with hPer2(V4). To examine the specificity of heme binding, hemin was titrated with increasing amounts of GST-hPer2(V4). The absorption peak of free hemin was blue shifted to 370 nm after the addition of the smallest amount of protein, whereas the amplitude of the peak increased accordingly with protein concentration (Fig. 4B, left panel). Titration curves show a well-defined inflection point corresponding to a molar stoichiometry of hemin and GST-hPer2(V4) of 1:1 (Fig. 4C). Specific binding of hemin to hPer2(V4-$SA_{841}PA$) was not detected by absorption experiments (Fig. 4A, left panel). Titration analysis showed initial diminution of the absorption peak of free hemin (388 nm) after hPer2(V4-$SA_{841}PA$) addition followed by a continuous shift around the hemin peak wavelength, likely caused by nonspecific binding by excess protein (Fig. 4B, middle panel, and C).

Evidence shows that the PAS domain in *m*ouse *Per*2 (mPer2) mediates heme binding (15), but there is no spectroscopic data illustrating binding details in this domain. We determined that hPer2 PAS domain heme binding is mediated by either methionine/histidine or bis-histidine coordination, since the free hemin absorption spectra (388 nm) shifts to a Soret peak at 412 nm (Fig. 4A, right panel) (see Fig. S2 in the supplemental material). Titration experiments also defined the stoichiometry of the interaction and established that hemin binds to PAS-A and -B subdomains, forming an equimolar complex in each case (Fig. 4B and C) (see Fig. S2 in the supplemental material). Altogether, these results demonstrate that (i) Fe(III)-heme binds to hPer2 at two distinct sites ($SC_{841}PA$ motif and PAS domain), (ii) binding is mediated by different coordination in HRM and PAS, and (iii) both subdomains in PAS are able to bind heme.

Degradation of hPer2 depends exclusively on binding of oxidized heme to HRM. Because hemin interacts strongly with both PAS and HRM (Fig. 4), we next examined whether either site was able to bind the reduced form of heme. To study this possibility, hemin was reduced by the addition of sodium dithionite and incubated with GST-hPer2(III), GST-hPer2(V4), or GST-hPer2(V4-$SA_{841}PA$), and their interactions were monitored by absorption spectra (Fig. 5A). As with ferric heme, ferrous heme has distinct absorption characteristics that shift upon protein binding. Accordingly, a Soret peak at 421 nm was observed exclusively in the presence of GST-hPer2(III) (Fig. 5A) and GST-hPer2(II-IIIPAS-B) (see Fig.

S2C in the supplemental material), suggesting that only this domain is able to bind both forms of heme. Neither GST-hPer2(V4) nor GSThPer2(V4-SA$_{841}$PA) exhibits any apparent peak in the spectra when incubated in the presence of a reducing agent, indicating that ferrous heme is not a suitable ligand for HRM. Therefore, we conclude that both forms of heme are able to bind PAS but that only oxidized heme binds to HRM, which suggests that this interaction takes place exclusively under specific redox conditions.

We next asked whether degradation of hPer2 depends on the redox state of the bound heme iron. To address this question, we used a cell-free system and evaluated hPer2 turnover in the presence of oxidized and reduced forms of heme (Fig. 5B). hPer2 stability was initially monitored in CHO cell extracts in the absence or presence of DTT (control). As expected, hPer2 remained stable in either condition, suggesting that factors other than heme are not required for hPer2 degradation (Fig. 5B, top panels). In agreement with Fig. 1, the sole addition of hemin (25 or 50 μM) showed an increased rate of hPer2 degradation compared to controls (Fig. 5B, left panels). Interestingly, the stability of hPer2 was restored when hemin was preincubated with DTT before its addition to the extract, suggesting that the redox state of the heme iron is a determinant of hPer2 stability (Fig. 5B, right panels, and C). To rule out the possibility that DTT reduced proteolysis of hPer2 by a nonspecific toxic effect in the extract, we measured the degradation of a nonrelated protein (a cyclin-dependent inhibitor p27Xic1T$_{204}$D) in the presence or absence of DTT (Fig. 5D). As a test of the role of HRM in hemin-mediated degradation of hPer2, we examined whether the levels of hPer2(II-III) were altered in either redox condition (Fig. 5E and F). Labeled hPer2(II-III) showed steady levels in a cellfree assay throughout the time course analyzed independently of the redox state of the heme iron (Fig. 5E and F). Thus, a heme-binding site other than PAS must be responsible for hPer2 degradation, supporting the role of HRM in mediating hPer2 stability.

It is established that reactive oxygen species encompass a variety of diverse chemical species, including superoxide anions hydroxyl radicals, and hydrogen peroxide. These various radical species can either be generated exogenously from several different sources (i.e., radiation, hyperthermia, and growth factors) or produced intracellularly as a consequence of metabolic activities, thus perturbing the normal redox balance and shifting cells into a state of oxidative stress. Therefore, we explored the consequences of inducing oxidative stress by diverse sources from different origins on hPer2 stability. Our data show that neither the addition of hydrogen peroxide, high metal concentration, and lipopolysaccharides, nor treatment with ionizing radiation and heat shock resulted in altered levels of hPer2, suggesting that hPer2 degradation is not a general response to oxidative stress conditions (see Fig. S5 in the supplemental material). Moreover, our data point directly toward a heme-mediated response, since the addition of Fe(III), per se, did not cause hPer2 degradation in vitro, but Fe(III)-heme (hemin) addition does (see Fig. S5 in the supplemental material), suggesting that iron must be converted to heme, before it can trigger hPer2 degradation.

It has long been recognized that the conformational stability of a protein and its proteolytic susceptibility are linked. The reason for this linkage lies in the assumption that certain protein conformational states are better substrates for proteases, with highly ordered conformations being relatively poor substrates owing to the lack of conformational freedom of the polypeptide chain (24). Therefore, we explored whether binding of heme influences the conformation of the protein using CD spectroscopy. Experiments were carried out in the presence of increasing concentrations of hemin and the apo forms of hPer2(II-III), hPer2(V4-VII), and hPer2(V4-VII-SA$_{841}$PA). Prediction of the secondary structure of hPer2(V4-VII) revealed the presence of a 24% alpah-helical, 18% beta-strand, and 19% beta-turn content (Fig. 6A). The hPer2(V4-VII) secondary structure elements were disrupted after treatment of the protein with guanidium hydrochloride (Fig. 6A). The hPer2(V4-VII-SA$_{841}$PA) fragment showed essentially the same overall fold as the wild-type construct, suggesting that the Cys$_{841}$ mutation does not alter the overall structure of the C-terminal domain (Fig. 6B), supporting a direct role for HRM in heme binding. The N terminus of hPer2(II-III) revealed a 5% alpha-helical, 29% beta-strand, and

21% beta-turn content, in agreement with the structural data from other PAS domain-containing proteins (Fig. 6C) (5). Neither hPer2(V4-VII) nor hPer2(IIIII) showed a significant rearrangement of their secondary structure even at twofold excess of ligand (Fig. 6A and C), suggesting that hPer2 degradation might result from its inability to form a stable heterodimer with hCry1 rather than a ligand-induced unfolding state. To test this possibility, pulldown experiments were performed using GST-hCry1-bound beads in the presence or absence of hemin and radiolabeled hPer2 fragments (Fig. 6D). In agreement with its role in hCry1 binding, the C-terminal fragment of hPer2 showed a reduced interaction to GST-hCry1 in the presence of hemin, suggesting that competition prevents this association. The labeled PAS domain-containing protein was unable to interact with hCry1 independently of hemin addition and does restrict the heme effect on hPer2/hCry1 formation to the C-terminal portion of hPer2.

HRM is required for degradation of hPer2 in vivo. To gain further insight into the role of HRM in the degradation of Per2 in vivo, we transiently transfected CHO cells with either *myc*hPer2 or *myc*-hPer2-SA$_{841}$PA and evaluated their subcellular localization and intracellular levels in response to hemin addition by immunofluorescence microscopy (Fig. 7A). In agreement with previous observations (40), immunofluorescence staining showed that *myc*-hPer2 was distributed in both nuclear and cytosolic compartments and that its accumulation was remarkably higher in the former (Fig. 7A). The cellular distribution of *myc*-hPer2-SA$_{841}$PA mutant was similar to that of the wild-type protein, and thus, we conclude the Cys$_{841}$Ala mutation does not alter hPer2 localization (Fig. 7A). Hemin addition to *myc*-hPer2-transfected cells resulted in decreased levels of the nuclear protein without increasing hPer2 levels in the cytosolic compartment, suggesting that degradation, rather than translocation, was triggered by hemin (Fig. 7A and B). Supporting the role of HRM in heme-mediated hPer2 degradation in vivo, the addition of hemin to *myc*-hPer2-SA$_{841}$PAtransfected cells did not result in apparent changes in mutant protein levels (Fig. 7A). Profile plotting of signal intensity along cross sections of cells transfected with wild-type and hPer2 mutants confirmed hemin-induced nuclear degradation of hPer2 and unambiguously confirmed that this phenomenon is mediated by HRM (Fig. 7B).

To further support the concept that HRM is sufficient to promote heme-mediated hPer2 degradation and that heme binding to PAS domain plays a distinct role (15), we transfected cells with *myc*-hPer2, *myc*-hPer2-SA$_{841}$PA, or *myc*-hPer2(II-III) and evaluated their total protein levels in response to hemin addition (Fig. 7C). The remarkable stability of *myc*-hPer2(II-III) observed in the presence of hemin contrasted greatly with the levels of *myc*hPer2 detected under the same condition, suggesting that binding of heme to the PAS domain does not alter its stability in vivo (Fig. 7C). The presence of equivalent levels of *myc*-hPer2-SA$_{841}$PA in the absence or presence of hemin further supports our model.

Binding of heme to HRM prevents the formation of the hPer2/hCry1 complex. The C terminus of Per2 physically associates with Cry proteins (9, 19), and the complex translocates to the nucleus where it acts as a negative regulator by directly interacting with Clock/Bmal1 (31). Thus, we first asked whether heme treatment of cells alters the intracellular levels of the hPer2/hCry1 complex (Fig. 8). Immunoprecipitation assays of hemin-treated *myc*-hPer2/FLAG-hCry1 cells were analyzed for the presence of heterodimers by immunoblotting (Fig. 8A). Results show reduced levels of bound hCry1 in hemin-treated samples, indicating that heme alters hPer2/ hCry1 levels in cells (Fig. 8A). To rule out the possibility that heme can cause hCry1 degradation and disrupt hPer2/hCry1 interaction, transfected CHO cells were incubated with hemin, and hCry1 levels were monitored at different times. As shown in Fig. S3A in the supplemental material, hCry1 levels remained invariable throughout the time course analyzed, suggesting that hCry1 stability is independent of the presence of heme. A similar result was obtained when hCry1 stability was tested in the presence of hemin in a cell-free assay (see Fig. S3B in the supplemental material).

We then examined whether heme binding to hPer2 prevents the formation of hPer2/hCry1 or disrupts an already preformed complex instead. To evaluate either model, we first recapitulated the cellular events leading to heme-

dependent reduction of hPer2/hCry1 levels in vitro (Fig. 8B). Recombinant GSThCry1, ^{35}S-labeled hPer2, and hemin were simultaneously incubated, and the amount of ^{35}S-labeled hPer2 present in the complex was analyzed by pull-down experiments (Fig. 8B and 6D). As was the case with transfected cell extracts, our in vitro assay showed lower levels of ^{35}S-labeled hPer2 associated with GST-hCry1 in the presence of hemin, supporting a model where ligand binding compromises hPer2/hCry1 complex formation. Because of the nature of our in vitro assay, only two proteins and hemin were present, which also suggests that heme binding to the C terminus of hPer2 prevents or disrupts its association with hCry1 and that heme-mediated degradation of hPer2 might be a consequence of lack of association.

Next, we established which event of the complex formation is inhibited by heme binding. In the first scenario, hPer2/GSThCry1 complex was allowed to form and later incubated wit hemin (Fig. 8C). In a parallel experiment, hPer2 was preincubated with hemin, added to GST-hCry1, and analyzed by pulldown experiments (Fig. 8C). Results demonstrate that more hPer2 is bound to GST-hCry1 when the complex is preformed, suggesting that hemin is unable to disrupt a stable heterodimer.

Expression of a non-heme-responsive HRM form of hPer2 alters the pattern of circadian gene expression. The observation that circadian gene expression can persist for several days in serum-free medium after an initial serum shock (1, 2) prompted us to test the effects of hPer2 and hPer2(SA$_{841}$PA) mutant on the mRNA accumulation profile of circadian genes. We investigated one of the known downstream effectors of Per2 signaling, *Rev-erb_*, a transcript that is lowest at times when Per2 expression peaks in the nucleus (26). Circadian *Rev-erb_* expression is controlled by components of the general feedback loop, thus influencing the period length and phaseshifting properties of the clock (26). In agreement with our model, cells transfected with hPer2 exhibited reduced levels of *Rev-erb_* compared with nontransfected cells (Fig. 9A, right panel), an effect that is reversed when cells were pretreated with hemin (Fig. 9A, bottom left panel). Moreover, transfection with hPer2(SA$_{841}$PA) resulted in sustained downregulation of *Rev-erb_* transcription throughout the analyzed time course (Fig. 9A, bottom right panel). As predicted, the addition of hemin to hPer2(SA$_{841}$PA)-transfected cells did not result in altered levels of *Rev-erb_*, since the ligand can no longer bind the mutant protein and is therefore unable to act on its stability.

Overall, our observations favor a scenario where heme plays an essential role in controlling hPer2 cellular levels by targeting hPer2 for degradation and preventing hPer2/hCry1 complex accumulation (Fig. 9B). Our tryptophan fluorescence spectroscopy data show that both PAS and HRM bind heme with roughly equal affinity in the nanomolar range {$K_{d\ hPer2(V4\text{-}VII)}$ [dissociation constant], 9.20 _ 0.94 nM; $K_{d\ hPer2(II\text{-}III)}$, 12.31 _ 0.43 nM; see Fig. S4 in the supplemental material}. Interestingly, whereas ferrous heme will bind only to the PAS domain (Fig. 5A), its ferric form could, in principle, target either binding site. At this point, we hypothesize that binding of ferric heme to either PAS or HRM might depend on their availability. For example, preassociation of hPer2 to hCry1 prevents the access of heme to HRM but not PAS (Fig. 8 and 9B) and thus affects signaling downstream. Accordingly, binding of heme to PAS in the mPer2/hCry1 complex regulates the transcriptional activity of Bmal1/NPAS2 and the expression of the *alas1* gene (15). Conversely, the absence of hCry1 will allow heme to bind HRM (or both HRM and PAS simultaneously) and promote instability of hPer2 (this study), an event that is exclusively mediated by HRM, since heme binding to PAS does not alter hPer2 instability (Fig. 1B). In this scenario, downregulation of hPer2 directly impacts the oscillatory expression of circadian genes. Thus, this novel pathway ensures an alternative mechanism to physiologically controlling the circadian clock by acting on gene expression.

DISCUSSION

The mammalian circadian system influences most physiological activities, including sleep/wake cycles, cardiovascular

activity, body temperature, blood pressure, glucose and fat metabolism, renal plasma flow, liver metabolism and detoxification, and hormonal secretion (32). Cross talk between the body's circadian rhythm and metabolic systems has been identified within both the gluconeogenic and lipogenic pathways and in organisms as diverse as flies and mammals. Examples include the circadian oscillatory expression of the sterol-regulatory element-binding proteins 1a and 1c, a group of transcription factors that bind to the sterol regulatory element to control the hepatic transcriptome and thus the hepatic physiology. In addition, the orphan nuclear receptor Rev-erb_, a negative regulator of the circadian core gene *bmal1*, is expressed according to a robust circadian pattern and is induced during normal adipogenesis. Conversely, the retinoic acid-related orphan receptors also modulate *bmal1* expression while regulating lipid flux, lipogenesis, and lipid storage in skeletal muscle, providing an additional nodal point interrelating metabolic and circadian physiology. Further studies linked carbohydrate metabolism and circadian rhythms in fruit flies, and strong evidence supports a cross talk mechanism between nuclear hormone receptors and the core circadian complex Clock/Bmal1 in adipogenesis (for a review, see reference 18).

An additional level of complexity arises from experiments showing that many heme-containing molecules regulate cellular homeostasis which, consistent with the circadian oscillatorynature of heme levels, led us to propose heme as a candidate bridge molecule for the circadian and metabolic mechanisms. We and other groups have reported that heme directly targets circadian clock components modulating both gene transcription and protein stability (6, 15, 43; this article). We established that heme directly binds to a novel regulatory motif in hPer2 in a redox-dependent manner, resulting in hPer2 instability and altered hPer2/hCry1 formation. Therefore, we propose that hPer2 acts as a heme sensor-transducer molecule, coupling metabolic signals to the circadian oscillator.

Control of Per2 stability plays a key role in driving circadian rhythmicity (31). During the transcription-translational feedback loop, Per2 is rapidly degraded as a result of phosphorylation by the double-time kinase in *Drosophila* (27) or CKIε in mammals (3), altering the levels of Per2 available for heterodimerization and nuclear translocation. Although phosphorylation remains the primary mechanism responsible for Per2 degradation, alternative mechanisms to control its stability might exist. We tested the simplest model in which binding of heme to hPer2 induces protein instability in a phosphorylation-independent fashion. Indeed, heme favors hPer2 degradation both in vitro and in vivo. More importantly, this event is independent of both phosphorylation by CKIε and binding of heme to the PAS domain, indicating that degradation of hPer2 can occur by alternative mechanisms. Period protein turnover is mediated by ubiquitination and further degradation by the proteasome pathway (39). Our data agreed, showing that inhibitors of proteasome function restore hPer2 levels, supporting a model where heme-mediated degradation of hPer2 depends on ubiquitination. Similarly, heme-mediated ubiquitination and degradation exist in iron regulatory proteins in other systems (13). Specifically, IRP2 oxidation, which is mediated by heme binding to its regulatory domain, triggers IRP2 ubiquitination-dependent degradation regulating the expression of genes involved in iron metabolism (13, 14, 41). In addition, the DNA-binding activity of the transcriptional repressor Bach1 dramatically decreases upon heme binding through multiple HRMs (23, 36), inducing nuclear export of Bach1 (37), polyubiquitination, and degradation of the repressor (44). Heme also binds to the bacterial iron response regulator through two distinct regions including an HRM, a necessary interaction for normal degradation (28, 29, 42). In this scenario, both redox states are required for rapid turnover of Irr, although its stability is independent of ubiquitination and likely mediated by an unknown specific protease (42). Like IRP2 and Irr, heme-dependent degradation of hPer2 is mediated by a CP core of a HRM. Unlike IRP2, where the Cys and His residues within the HRM participate in coordination and are responsible for axial ligand of ferric and ferrous heme (13), the HRM of hPer2 lacks the His component found in the HRM of IRP2 and exclusively binds ferric heme. More importantly, whereas oxidized heme binds to bothHRMand PAS of hPer2, it is only its interaction with the former that is responsible

for hPer2 degradation. This is the first demonstration of ligandinduced instability of a clock gene product and is a novel mode of regulation of the circadian feedback loop.

To understand the mechanism underlying heme-hPer2 recognition, we studied whether conformational changes are associated with ligand binding and heterodimeric complex formation. It is not known whether or to what extent heme binding to hPer2 plays a role in hPer2/hCry1 complex formation. Examples show slight secondary structural changes in helicity in the electron transport protein cytochrome b_{562} upon heme binding (16), whereas large changes in secondary structure are revealed when the His-rich protein II is compared to the apoprotein after ferric heme addition (33). Our secondary structural studies of the C-terminal domain of hPer2 show that heme binding does not induce major conformational changes in the protein, suggesting that degradation of hPer2 does not result from unfolding upon ligand binding but is most likely mediated by an unknown, specific ubiquitin ligase enzyme. Much has been done to identify the molecules responsible for selective recognition of oxidized target proteins, including the recent characterization of the heme-oxidized IRP2 ubiquitin ligase-1 responsible for IRP2 turnover (13, 41). Interestingly, mPer2 ubiquitination is reduced by its interaction with Cry and is mediated by the Cry-binding domain residing in the Cterminal portion of mPer2 (9, 19), a mode of regulation closely resembling the organization of the Per/Tim loop in *Drosophila* (17).

All of these findings raise the question of whether heme binding to the C terminus of hPer2 prevents the formation of the hPer2/hCry1 complex or rather perturbs the stability of an already preformed heterodimer. Here, we provide evidence that heme acts by preventing hPer2 from binding to hCry1 when bound to HRM, whereas heme-PAS binding neither promotes hPer2 degradation nor affects hCry1 association. Heme binding to PAS plays a role in mPer2 interaction with the Bmal1/NPAS2 complex and in its transcriptional activity (15). Accordingly, cyanocobalamin, a vitamin B_{12} analogue with a similar porphyrin ring structure to heme, greatly decreases the binding of NPAS2 and mPer2 to a heme-agarose matrix (15). The overall data are reconciled in a model where heme binding to either HRM or PAS in hPer2 targets different circadian complexes for regulation, likely connecting the cellular response to changes in heme levels. Furthermore, we propose that selectivity of binding is dictated by the redox state of the iron core in the heme molecule. Last, we demonstrate that transcription of the orphan nuclear receptor *Rev-erb_*, a major regulator of the circadian oscillator that influences period length and affects the phase-shifting properties of the clock, is responsive to heme binding to the HRM of hPer2. These experiments add a new level of regulation in circadian gene expression by directly coupling metabolic sensing to the transcriptional control of the molecular oscillator.

ACKNOWLEDGMENTS

We thank William Huckle (Virginia Tech) and Mark O'Brian (SUNY, Buffalo) for critical reading of the manuscript and all members of the Finkielstein laboratory for help and discussions. We are grateful to Steven L. McKnight (University of Texas Southwestern Medical Center) for providing us with the hPer2 and hCry1 cDNAs. This work was supported by the Jeffress Memorial Trust, American Heart Association, and Susan G. Komen Foundation (C.V.F.) and Wendy Will Case and Concern Foundations (D.G.S.C.). J.Y. is partially funded by an AdvanceVT postdoctoral fellowship (NSF SBE-0244916). A.L. is a Wilkins-Fralin Research Fellow and Sigma Xi Scholar. K.D.K. and K.E.D. are Sigma Xi Scholars.

J.Y. performed all experiments except those mentioned below. A.L. and D.G.S.C. performed and analyzed CD experiments, C.V.F. performed immunofluorescence experiments, and K.D.K. performed the in vitro hPer2/hCry1 binding and fluorescence spectroscopy experiments. D.G.S.C. processed and analyzed the fluorescence data. K.E.D., C.S.S., and S.P.M. performed the experiments described in the supplemental material and provided technical support at various stages of the project. C.V.F., D.G.S.C., and J.Y. analyzed the overall data. C.V.F. wrote the manuscript.

REFERENCES

1. **Balsalobre, A., F. Damiola, and U. Schibler.** 1998. A serum shock induces circadian gene expression in mammalian tissue culture cells. Cell **93:**929–937.
2. **Balsalobre, A., L. Marcacci, and U. Schibler.** 2000. Multiple signaling pathways elicit circadian gene expression in cultured Rat-1 fibroblasts. Curr. Biol. **10:**1291–1294.
3. **Camacho, F., M. Cilio, Y. Guo, D. M. Virshup, K. Patel, O. Khorkova, S. Styren, B. Morse, Z. Yao, and G. A. Keesler.** 2001. Human casein kinase Idelta phosphorylation of human circadian clock proteins period 1 and 2. FEBS Lett. **489:**159–165.
4. **Chen, J. J., and I. M. London.** 1995. Regulation of protein synthesis by heme-regulated eIF-2 alpha kinase. Trends Biochem. Sci. **20:**105–108.
5. **Crews, S. T., and C. M. Fan.** 1999. Remembrance of things PAS: regulation of development by bHLH-PAS proteins. Curr. Opin. Genet. Dev. **9:**580–587.
6. **Dioum, E. M., J. Rutter, J. R. Tuckerman, G. Gonzalez, M. A. Gilles- Gonzalez, and S. L. McKnight.** 2002. NPAS2: a gas-responsive transcription factor. Science **298:**2385–2387.
7. **Eide, E. J., M. F. Woolf, H. Kang, P. Woolf, W. Hurst, F. Camacho, E. L. Vielhaber, A. Giovanni, and D. M. Virshup.** 2005. Control of mammalian circadian rhythm by CKIε-regulated proteasome-mediated PER2 degradation. Mol. Cell. Biol. **25:**2795–2807.
8. **Gilles-Gonzalez, M. A., and G. Gonzalez.** 2005. Heme-based sensors: defining characteristics, recent developments, and regulatory hypotheses. J. Inorg. Biochem. **99:**1–22.
9. **Griffin, E. A., Jr., D. Staknis, and C. J. Weitz.** 1999. Light-independent role of CRY1 and CRY2 in the mammalian circadian clock. Science **286:**768–771.
10. **Gu, Y. Z., J. B. Hogenesch, and C. A. Bradfield.** 2000. The PAS superfamily: sensors of environmental and developmental signals. Annu. Rev. Pharmacol. Toxicol. **40:**519–561.
11. **Hirai, K., M. Martinkova, J. Igarashi, I. Saiful, S. Yamauchi, S. El-Mashtoly, T. Kitagawa, and T. Shimizu.** 2007. Identification of Cys385 in the isolated kinase insertion domain of heme-regulated eIF2alpha kinase (HRI) as the heme axial ligand by site-directed mutagenesis and spectral characterization. J. Inorg. Biochem. **101:**1172–1179.
12. **Hon, T., A. Hach, H. C. Lee, T. Cheng, and L. Zhang.** 2000. Functional analysis of heme regulatory elements of the transcriptional activator Hap1. Biochem. Biophys. Res. Commun. **273:**584–591.
13. **Ishikawa, H., M. Kato, H. Hori, K. Ishimori, T. Kirisako, F. Tokunaga, and K. Iwai.** 2005. Involvement of heme regulatory motif in heme-mediated ubiquitination and degradation of IRP2. Mol. Cell **19:**171–181.
14. **Iwai, K., R. D. Klausner, and T. A. Rouault.** 1995. Requirements for ironregulated degradation of the RNA binding protein, iron regulatory protein 2. EMBO J. **14:**5350–5357.
15. **Kaasik, K., and C. C. Lee.** 2004. Reciprocal regulation of haem biosynthesis and the circadian clock in mammals. Nature **430:**467–471.
16. **Kamiya, N., Y. Okimoto, Z. Ding, H. Ohtomo, M. Shimizu, A. Kitayama, H. Morii, and T. Nagamune.** 2001. How does heme axial ligand deletion affect the structure and the function of cytochrome b_{562}? Protein Eng. **14:**415–419.
17. **Kloss, B., A. Rothenfluh, M. W. Young, and L. Saez.** 2001. Phosphorylation of period is influenced by cycling physical associations of double-time, period, and timeless in the *Drosophila* clock. Neuron **30:**699–706.
18. **Kohsaka, A., and J. Bass.** 2007. A sense of time: how molecular clocks organize metabolism. Trends Endocrinol. Metab. **18:**4–11.
19. **Kume, K., M. J. Zylka, S. Sriram, L. P. Shearman, D. R. Weaver, X. Jin, E. S. Maywood, M. H. Hastings, and S. M. Reppert.** 1999. mCRY1 and mCRY2 are essential components of the negative limb of the circadian clock feedback loop. Cell **98:**193–205.
20. **Lathrop, J. T., and M. P. Timko.** 1993. Regulation by heme of mitochondrial protein transport through a conserved amino acid motif. Science **259:**522–525.
21. **McCoubrey, W. K., Jr., T. J. Huang, and M. D. Maines.** 1997. Heme oxygenase-2 is a hemoprotein and binds heme through heme regulatory motifs that are not involved in heme catalysis. J. Biol. Chem. **272:**12568–12574.
22. **Nagai, T., K. Igarashi, J. Akasaka, K. Furuyama, H. Fujita, N. Hayashi, M. Yamamoto, and S. Sassa.** 1998. Regulation of NF-E2 activity in erythroleukemia cell differentiation. J. Biol. Chem. **273:**5358–5365.
23. **Ogawa, K., J. Sun, S. Taketani, O. Nakajima, C. Nishitani, S. Sassa, N. Hayashi, M. Yamamoto, S. Shibahara, H. Fujita, and K. Igarashi.** 2001. Heme mediates derepression of Maf recognition element through direct binding to transcription repressor Bach1. EMBO J. **20:**2835–2843.
24. **Pace, C. N., and A. J. Barrett.** 1984. Kinetics of tryptic hydrolysis of the arginine-valine bond in folded and unfolded ribonuclease T1. Biochem. J. **219:**411–417.
25. **Ponka, P.** 1999. Cell biology of heme. Am. J. Med. Sci. **318:**241–256.
26. **Preitner, N., F. Damiola, L. Lopez-Molina, J. Zakany, D. Duboule, U. Albrecht, and U. Schibler.** 2002. The orphan nuclear receptor REV-ERBalpha controls circadian transcription within the positive limb of the mammalian circadian oscillator. Cell **110:**251–260.
27. **Price, J. L., J. Blau, A. Rothenfluh, M. Abodeely, B. Kloss, and M. W. Young.** 1998. *double-time* is a novel *Drosophila* clock gene that regulates PERIOD protein accumulation. Cell **94:**83–95.
28. **Qi, Z., I. Hamza, and M. R. O'Brian.** 1999. Heme is an effector molecule for iron-dependent degradation of the bacterial iron response regulator (Irr) protein. Proc. Natl. Acad. Sci. USA **96:**13056–13061.
29. **Qi, Z., and M. R. O'Brian.** 2002. Interaction between the bacterial iron response regulator and ferrochelatase mediates genetic control of heme biosynthesis. Mol. Cell **9:**155–162.
30. **Raghuram, S., K. R. Stayrook, P. Huang, P. M. Rogers, A. K. Nosie, D. B. McClure, L. L. Burris, S. Khorasanizadeh, T. P. Burris, and F. Rastinejad.** 2007. Identification of heme as the ligand for the orphan nuclear receptors REV-ERBalpha and REV-ERBbeta. Nat. Struct. Mol. Biol. **14:**1207–1213.
31. **Reppert, S. M., and D. R. Weaver.** 2002. Coordination of circadian timing in mammals. Nature **418:**935–941.
32. **Schibler, U., J. Ripperger, and S. A. Brown.** 2003. Peripheral circadian oscillators in mammals: time and food. J. Biol. Rhythms **18:**250–260.
33. **Schneider, E. L., and M. A. Marletta.** 2005. Heme binding to the histidinerich protein II from *Plasmodium falciparum*. Biochemistry **44:**979–986.
34. **Sreerama, N., and R. W. Woody.** 2000. Estimation of protein secondary structure from circular dichroism spectra: comparison of CONTIN, SELCON, and CDSSTR methods with an expanded reference set. Anal. Biochem. **287:**252–260.
35. **Steiner, H., G. Kispal, A. Zollner, A. Haid, W. Neupert, and R. Lill.** 1996. Heme binding to a conserved Cys-Pro-Val motif is crucial for the catalytic function of mitochondrial heme lyases. J. Biol. Chem. **271:**32605–32611.
36. **Sun, J., H. Hoshino, K. Takaku, O. Nakajima, A. Muto, H. Suzuki, S. Tashiro, S. Takahashi, S. Shibahara, J. Alam, M. M. Taketo, M. Yamamoto, and K. Igarashi.** 2002. Hemoprotein Bach1 regulates enhancer availability of heme oxygenase-1 gene. EMBO J. **21:**5216–5224.
37. **Suzuki, H., S. Tashiro, S. Hira, J. Sun, C. Yamazaki, Y. Zenke, M. Ikeda-Saito, M. Yoshida, and K. Igarashi.** 2004. Heme regulates gene expression by triggering Crm1-dependent nuclear export of Bach1. EMBO J. **23:**2544– 2553.
38. **Whitmore, L., and B. A. Wallace.** 2004. DICHROWEB, an online server for protein secondary structure analyses from circular dichroism spectroscopic data. Nucleic Acids Res. **32:**W668–W673.
39. **Yagita, K., F. Tamanini, M. Yasuda, J. H. Hoeijmakers, G. T. van der Horst, and H. Okamura.** 2002. Nucleocytoplasmic shuttling and mCRY-dependent inhibition of ubiquitylation of the mPER2 clock protein. EMBO J. **21:**1301–1314.
40. **Yagita, K., S. Yamaguchi, F. Tamanini, G. T. van Der Horst, J. H. Hoeijmakers, A. Yasui, J. J. Loros, J. C. Dunlap, and H. Okamura.** 2000. Dimerization and nuclear entry of mPER proteins in mammalian cells. Genes Dev. **14:**1353–1363.
41. **Yamanaka, K., H. Ishikawa, Y. Megumi, F. Tokunaga, M. Kanie, T. A. Rouault, I. Morishima, N. Minato, K. Ishimori, and K. Iwai.** 2003. Identification of the ubiquitin-protein ligase that recognizes oxidized IRP2. Nat. Cell Biol. **5:**336–340.
42. **Yang, J., K. Ishimori, and M. R. O'Brian.** 2005. Two heme binding sites are involved in the regulated degradation of the bacterial iron response regulator (Irr) protein. J. Biol. Chem. **280:**7671–7676.

43. **Yin, L., N. Wu, J. C. Curtin, M. Qatanani, N. R. Szwergold, R. A. Reid, G. M. Waitt, D. J. Parks, K. H. Pearce, G. B. Wisely, and M. A. Lazar.** 2007. Rev-erbalpha, a heme sensor that coordinates metabolic and circadian pathways. Science **318:**1786–1789.
44. **Zenke-Kawasaki, Y., Y. Dohi, Y. Katoh, T. Ikura, M. Ikura, T. Asahara, F. Tokunaga, K. Iwai, and K. Igarashi.** 2007. Heme induces ubiquitination and degradation of the transcription factor Bach1. Mol. Cell. Biol. **27:**6962–6971.
45. **Zhang, L., and L. Guarente.** 1995. Heme binds to a short sequence that serves a regulatory function in diverse proteins. EMBO J. **14:**313–320.
46. **Zheng, B., U. Albrecht, K. Kaasik, M. Sage, W. Lu, S. Vaishnav, Q. Li, Z. S. Sun, G. Eichele, A. Bradley, and C. C. Lee.** 2001. Nonredundant roles of the mPer1 and mPer2 genes in the mammalian circadian clock. Cell **105:**683–694.

Figure Legends

FIG. 1. Heme modulates hPer2 stability in vitro and in vivo. (A, top) ^{35}S-labeled hPer2 ([^{35}S]-hPer2) [^{35}S-hPer2(II-III) in panel B and ^{35}S-hPer2(S$_{662}$A) in panel C] was added to CHO cell extracts in the absence or presence of hemin (10 μM and 100 μM) and incubated at 37°C. Aliquots were removed at 0, 1, and 2 h and resolved by SDS-PAGE and autoradiography. In other experiments, CHO extracts were preincubated with MG-132 before the addition of ^{35}S-hPer2 and hemin (10 μM). Bands were quantified using an AlphaImager and normalized to the input amount (at time zero in bottom panels). The figure shows data from a single experiment that was repeated three times with similar results. The arrows on the right denote radiolabeled protein. The positions of molecular mass markers (in kilodaltons) are indicated to the left of the gels. (D) CHO cells were incubated with hemin (10 μM) for 2, 4, 6, 8, 10, or 12 h in serum-free medium. Samples were collected at the indicated times, and endogenous levels of hPer2 were analyzed by immunoblotting (top panel). Bands were quantified using an AlphaImager and normalized to tubulin levels (bottom right panel). Total RNA was isolated from cells harvested at each time point (in hours) and converted to cDNA in reactions that contain equivalent amounts of total RNA. Gene-specific primers (Per2 and GAPDH) were used for PCR amplification. GAPDH was used as internal control (bottom left panel). (E) CHO cells were treated with succinylacetone (SA) to deplete cells of endogenous heme. After removal of the medium, cells were incubated with either serum-free medium (control), SA, or SA plus hemin (10 μM). Extracts were subjected to SDS-PAGE and immunoblotting. Total protein levels were monitored by either tubulin or actin expression (bottom panels).

FIG. 2. Heme binds hPer2 in two distinct regions. (A) Schematic representation of hPer2 (1,255 residues) architecture including the PAS domain (residues 186 to 434) and the PAS-A (residues 186 to 235) and PAS-B (residues 322 to 374) subdomains. Fragments hPer2(I) (residues 1 to 172), hPer2(II) (residues 173 to 355), hPer2(III) (residues 356 to 574), hPer2(II-III) (residues 173 to 574), and hPer2(V4-VII) (residues 822 to 1,255) are represented below. (B) GST-tagged hPer2 fragments were purified using affinity chromatography (left panel). Samples were analyzed for hemin binding using hemin-agarose (right panel).

FIG. 3. A novel heme-regulatory motif is present in hPer2. (A) Sequence alignment of the surrounding residues of the putative HRMs (SC$_{841}$PA and AC$_{962}$PA) in hPer2 and its homologs in other species. Multiple alignment was performed with the program BenchWork and refined manually. The numbers at the beginning and end of the top sequence correspond to the positions of the first and the last amino acid residues in hPer2. Conserved residues (blue), similar residues (pink), identical residues (purple), and nonconserved residues (black) are indicated. The CP cores in both HRMs of hPer2 are boxed. (B) Absorption spectra of hemin (1 μM) in the presence of various constructs of hPer2(V4-VII) were recorded between 300 and 700 nm on a Beckman DU640 spectrophotometer. (C) GST-hPer2(V4) (residues 822 to 872) and -hPer2(V4-SA$_{841}$PA) were purified and analyzed for heme binding using agarose-hemin beads. The arrow on the right denotes the recombinant protein. The positions of molecular mass markers (Mks) (in kilodaltons) are indicated to the left of the gel.

FIG. 4. Heme binds to the PAS domain and the HRM motif. (A) Absorption spectra of ferric heme (hemin) for GST-hPer2(V4), -hPer2(V4-SA$_{841}$PA), and -hPer2(III). (B) Absorption spectra of hemin after the addition of increasing concentration of GST-hPer2(V4), GST-hPer2(V4-SA$_{841}$PA), and GST-hPer2(III) up to 8 mol equivalent of the hemin amount (black arrow). Free hemin spectrum is indicated with a red arrow. (C) Titration curves of hemin with increasing amounts of the indicated protein are represented as absorbance at 370 nm [GST-hPer2(V4)], 382 nm [GST-hPer2(V4-SA$_{841}$PA)], and 413 nm [GST-hPer2(III)] as a function of the molar ratios of the protein to hemin.

FIG. 5. Degradation of hPer2 depends exclusively on the redox state of the heme bound to HRM. (A) Absorption spectra of ferrous heme (inset) in the presence of GST, GST-hPer2(III), GST-hPer2(V4), and GST-hPer2(V4-SA$_{841}$PA). (B) CHO cell extracts were incubated with ^{35}S-labeled hPer2 ([^{35}S]-hPer2) in the absence (control) or presence of hemin (25 or 50 _M). In a duplicate set of reactions, hemin was preincubated with DTT before adding radiolabeled protein. Aliquots were taken at different times and analyzed by SDS-PAGE and autoradiography. (C) Bands in panel B were quantified using an AlphaImager system, and values were normalized to the input protein

(time zero). The figure shows data from a single experiment that was repeated three times with similar results. (D) ^{35}S-labeled p27Xic1T$_{204}$D ([^{35}S]- p27Xic1T$_{204}$D) was used as control of extract quality upon DTT addition. Samples were analyzed and later quantified as described above for panels B and C, respectively. (E) Cell-free assays of ^{35}S-labeled hPer2(II-III) {[^{35}S]-hPer2(II-III)} in the absence or presence of hemin with or without DTT addition were performed essentially as described above for panel B. (F) Bands in panel E were quantified as indicated above.

FIG. 6. CD analysis of the heme-binding regions in hPer2. (A) Far-UV CD spectra of untagged hPer2(V4-VII) were collected in the absence (dashed line) or presence (solid line) of hemin (twofold) are shown for simplicity and are similar to the spectra for one- and fourfold excess hemin. Protein folding was confirmed by preincubating the protein with 6 M guanidinium chloride (GdHCl) prior to data recording (gray line). Mean residue ellipticity (MRE) (in degrees cm^2 dmol^{-1} residue^{-1}) is shown on the *y* axis (B) Comparison of the CD spectra of hPer2(V4-VII) (solid line) and hPer2(V4-VII-SA$_{841}$PA) (dashed line) recorded under the same experimental conditions for panel A. (C) CD spectra of free hPer2(IIIII) (solid line) and after twofold excess of hemin (dashed line). (D) GST-hCry1-bound beads were incubated with either ^{35}S-labeled hPer2(II-III) {[^{35}S]-hPer2(II-III)} or ^{35}S-labeled hPer2(V4-VII) in the absence or presence of hemin (10 μM). Complexes were monitored by SDS-PAGE and autoradiography. Bands were quantified using an AlphaImager. Results similar to those presented here were observed in two independent experiments. The positions of molecular mass markers (in kilodaltons) are shown to the left or right of the gel.

FIG. 7. The HRM modulates hPer2 stability in CHO cells. (A) CHO cells were transfected with either *myc*-tagged hPer2 or -hPer2(SA$_{841}$PA) plasmids and incubated with hemin. Expressed proteins and DNA were detected using a Cy3-conjugated anti-*myc* antibody and DAPI, respectively. (B) Profile plots of signal intensity across the cell. Recombinant protein and DNA levels were scored along the white lines shown in panel A and represented as intensity values (red for protein; black for DNA). (C) CHO cells were transfected with either *myc*-hPer2, -hPer2(SA$_{841}$PA), or -hPer2(II-III) and treated with or without hemin. Cell extracts were analyzed for the presence of recombinant proteins by immunoblotting using an anti-*myc* antibody. Bands were quantified using an AlphaImager system, and values were normalized to ß-galactosidase activity. Results similar to those presented here were observed in three independent experiments.

FIG. 8. Binding of heme prevents hPer2/hCry1 heterodimerization. (A) CHO cells were cotransfected with either *myc*-hPer2 or pCS2_(*myc*)$_6$ empty vector and FLAG-hCry1 and treated with hemin (10 μM) as shown in Fig. 7. Extracts were incubated with anti-*myc*-tagged beads, and samples were analyzed by SDS-PAGE and immunoblotting using anti-*myc* and anti-FLAG antibodies (Ab). IP, immunoprecipitation; WB, Western blotting. (B) GST-hCry1-bound beads were incubated with ^{35}S-labeled hPer2 ([^{35}S]-hPer2) in the absence and presence of hemin (10 μM), and binding was monitored by SDS-PAGE and autoradiography. Bands were quantified using an AlphaImager. (C) GST-hCry1-bound beads were incubated with ^{35}S-labeled hPer2 before or after hemin (10 μM) addition. In all cases, beads were exhaustively washed, and samples were analyzed by SDS-PAGE and autoradiography. The figure shows data from a single experiment that was repeated three times with similar results.

FIG. 9. HRM-heme binding modulates the expression of Rev-erb_. (A) CHO cells were transfected with *myc*-hPer2, *myc*-hPer2(SA$_{841}$PA), or empty vector (control) before the cells were shifted to a medium containing 50% horse serum and incubated for 2 h (time zero [see Materials and Methods]). Synchronized cells were then maintained in 5 mM succinylacetone followed by hemin (10 μM) addition (at 24 h). Total RNA was prepared from about 10^7 cells at the times (in hours after serum shock) indicated in the panels, and the relative levels of *Rev-erb_* and *GAPDH* were determined by reverse transcription-PCR. *Rev-erb_* levels were normalized to those of the housekeeping gene. (B) A proposed model for the role of heme binding in hPer2/hCry1 complex formation is depicted. C, C terminus; N, N terminus, ub, ubiquitin; Fe$_{3+}$, ferric heme; Fe$_{2+}$, ferrous heme.

Figure 1

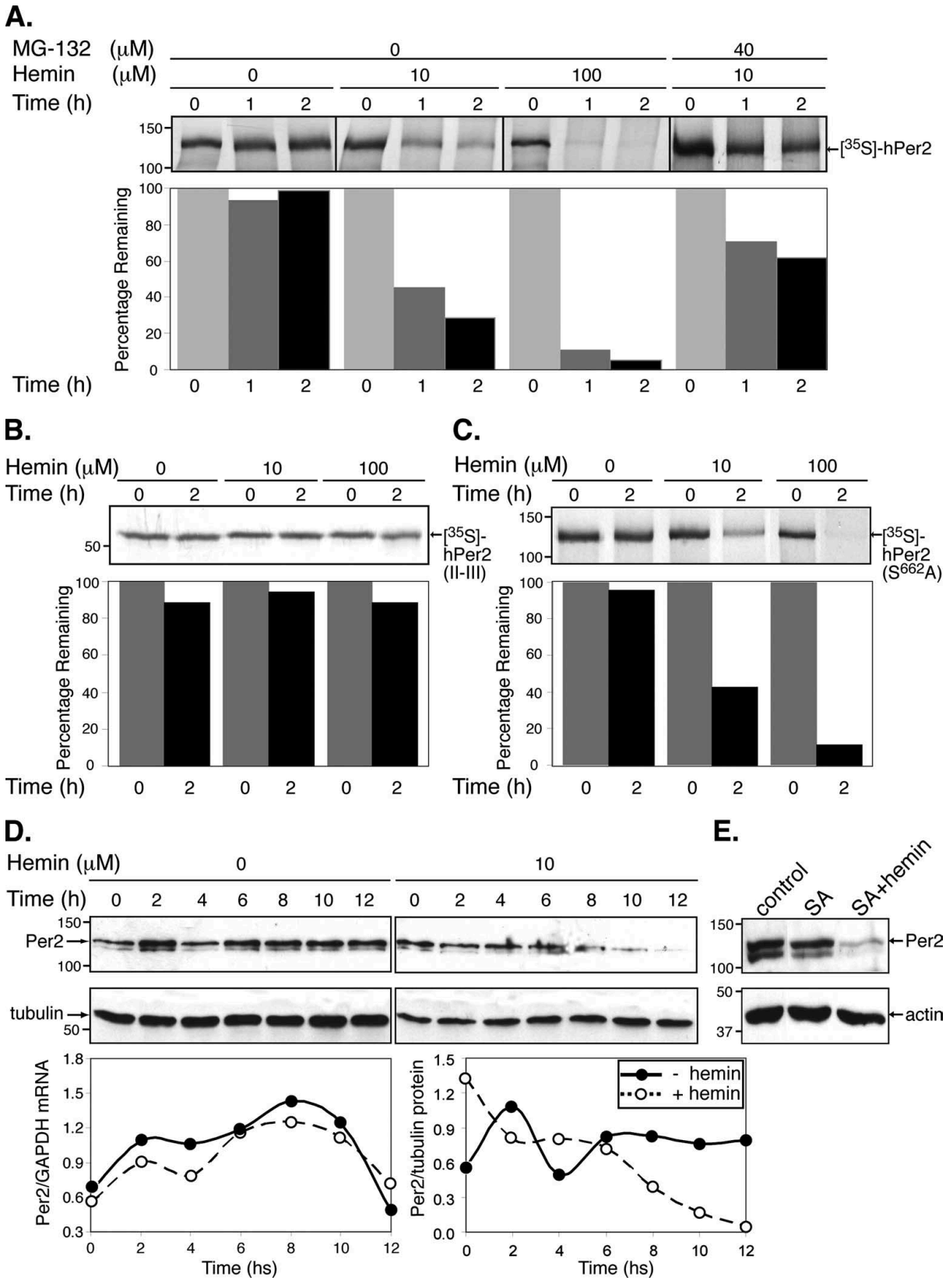
A.
MG-132 (μM)
Hemin (μM)
Time (h)
[35S]-hPer2
Percentage Remaining
B.
[35S]-hPer2 (II-III)
C.
[35S]-hPer2 (S662A)
D.
Per2
tubulin
Per2/GAPDH mRNA
Per2/tubulin protein
- hemin
+ hemin
Time (hs)
E.
control
SA
SA+hemin
actin

Figure 2

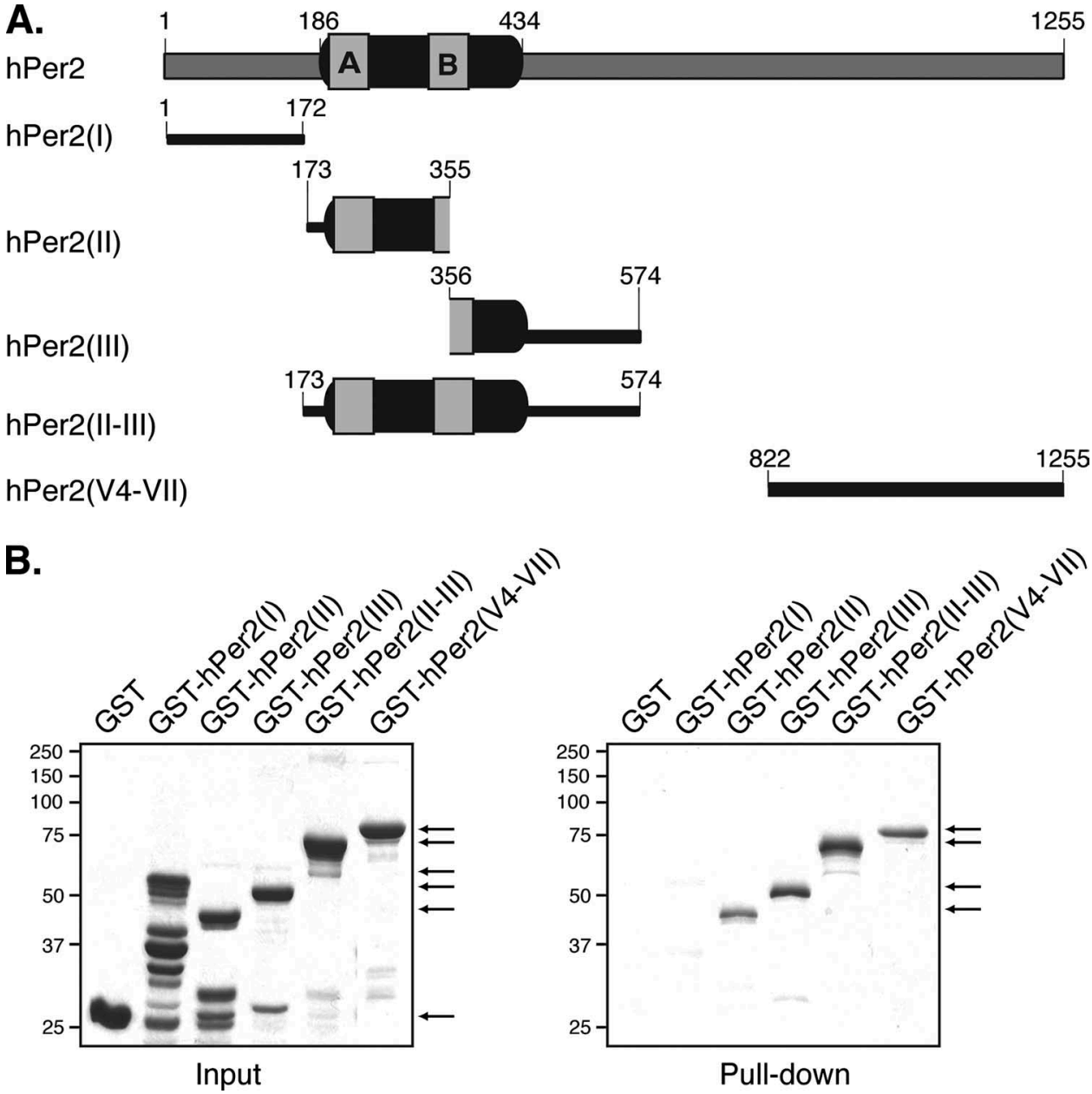
A.
1
186
434
1255
hPer2
A
B
1
172
hPer2(I)
173
355
hPer2(II)
356
574
hPer2(III)
173
574
hPer2(II-III)
822
1255
hPer2(V4-VII)
B.
GST
GST-hPer2(I)
GST-hPer2(II)
GST-hPer2(III)
GST-hPer2(II-III)
GST-hPer2(V4-VII)
250
150
100
75
50
37
25
Input
Pull-down

Figure 3

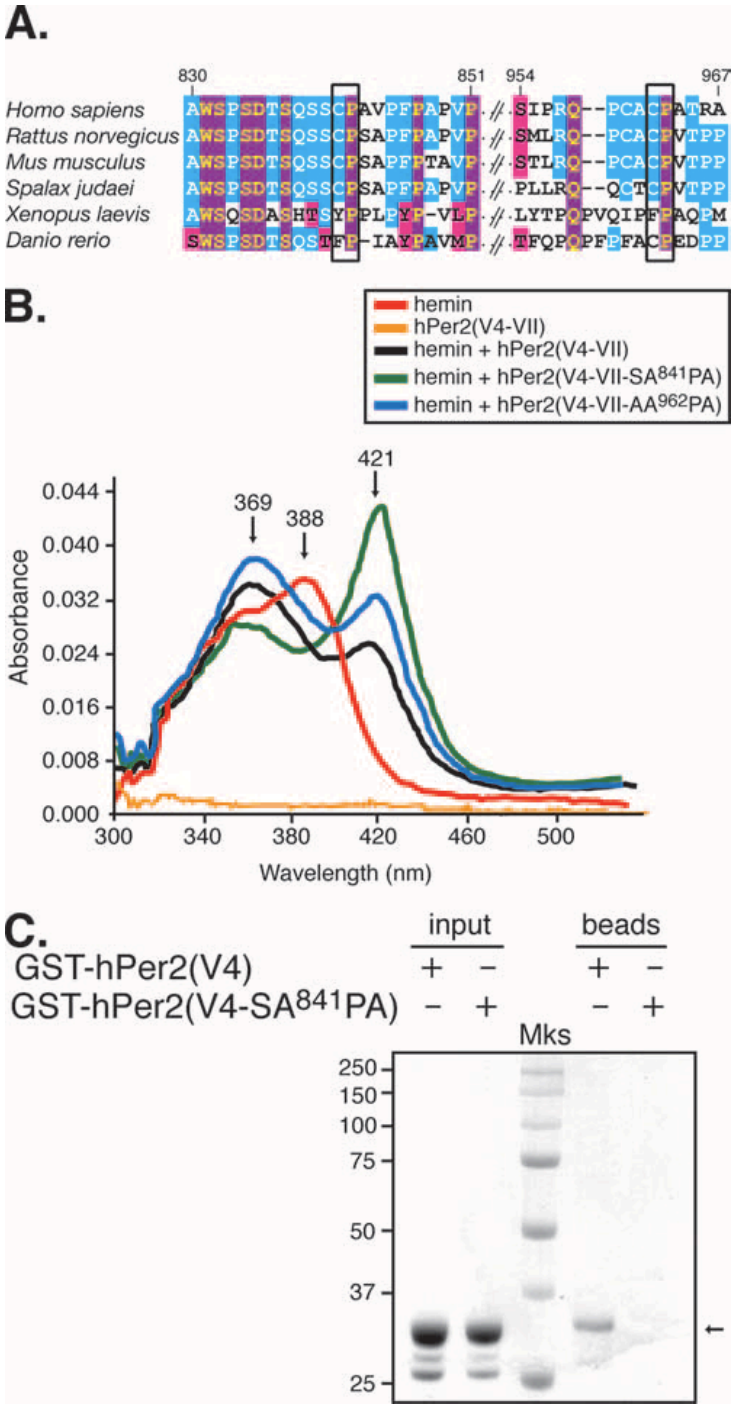
A.
830
851
954
967
Homo sapiens
Rattus norvegicus
Mus musculus
Spalax judaei
Xenopus laevis
Danio rerio
B.
hemin
hPer2(V4-VII)
hemin + hPer2(V4-VII)
hemin + hPer2(V4-VII-SA841PA)
hemin + hPer2(V4-VII-AA962PA)
421
369
388
Absorbance
0.044
0.040
0.032
0.024
0.016
0.008
0.000
300
340
380
420
460
500
Wavelength (nm)
C.
input
beads
GST-hPer2(V4)
GST-hPer2(V4-SA841PA)
Mks
250
150
100
75
50
37
25

Figure 4

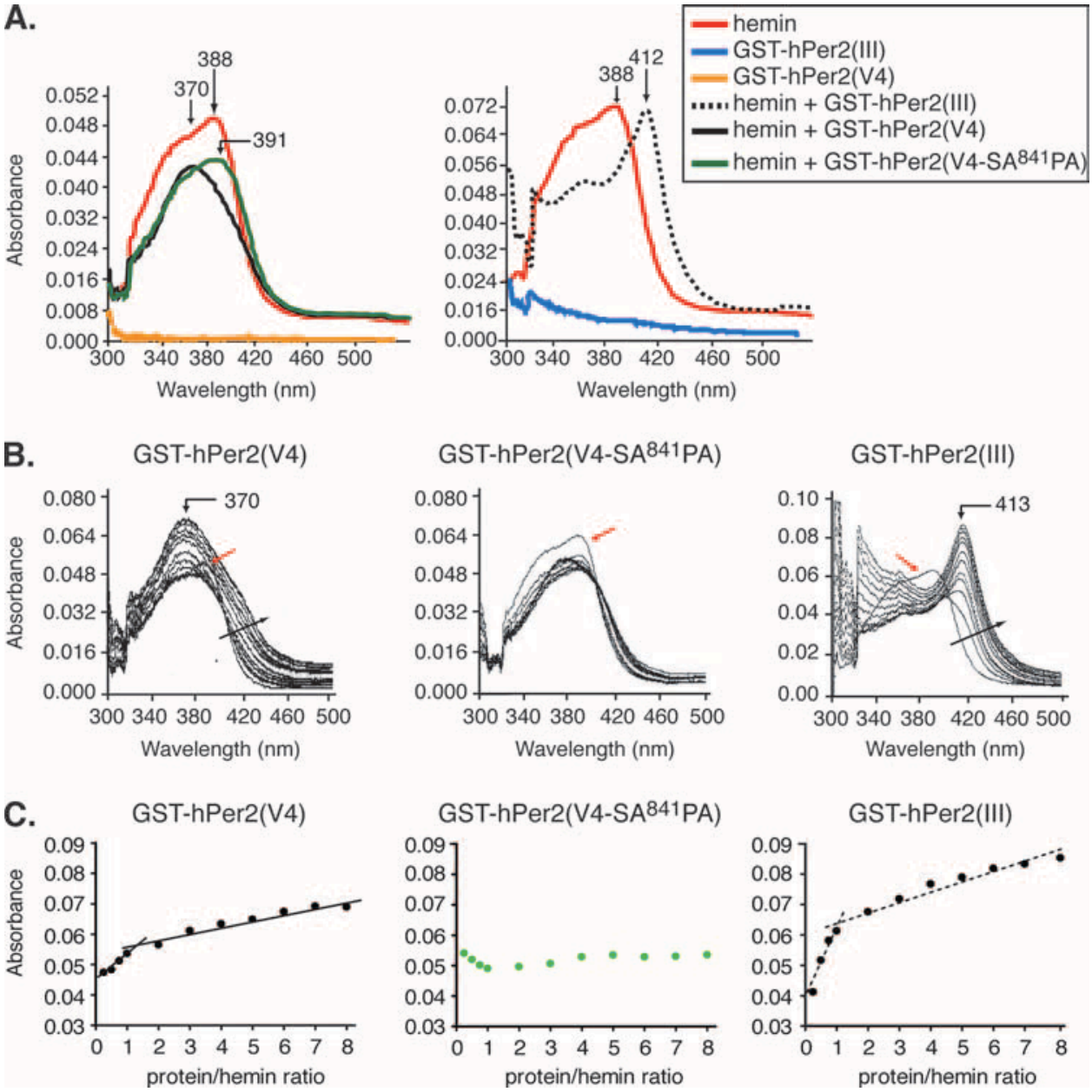
A.
hemin
GST-hPer2(III)
GST-hPer2(V4)
hemin + GST-hPer2(III)
hemin + GST-hPer2(V4)
hemin + GST-hPer2(V4-SA841PA)
Absorbance
Wavelength (nm)
388
370
391
412
B.
GST-hPer2(V4)
GST-hPer2(V4-SA841PA)
GST-hPer2(III)
370
413
C.
protein/hemin ratio

Figure 5

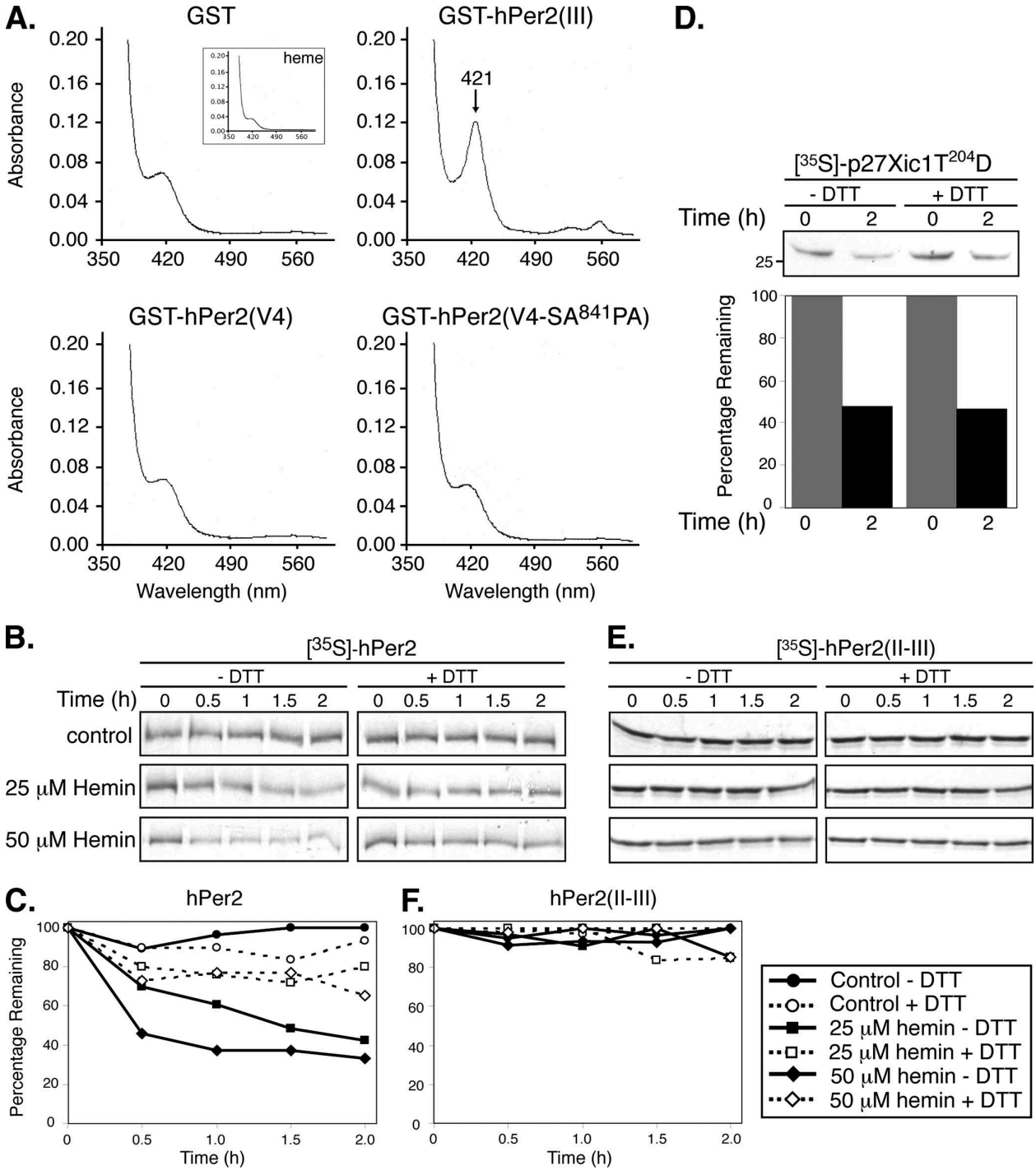
A.
GST
GST-hPer2(III)
heme
421
GST-hPer2(V4)
GST-hPer2(V4-SA841PA)
Absorbance
Wavelength (nm)
D.
[35S]-p27Xic1T204D
- DTT
+ DTT
Time (h)
Percentage Remaining
B.
[35S]-hPer2
control
25 μM Hemin
50 μM Hemin
E.
[35S]-hPer2(II-III)
C.
hPer2
F.
hPer2(II-III)
Control - DTT
Control + DTT
25 μM hemin - DTT
25 μM hemin + DTT
50 μM hemin - DTT
50 μM hemin + DTT

Figure 6

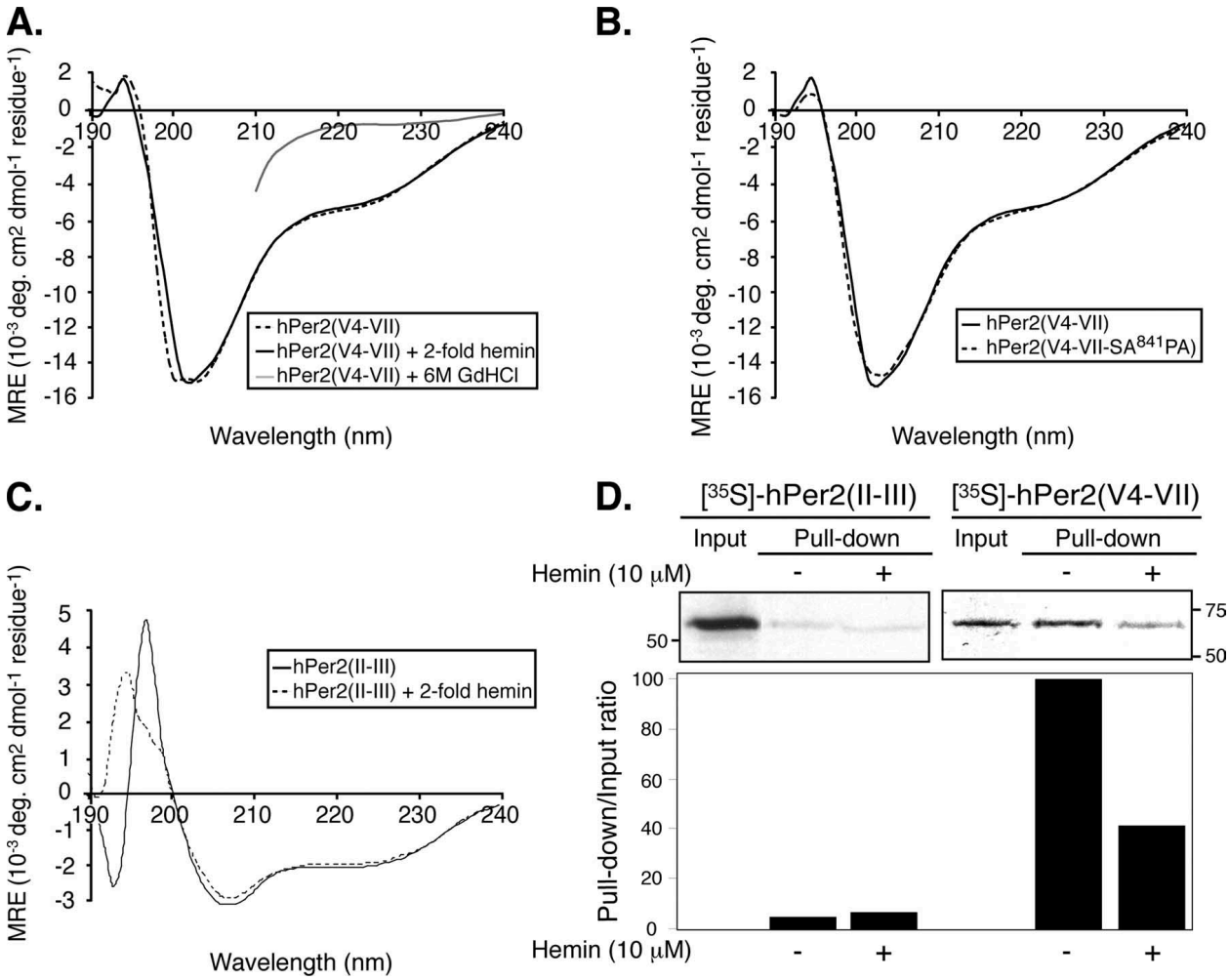
A.
MRE (10-3 deg. cm2 dmol-1 residue-1)
Wavelength (nm)
hPer2(V4-VII)
hPer2(V4-VII) + 2-fold hemin
hPer2(V4-VII) + 6M GdHCl
B.
MRE (10-3 deg. cm2 dmol-1 residue-1)
Wavelength (nm)
hPer2(V4-VII)
hPer2(V4-VII-SA841PA)
C.
MRE (10-3 deg. cm2 dmol-1 residue-1)
Wavelength (nm)
hPer2(II-III)
hPer2(II-III) + 2-fold hemin
D.
[35S]-hPer2(II-III)
[35S]-hPer2(V4-VII)
Input
Pull-down
Hemin (10 μM)
Pull-down/Input ratio

Figure 7

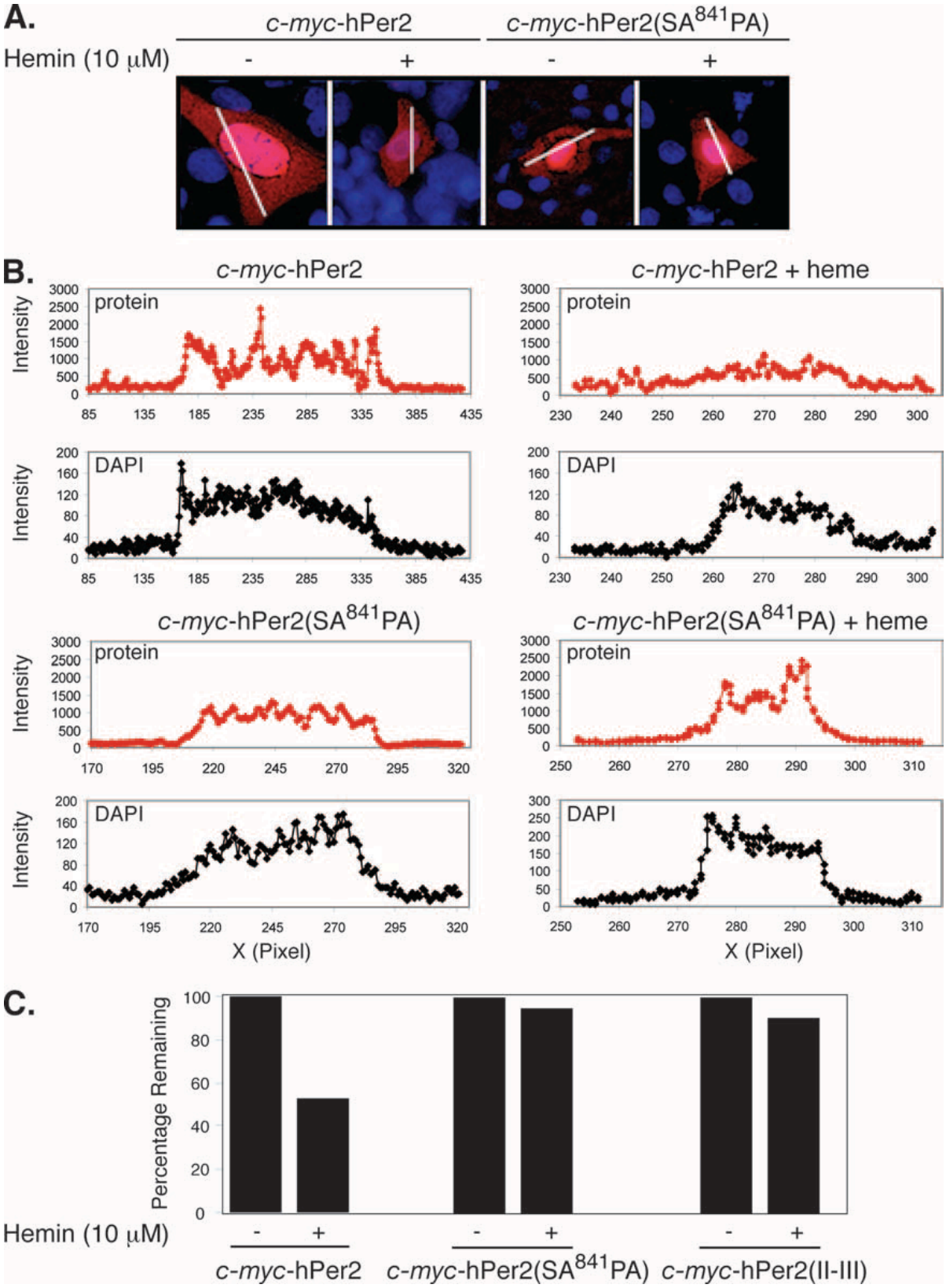
A.
c-myc-hPer2
c-myc-hPer2(SA841PA)
Hemin (10 μM)
- + - +
B.
c-myc-hPer2
c-myc-hPer2 + heme
c-myc-hPer2(SA841PA)
c-myc-hPer2(SA841PA) + heme
protein
DAPI
Intensity
X (Pixel)
C.
Percentage Remaining
Hemin (10 μM)
c-myc-hPer2
c-myc-hPer2(SA841PA)
c-myc-hPer2(II-III)

Figure 8

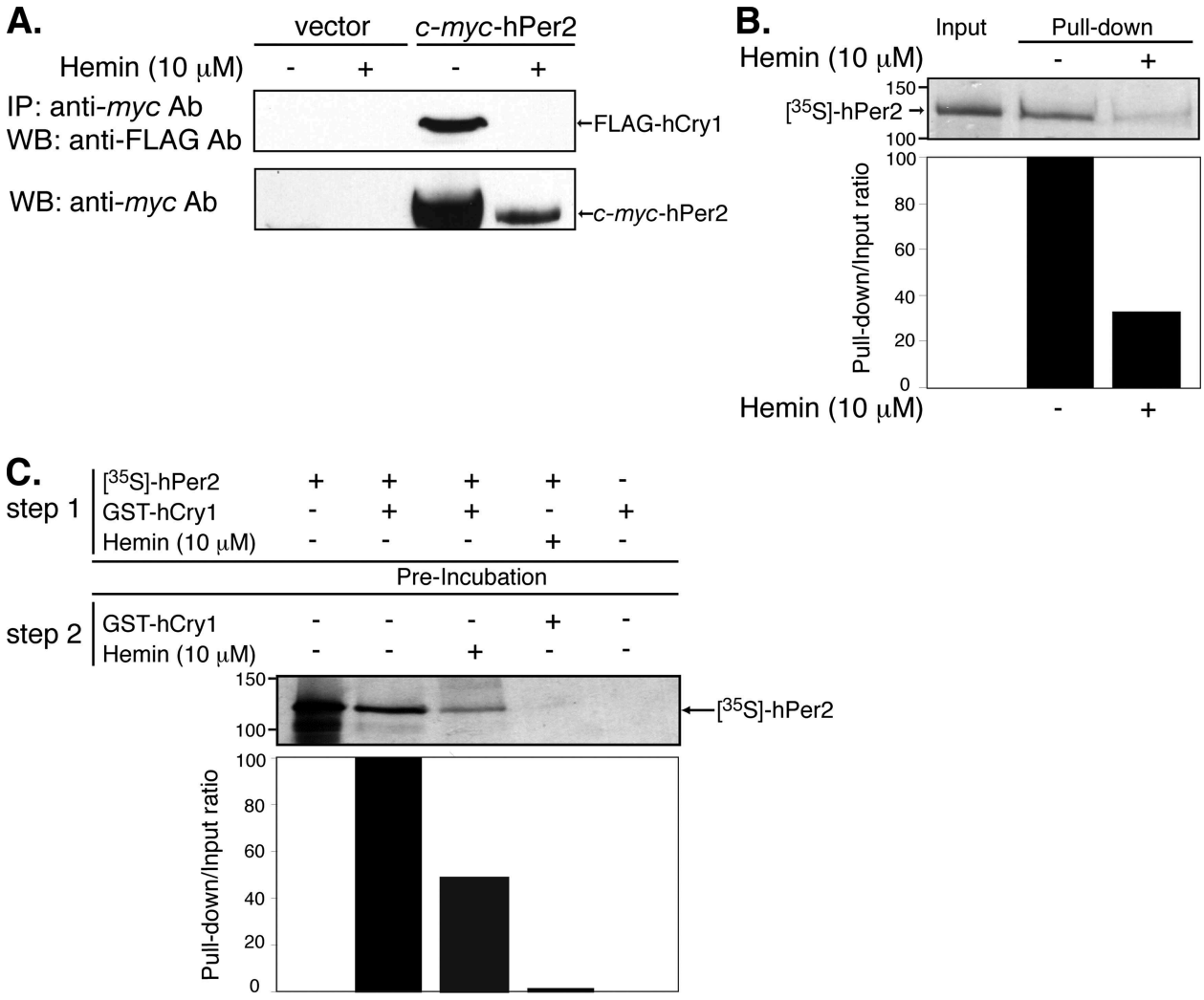
A.
vector
c-myc-hPer2
Hemin (10 μM)
- + - +
IP: anti-myc Ab
WB: anti-FLAG Ab
←FLAG-hCry1
WB: anti-myc Ab
←c-myc-hPer2
B.
Input
Pull-down
Hemin (10 μM)
- +
[35S]-hPer2
150
100
Pull-down/Input ratio
100
80
60
40
20
0
Hemin (10 μM)
- +
C.
step 1
[35S]-hPer2 + + + + -
GST-hCry1 - + + - +
Hemin (10 μM) - - - + -
Pre-Incubation
step 2
GST-hCry1 - - - + -
Hemin (10 μM) - - + - -
150
100
←[35S]-hPer2
Pull-down/Input ratio
100
80
60
40
20
0

Figure 9

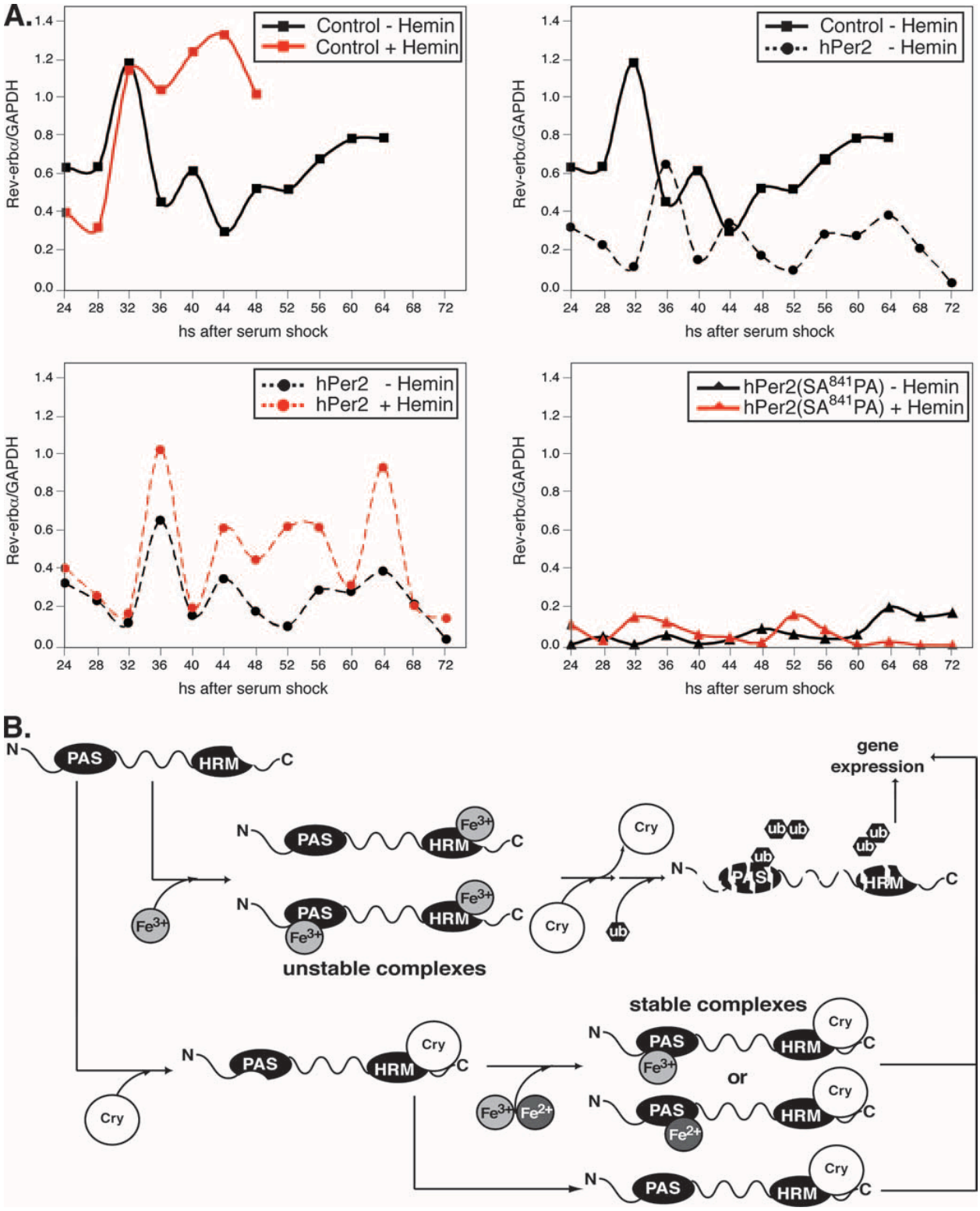
A.
Control - Hemin
Control + Hemin
hPer2 - Hemin
hPer2 + Hemin
hPer2(SA841PA) - Hemin
hPer2(SA841PA) + Hemin
Rev-erbα/GAPDH
hs after serum shock
B.
PAS
HRM
Cry
ub
gene expression
unstable complexes
stable complexes
or

B. Heme Binding to the Translationally Controlled Tumor Protein Induces Oligomerization. Andrew Lucas, Jianhua Yang, Daniel G.S. Capelluto, and Carla Finkielstein. *Publication in process*

Lucas et al. **Figure 1**

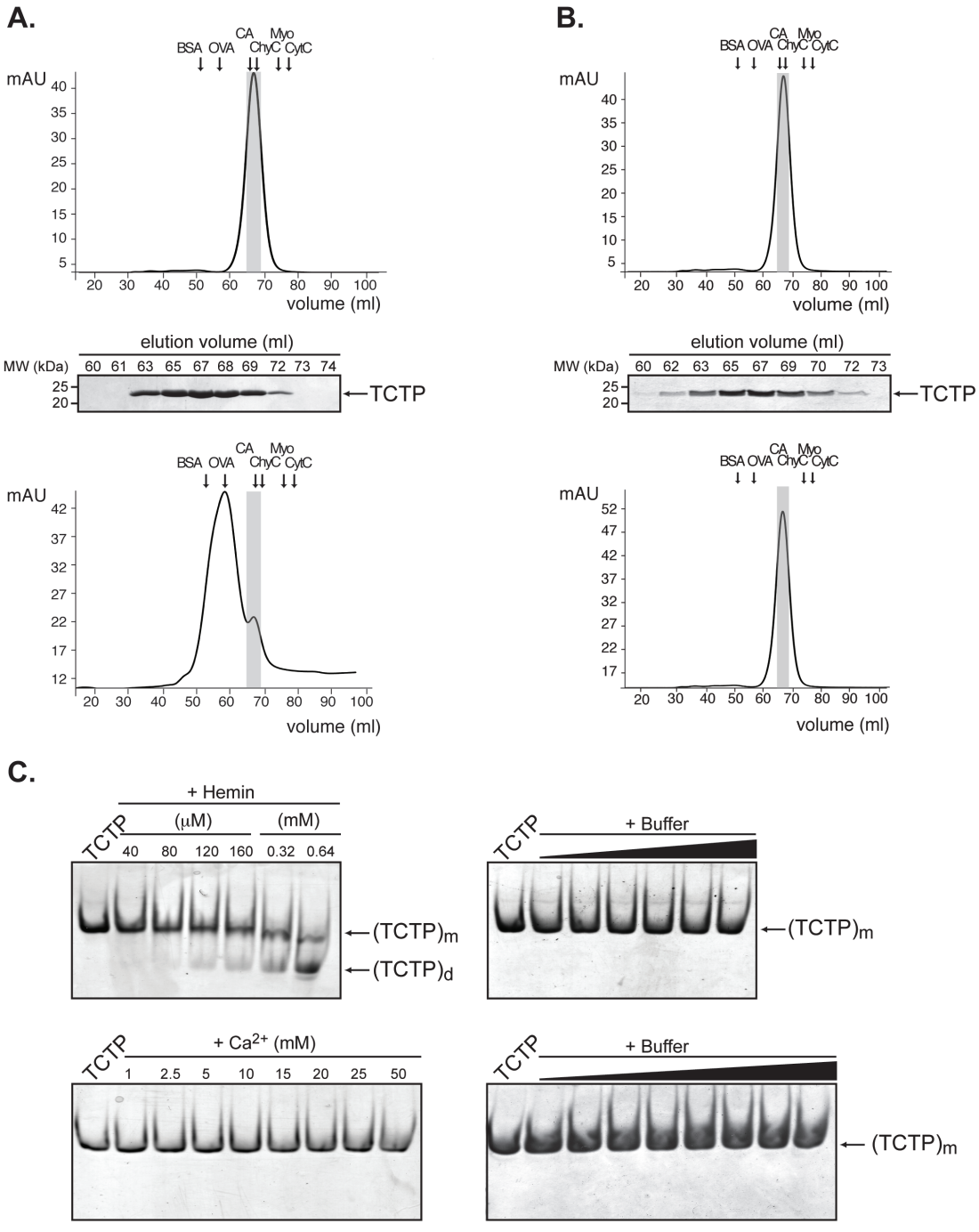

Lucas et al.

Figure 2

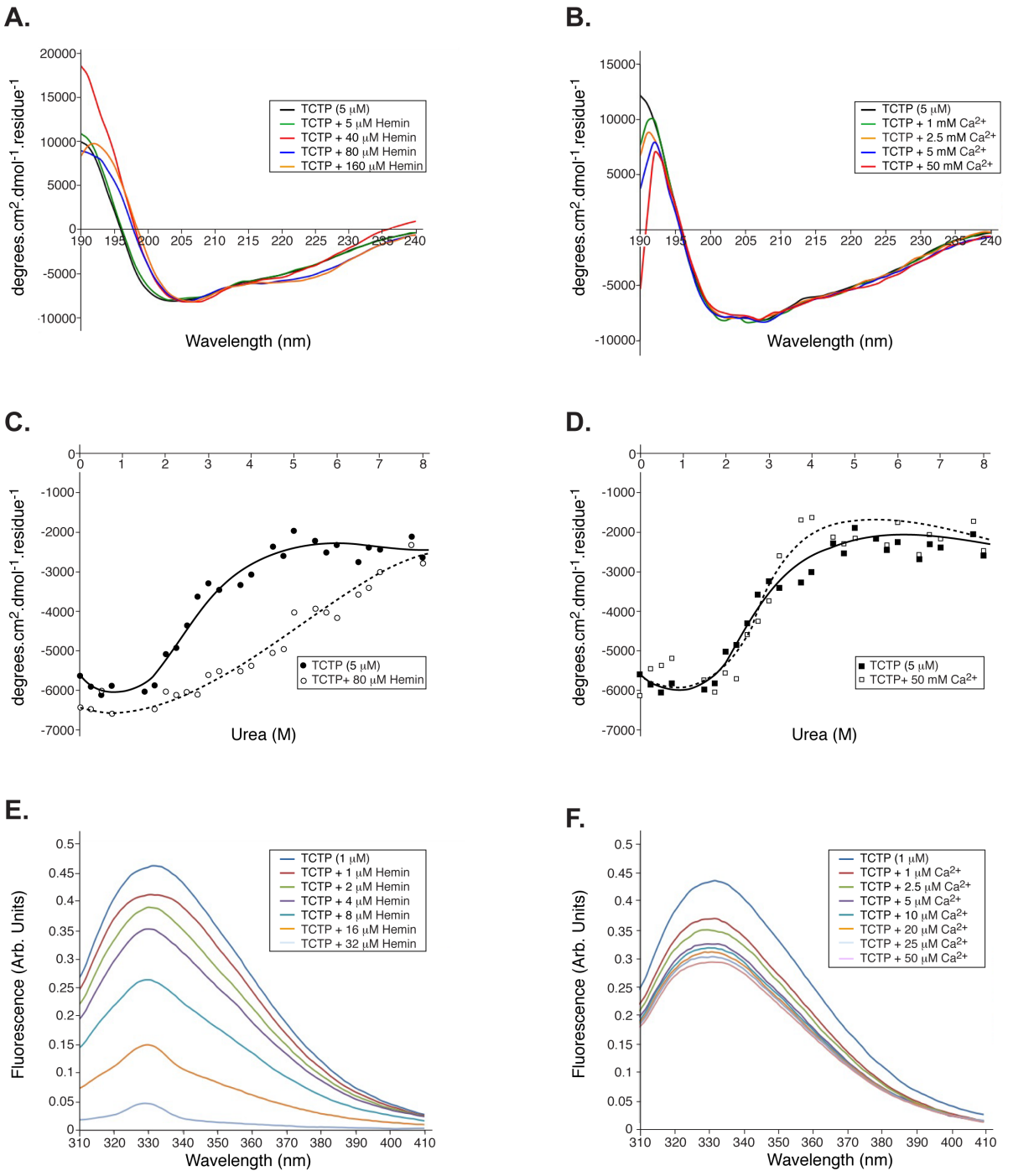

Lucas et al. **Figure 3**

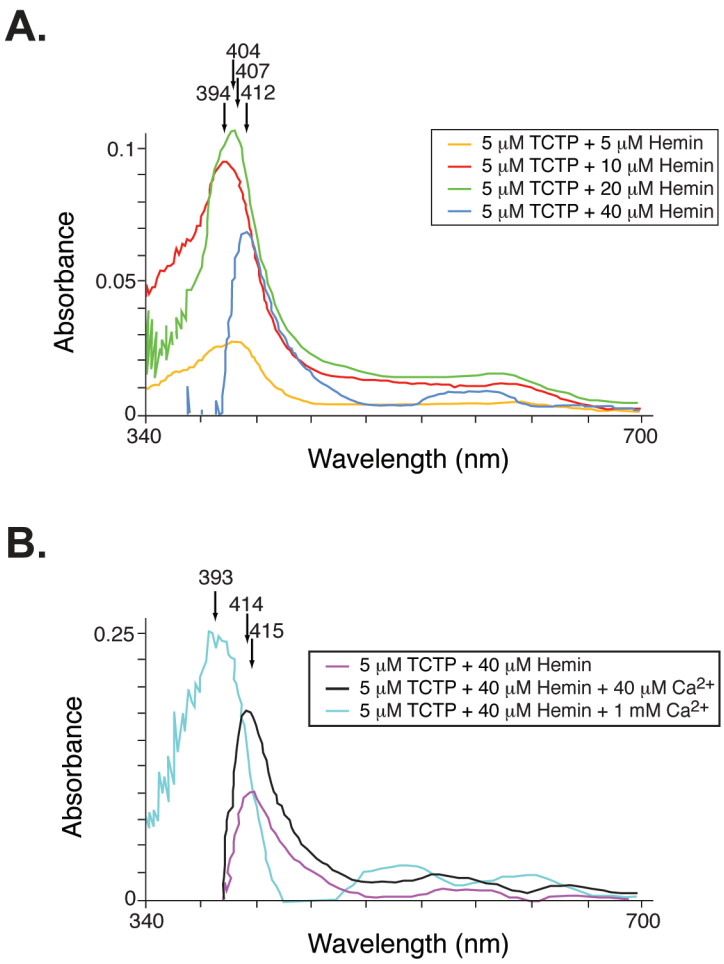

A.

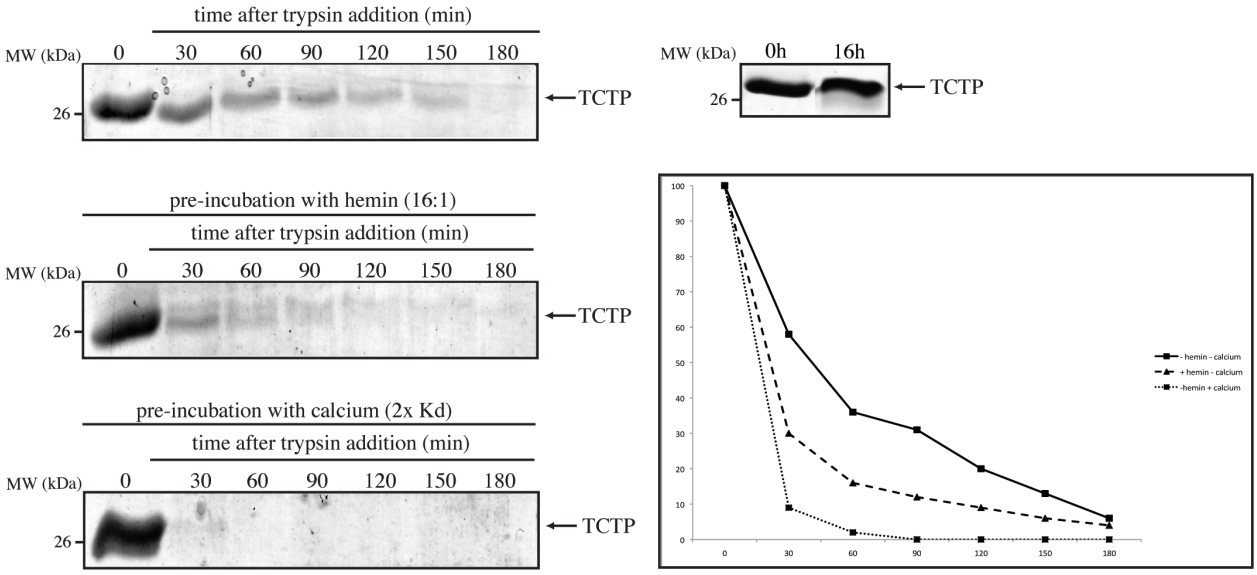
time after trypsin addition (min)
MW (kDa)
0
30
60
90
120
150
180
26
TCTP
MW (kDa)
0h
16h
26
TCTP
pre-incubation with hemin (16:1)
time after trypsin addition (min)
MW (kDa)
0
30
60
90
120
150
180
26
TCTP
pre-incubation with calcium (2x Kd)
time after trypsin addition (min)
MW (kDa)
0
30
60
90
120
150
180
26
TCTP
100
90
80
70
60
50
40
30
20
10
0
0
30
60
90
120
150
180
- hemin - calcium
+ hemin - calcium
-hemin + calcium

B.

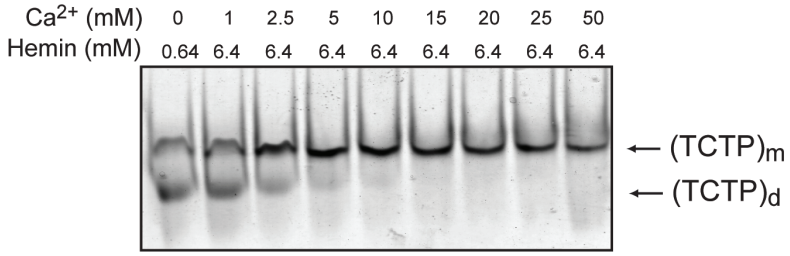
Ca2+ (mM)
0
1
2.5
5
10
15
20
25
50
Hemin (mM)
0.64
6.4
6.4
6.4
6.4
6.4
6.4
6.4
6.4
(TCTP)m
(TCTP)d

Lucas et al. **Figure 5**

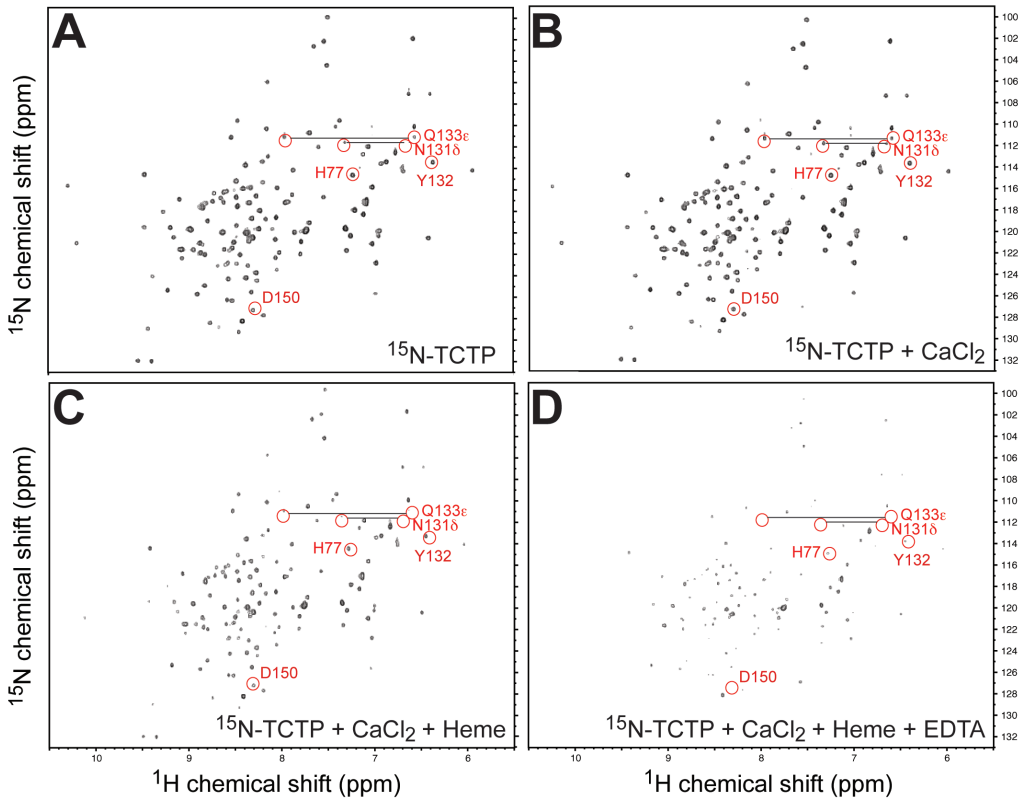

Lucas et al. **Figure 6**

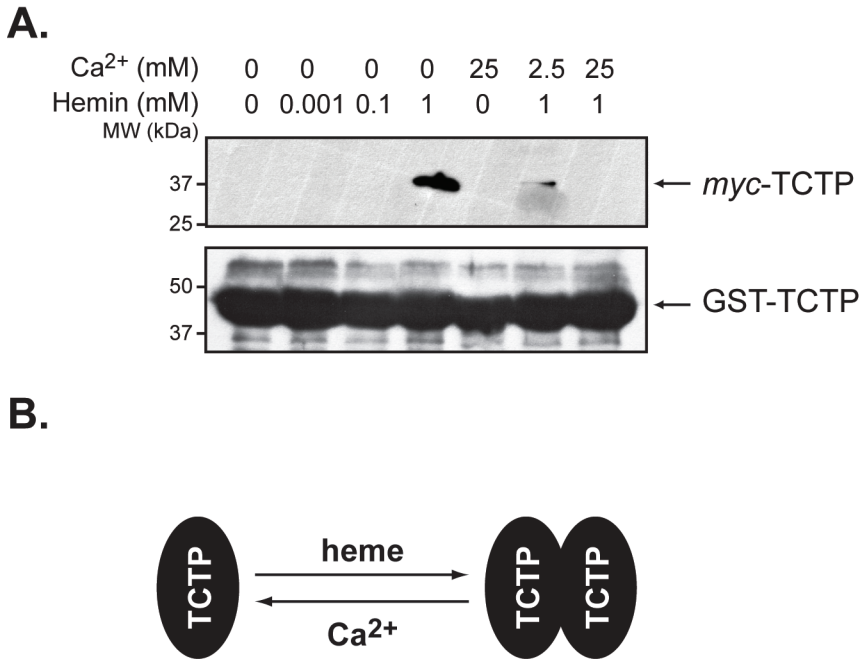

Figure Legends

Figure 1. Analysis of TCTP/heme and TCTP/calcium interaction using gel filtration chromatography and non-denaturing gel electrophoresis. Samples of TCTP were run through a gel filtration column to show a pure, symmetrical absorbance curve. However, with the addition of 1mM heme, a shift is observed in the region about double the molecular weight of TCTP. TCTP samples incubated with calcium chloride showed no change in oligomeric state, represented by a single peak. Pre-incubated sample of TCTP and heme at various ratios were run in non-denaturing gels and we see the formation of a second dimeric band forming after ~4:1 heme:protein ratio. TCTP samples incubated with calcium lack the formation of the oligomeric band that we see when TCTP is incubated with heme.

Figure 2. Analysis of TCTP/heme and TCTP/calcium interaction shows structural conformation change and change to denaturation effects. Scanning the far-UV range, we see that when heme is becoming in excess, TCTP gains structure (A); specifically, denoting an alpha helical structure from a mainly beta structure. However, when incubated with urea (C), the samples containing heme degraded at a slower rate and compared to its counterpart. Fluorescence spectroscopy also demonstrates a near complete quenching as 32:1 heme:protein ratio (E), with a calculated IC50 at 16 μM. Samples incubated with calcium causes no change in overall secondary structure (B), even when added in two-fold excess of its Kd. Samples incubated with urea show no change (D), where the samples mimicked the denaturation of TCTP WT. Fluorescence spectroscopy showed TCTP samples titrated with calcium had an IC50 around 3 mM.

Figure 3. Absorption spectra of TCTP/heme and the effects of calcium. A) The subtracted absorption spectra of TCTP (5 μM) with various levels of heme and calcium between 300 nm and 700 nm. A shift in the Soret peak (394 nm to 412 nm) is observed with increasing level of hemin, which suggests association to either methionine or histidine residues. B) When calcium is added to a sample containing heme, we observe a shift back towards 394 nm, demonstrating the dissociation of heme due to calcium.

Figure 4. Determination of novel interactions between TCTP with heme and calcium interaction demonstrates calcium dissociates the heme induced dimer. The addition of trypsin allows us to determine if a significant tertiary structure change is occurring though digestion. With the addition of 100uM heme, we see a drastic change in the time it takes to digest TCTP; concluding that the structure changes to allow such a digestion. However, addition of calcium to TCTP results in an even faster cleavage by trypsin than the addition of heme, and resulting in different cleavage fragments. Thru non-denaturing gel electrophoresis, samples pre-incubated with excess heme were titrated with calcium chloride. The results were that we saw a disappearance of the oligomer band, allowing us to conclude that calcium dissociates the heme-induced oligomer formation.

Figure 5. NMR titration proves TCTP dimer formation and dissociation. N-15 labeled TCTP samples (A) were incubated with calcium chloride (B); as calcium does not affect TCTP structure, no change in spectra is observed. When hemin is added into the sample (C), we begin to see a line broadening effect due to protein leveing the visible spectra range due to oligoerization. Finally, we add EDTA (D) to absorb all of the calcium in the system and see an even greater line broadening as calcium is no longer present to interfere in dimer formation.

Figure 6. Pulldown of TCTP when mixed with heme shows dimer formation while calcium shows dissociation. Chinese hamster ovary (CHO) cells were transfected with myc-TCTP. Cell extracts were then added to GST-TCTP beads and treated with various levels of heme and/or calcium chloride. We see with increased levels of heme, we observe an increased formation of a TCTP oligomer, proving the reaction in an in vitro cell system. However, we also see the dissociation of the heme induced oligomer with increased levels of calcium, denoting a possible regulator for the TCTP oligomer.

Appendix A: Literature Reference

Chapter 1: Background and Significance

1. Boutros, M. a. M. M. (1999) Dishevelled: at the crossroads of divergent intracellular signaling pathways, *Mechanisms of Development 83*, 27-37.
2. Wallingford, J. B. (2005) The developmental biology of Dishevelled: an enigmatic protein governing cell fate and cell polarity, *Development 132*, 4421-4436.
3. Wharton, K. A. (2003) Runnin' with the Dvl: Proteins That Associate with Dsh/Dvl and Their Significance to Wnt Signal Transduction, *Developmental Biology 253*, 1-17.
4. Wharton, K. A. (2003) Runnin' with the Dvl: Proteins That Associatewith Dsh/Dvl and Their Significance to Wnt Signal Transduction, *Developmental Biology 253*, 1-17.
5. Tada, M., and J.C. Smith. (2000) Xwnt11 is a target of Xenopus Brachyury: regulation of gastrulation movements via Dishevelled, but not through the canonical Wnt pathway, *Development 127*, 2227-2238.
6. Capelluto, D. G. S., Tatiana G. Kutateladze, Raymond Habas, Carla V. Finkielstein, Xi Hek and Michael Overduin. (2002) The DIX domain targets dishevelled to actin stress fibres and vesicular membranes, *Nature 419*, 726-729.
7. Kornau, H. C., Schenker, L. T., Kennedy, M. B. and Seeburg, P. H. (1995) Domain interaction between NMDA receptor subunits and the postsynaptic density protein PSD-95, *Science 269*, 1737-1740.
8. Wong, H. C., Junhao Mao, Jason T. Nguyen, Shamala Srinivas, Weixing Zhang, Bo Liu, Lin Li, Dianqing Wu, and Jie Zheng. (2000) Structural basis of the recognition of the Dishevelled DEP domain in the Wnt signaling pathway, *Nature Structural Biology 7*, 1178-1184.
9. Wallingford, J. B. a. R. H. (2005) The developmental biology of Dishevelled: an enigmatic protein governing cell fate and cell polarity, *Development 132*, 4421-4436.
10. Pan, W. J., and Shu Zhao Pang, Tao Huang, Hui Yun Guo, Dianqing Wu, Lin Li. (2004) Characterization of Function of Three Domains in Dishevelled-1: DEP Domain is Responsible for Membrane Translocation of Dishevelled-1, *Cell Research 14*, 324-330.
11. Wong, H. C., Junhao mao, Jason T. Nguyen, Shamala Srinivas, Weixing Zhang, Bo Liu, Lin Li, Dianqing Wu, and Jie Zheng. (2000) Structural basis of the Recognition of the Dishevelled DEP domain in the Wnt signaling pathway, *Nature Structural Biology 7*, 1178-1184.
12. Schweisguth, F. (2009) When you are Dishevelled, fat is good and acid is bad!, *Nature Cell Biology 11*, 237-239.
13. Simons, M., William J. Gault, Daniel Gotthardt, Rajeev Rohatgi, Thomas J. Klein, Youming Shao, Ho-Jin Lee, Ai-Luen Wu, Yimin Fang, Lisa M. Satlin, Julian T. Dow, Jie Chen, Jie Zheng, Michael Boutros and Marek Mlodzik. (2009) Electrochemical cues regulate assembly of the Frizzled/Dishevelled complex at the plasma membrane during planar epithelial polarization, *Nature Cell Biology 11*, 286-294.
14. Simons, M., William J. Gault, Daniel Gotthardt, Rajeev Rohatgi, Thomas J. Klein, Youming Shao, Ho-Jin Lee, Ai-Luen Wu, Yimin Fang, Lisa M. Satlin, Julian T. Dow, jie Chen, Jie Zheng, Michael Boutros, and Marek Mlodzik. (2009) Electrochemical cues regulate assembly of the Frizzled/Dishevelled complex at the plasma membrane during planar epithelial polarization, *Nature Cell Biology 11*, 286-294.

15. Schweisguth, F. (2009) When you are Dishevelled, fat is good and acid is bad!, *Nature Cell Biology 11*, 237-239.
16. van Gijn, M. E., Mat J.A.P. Daemen, Jos F.M. Smits, W. Matthijs Blankesteijn. (2002) The wnt-frizzled cascade in cardiovascular disease, *Cardiovascular Research 55*, 16-24.
17. Benzing, T., Matias Simons, and Gerd Walz. (2007) Wnt Signaling in Polycystic Kidney Disease, *Journal of the American Society of Nephrology 18*, 1389-1398.
18. Uematsu, K., Biao He, Liang You, Zhidong Xu, Frank McCormick and David Mark Jablons. (2003) Activation of the Wnt pathway in non small cell lung cancer: evidence of dishevelled overexpression, *Oncogene 22*, 7218-7221.
19. McDonald, S. A., Sean L Preston, Matthew J Lovell, Nicholas A Wright and Janusz AZ Jankowski. (2006) Mechanisms of Disease: from stem cells to colorectal cancer, *Nature Clinical Practice 3*, 267-274.
20. Westendorf, J. J., Rachel A. Kahler, Tania M. Schroeder. (2004) Wnt signaling in osteoblasts and bone diseases, *Gene 341*, 19-39.
21. Bienz, M. a. H. C. (2000) Linking colorectal cancer to Wnt signaling, *Cell Research 103*, 311-320.
22. Nagase, H. a. N. Y. (1993) Mutations of the APC (Adenomatous polyposis coli) gene *Human Mutation 2*, 425-434.
23. Smits, R., Kartheuser, A., Jagmohan-Changur, S., Leblanc, V., Breukel, C., de Vries, A., van Kucherlapati, R., KhanPm, and Fodde, R. (1997) Loss of Apc and the entire chromosome 18 but absence of mutations at the Ras and Tp53 genes in intestinal tumors from Apc1638N, a mouse model for Apc-driven carcinogenesis, *Carcinogenesis 18*, 321-327.
24. Pierre Laurent-Puig, C. B. r. a. T. S. (1998) APC gene: database of germline and somatic mutations in human tumors and cell lines, *Nucleic Acids Research 26*, 269-270.
25. Ferrari, G. V. a. N. C. I. (2000) Wnt signaling function in Alzheimer's disease, *Brain Research Reviews 33*, 1-12.
26. Zheng-Fischhofer, Q., J. Biernat, E.M. Mandelkow, S. Illenberger, R. Godemann, E. Mandelkow. (1998) Sequential phosphorylation of Tau by glycogen synthase kinase-3b and protein kinase A at Thr212 and Ser214 generates the Alzheimer-specific epitope of antibody AT100 and requires a paired-helical-filament-like conformation, *European jouranl of Biochemistry 252*, 542-552.

Chapter 3: Results

1. Pan, W. J. a. S. Z. P., Tao Huang, Hui Yun Guo, Dianqing Wu, Lin Li. (2004) Characterization of Function of Three Domains in Dishevelled-1: DEP Domain is Responsible for Membrane Translocation of Dishevelled-1, *Cell Research 14*, 324-330.
3. Simons, M., William J. Gault, Daniel Gotthardt, Rajeev Rohatgi, Thomas J. Klein, Youming Shao, Ho-Jin Lee, Ai-Luen Wu, Yimin Fang, Lisa M. Satlin, Julian T. Dow, jie Chen, Jie Zheng, Michael Boutros, and Marek Mlodzik. (2009) Electrochemical cues regulate assembly of the Frizzled/Dishevelled complex at the plasma membrane during planar epithelial polarization, *Nature Cell Biology 11*, 286-294.
4. Schweisguth, F. (2009) When you are Dishevelled, fat is good and acid is bad!, *Nature Cell Biology 11*, 237-239.

5. Dominguez, C., Bonvin A., Winkler G., van Schaik F., Timmers H., and Boelens, R. (2004) Structural Model of the UbcH5B/CNOT4 Complex Revealed by Combining NMR, Mutagenesis, and Docking Approaches, *Structure 12*, 633-444.
6. Pettersen EF, G. T., Huang CC, Couch GS, Greenblatt DM, Meng EC, Ferrin TE. (2004) UCSF Chimera--a visualization system for exploratory research anda analysis, *Journal of Computational Chemistry 25*, 1605-1612.
7. Simons, M., William J. Gault, Daniel Gotthardt, Rajeev Rohatgi, Thomas J. Klein, Youming Shao, Ho-Jin Lee, Ai-Luen Wu, Yimin Fang, Lisa M. Satlin, Julian T. Dow, Jie Chen, Jie Zheng, Michael Boutros and Marek Mlodzik. (2009) Electrochemical cues regulate assembly of the Frizzled/Dishevelled complex at the plasma membrane during planar epithelial polarization, *Nature Cell Biology 11*, 286-294.
8. Lee, S. A., Rosemary Eyeson, Matthew L. Cheever, Jinming Geng, Vladislav V. Verkhusha, Christopher Burd, Michael Overduin, and Tatiana G. Kutateladze. (2005) Targeting of the FYVE domain to endosomal membranes is regulated by a histadine switch, *PNAS 102*, 13052-13057.

Chapter 4: Discussion and Conclusions

1. Schweisguth, F. (2009) When you are Dishevelled, fat is good and acid is bad!, *Nature Cell Biology 11*, 237-239.
2. Smith, D. G., Giuseppe D. Ciccotosto, Deborah J. Tew, Keyla Perez, Cyril C. Curtain, John F. Boas, Colin L. Masters, Roberto Cappai, Kevin J. Barnham. (2010) Histidine 14 Modulates Membrane Binding and Neurotoxicity of the Alzheimer's Disease Amyloid-β Peptide, *Journal of Alzheimer's Disease 19*, 1387-1400.
3. Dubovskii, P. V., Daria V. Dementieva, Eduard V. Bocharov Yuri N. Utkin and Alexander S. Arseniev. (2001) Membrane Binding Motif of the P-type Cardiotoxin, *Journal of Molecular Biology 305*, 137-149.
4. Heidarian, E., and Bahram Haghighi. (2008) Evidence for Histidine Residues on Plasma Membrane Phosphatidate Phosphohydrolase from Rat Liver, *Iranian Journal of Basic Medical Sciences 11*, 166-173.
5. Gisselssona, A., Anna Szila ´gyia and Hans-Erik Akerlund. (2004) Role of histidines in the binding of violaxanthin de-epoxidase to the thylakoid membrane as studied by site-directed mutagenesis, *Physiologia Plantarum 122*, 337-343.
6. Laskowski, R. A., M.W. MacArthur, D.S. Moss, and J.M. Thornton. (1993) PROCHECK: a program to check the stereochemical quality of protein structures, *Journal of Applied Crystallography 26*, 283-291.
7. Lee, S. A., Rosemary Eyeson, Matthew L. Cheever, Jinming Geng, Vladislav V. Verkhusha, Christopher Burd, Michael Overduin, and Tatiana G. Kutateladze. (2005) Targeting of the FYVE domain to endosomal membranes is regulated by a histadine switch, *PNAS 102*, 13052-13057.
8. Frank, C., Heike Keilhack, Frank Opitz, Olaf Zschornig, and Frank-D. Bohmer. (1999) Binding of Phosphatidic Acid to the Protein-Tyrosine Phosphatase SHP-1 as a Basis for Activity Modulation, *Biochemistry 38*, 11993-12002.
9. Gerber, S. H., Josep Rizo, and Thomas C. Sudhof. (2002) Role of Electrostatic and Hydrophobic Interactions in Ca2-Dependent Phospholipid Binding by the C2A-Domain From Synaptotagmin I, *Diabetes 51*, S12-S18.

10. Salvatella, X., and Ernest Giralt. (2003) NMR-based methods and strategies for drug discovery, *The Royal Society of Chemistry 32*, 365-372.
11. Anstrom, D. M., Leslie Colip, Brian Moshofsky, Eric Hatcher and S. James Remington. (2005) Systematic replacement of lysine with glutamine and alanine in Escherichia coli malate synthase G: effect on crystallization, *Acta Crystallographica 61*, 1069-1074.
12. Aliverti, A., Wilfred R. Hagen, Giuliana Zanetti. (1995) Direct electrochemistry and EPR spectroscopy of spinach ferredoxin mutants with modified electron transfer properties, *FEBS Letters 368*, 220-224.
13. Thuduppathy, G. R., Oihana Terrones, Jeffrey W. Craig, Gorka Basanez, and R. Blake Hill. (2006) The N-Terminal Domain of Bcl-xL Reversibly Binds Membranes in a pH-Dependent Manner, *Biochemistry 45*, 14533-14542.
14. Zhang, P., GerardF. Graminski, and RichardN. Armstrong. (1991) Are the Histidine Residues of Glutathione&Transferase Important in Catalysis?, *Journal of Biological Chemistry 266*, 19475-19479.
15. Chowdary, T. K., Bakthisaran Raman, Tangirala Ramakrishna, and Chintalagiri Mohan Rao. (2004) Mammalian Hsp22 is a heat-inducible small heat-shock protein with chaperone-like activity, *Biochemistry Journal 381*, 379-387.
16. Wallon, G., Juri Rappsilber, Matthias Mann and Luis Serrano. (2000) Model for stathmin/OP18 binding to tubulin, *EMBO Journal 19*, 213-222.
17. Zhang, K.-L., Bastien Mangeat, Millan Ortiz, Vincent Zoete, Didier Trono, Amalio Telenti, Olivier Michielin. (2007) Model Structure of Human APOBEC3G, *PLoS ONE 2*, e378.
18. Jones, J. A., Robert Rawles, and Yusuf A. Hannun. (2005) Identification of a Novel Phosphatidic Acid Binding Domain in Protein Phosphatase-1, *Biochemistry 44*, 13235-13245.
19. Huang, S., Lisa Gao, Laurent Blanchoin, and Christopher J. Staiger. (2006) Heterodimeric Capping Protein from Arabidopsis Is Regulated by Phosphatidic Acid, *Molecular Biology of the Cell 17*, 1946-1958.
20. Drahos, K. E., John D. Welsh, Carla V. Finkielstein, and Daniel G.S. Capelluto. (2009) Sulfatides Partition Disabled-2 in Response to Platelet Activation, *PLoS One 4*, e8007.
21. Stahelin, R. V., Dimitrios Karathanassis, Karol S. Bruzik, Michael D. Waterfield, Jero ´ nimo Bravo, Roger L. Williams, and Wonhwa Cho. (2006) Structural and Membrane Binding ANalysis of the Phox Homology Domain of Phosphoinositide 3-Kinase-C2alpha, *Journal of Biological Chemistry 281*, 39396-39406.
22. Mann, K. G., M.E. Nesheim, W.R. Church, P. Haley, and S.Krishnaswamy. (1990) Surface-Dependent Reactions of the Vitamin K-Dependent Enzyme Complexes, *Blood 76*, 1-16.
23. Kukic, P., Damien Farrell, Chresten R. Søndergaard, Una Bjarnadottir, John Bradley, Gianluca Pollastri, and Jens Erik Nielsen. (2010) Improving the analysis of NMR spectra tracking pH-induced conformational changes: Removing artefacts of the electric field on the NMR chemical shift, *Proteins 78*, 971-984.
24. Nolting, D., Emad F. Aziz, Niklas Ottosson, Manfred Faubel, Ingolf V. Hertel, and Bernd Winter. (2007) pH-Induced Protonation of Lysine in Aqueous Solution Causes Chemical Shifts in X-ray Photoelectron Spectroscopy, *Journal of the American Chemical Society 129*, 14068-14073.

25. Tu, Z., Albert Young, Christopher Murphy and Jun F. Liang. (2009) The pH sensitivity of histidine-containing lytic peptides, *Journal of Peptide Science 15*, 790-795.
26. Zong, X., Juliane Stieber, Andreas Ludwig, Franz Hofmann, and Martin Biel. (2000) A Single Histidine Residue Determines the pH Sensitivity of the Pacemaker Channel HCN2, *Journal of Biological Chemistry 276*, 6313-6319.
27. Lakowicz, J. R. (2001) *Topics in Fluorescence Spectroscopy: Protein Fluorescence*, Vol. 6, pringer, New York.
28. Hoffman, L. R., I.D. Kuntz, and Judith M. White. (1997) Structure-Based Identification of an Inducer of the Low-pH Conformational Change in the Influenza Virus Hemagglutinin: Irreversible Inhibition of Infectivity, *Journal of Virology 71*, 8808-8820.
29. Kampmann, T., Daniela S. Mueller, Alan E. Mark, Paul R. Young, and Bostjan Kobe. (2006) The Role of Histidine Residues in Low-pH-Mediated Viral Membrane Fusion, *Structure 14*, 1481-1487.
30. Mueller, D. S., Thorsten Kampmann, Ragothaman Yennamalli, Paul R. Young, Bostjan Kobe and Alan E. Mark. (2008) Histidine protonation and the activation of viral fusion proteins, *Biochemical Society Transactions 36*, 43-45.
31. Simons, M., William J. Gault, Daniel Gotthardt, Rajeev Rohatgi, Thomas J. Klein, Youming Shao, Ho-Jin Lee, Ai-Luen Wu, Yimin Fang, Lisa M. Satlin, Julian T. Dow, jie Chen, Jie Zheng, Michael Boutros, and Marek Mlodzik. (2009) Electrochemical cues regulate assembly of the Frizzled/Dishevelled complex at the plasma membrane during planar epithelial polarization, *Nature Cell Biology 11*, 286-294.
32. Taneva, S. G., Anthony A. Donchev, Mitko I. Dimitrov, Arturo Muga. (2000) Redox- and pH-dependent association of plastocyanin with lipid bilayers: e¡ect on protein conformation and thermal stability, *Biochemica et Biophysica Acta 1463*, 429-438.
33. Srivastava, J., Diane L. Barber, and Matthew P. Jacobson. (2007) Intracellular pH Sensors: Design Principles and Functional Significance, *Physiology 22*, 30-39.
34. Liu, T., Margret Ryan, Frederick W. Dahlquist, and O. Hayes Griffith. (1997) Determination ofpK, values of the histidine side chains of phosphatidylinositol-specific phospholipase C from Bacillus cereus by NMR spectroscopy and site-directed mutagenesis, *Protein Science 6*, 1937-1944.
35. Lu, Z., Elizabeth A. DiBlasio-Smith, Kathleen L. Grant, Nicholas W. Warne, Edward R. LaVallie, Lisa A. Collins-Racie, Maximillian T. Follettie, Mark J. Williamson, and John M. McCoy. (1996) Histidine Patch Thioredoxins: Mutant Forms of Thioredoxin with Metal Chelating Affinity that Provide for Convenient Purifications of Thioredoxin Fusion Proteins, *Journal of Biological Chemistry 271*, 5059-5065.
36. Cao, L., Helen E. Broomhead, Mark T. Young, and R. Alan North. (2009) Polar Residues in the Second Transmembrane Domain of the Rat P2X2 Receptor That Affect Spontaneous Gating, Unitary Conductance, and Rectification, *Journal of Neuroscience 29*, 14257-14264.